Superradiant and stimulated-superradiant emission of bunched electron beams

A. Gover
University of Tel-Aviv, Tel-Aviv, Israel

R. Ianconescu
University of Tel-Aviv, Tel-Aviv and Shenkar College, Ramat Gan, Israel

A. Friedman
Ariel University, Ariel

C. Emma, N. Sudar, P. Musumeci, and C. Pellegrini
UCLA, Los Angeles, California, 90095, USA

(published 19 August 2019)

The fundamental coherent radiation emission processes from a bunched charged particles beam are outlined. In contrast to spontaneous emission of radiation from a random electron beam that is proportional to the number of particles, a prebunched electron beam can emit spontaneously coherent radiation proportional to the number of particles—squared, through the process of (spontaneous) superradiance (SP-SR) (in the sense of Dicke's). The coherent SP-SR emission of a bunched electron beam can be even further enhanced by a process of stimulated superradiance in the presence of a seed-injected radiation field. In this review, these coherent radiation emission processes for both single bunch and periodically bunched beams are considered in a model of radiation mode expansion. The general model of coherent spontaneous emission is extended to the nonlinear regime, particularly for undulator (wiggler) interaction: tapering-enhanced stimulated-superradiant amplification (TESSA). Processes of SP-SR and TESSA take place in tapered wiggler seed-injected free-electron lasers (FELs). In such FELs, operating in the x-ray regime, these processes are convoluted with other effects. However these fundamental emission concepts are useful guidelines for the strategy of wiggler tapering efficiency and power enhancement. Based on this model, previous theories and experiments are reviewed on coherent radiation sources based on SP-SR (coherent undulator radiation, synchrotron radiation, Smith-Purcell radiation, etc.), in the THz regime and on-going works on tapered wiggler efficiency-enhancement concepts in all optical frequency regimes up to x rays.

DOI: 10.1103/RevModPhys.91.035003

CONTENTS

I. INTRODUCTION

Free electrons emit electromagnetic radiation when subjected to an external force, e.g., synchrotron radiation (Nodvick and Saxon, 1954; Green, 1976; Michel, 1982; Krinsky, 1983; Hirschmugl, Sagurton, and Williams, 1991; Tamada *et al.*, 1993; Berryman *et al.*, 1996; Wang, Krafft, and Sinclair, 1998; Giovenale *et al.*, 1999; Andersson, Johnson, and Nelander, 2000; Arp, 2001; Carr *et al.*, 2001, 2002; Abo-Bakr *et al.*, 2002; Byrd *et al.*, 2002, 2004; Geloni *et al.*, 2003; Adams, 2004; Sannibale *et al.*, 2004), undulator radiation (Bonifacio, Pellegrini, and Narducci, 1984b; Gover, Friedman, and Luccio, 1987; Jeong *et al.*, 1992; Ciocci *et al.*, 1993; Doria *et al.*, 1993; Jaroszynsky *et al.*, 1993; Asakawa *et al.*, 1994; Gover *et al.*, 1994; Cohen *et al.*, 1995; Mayhew *et al.*, 1997; Gallerano *et al.*, 1999; McNeil, Robb, and Jaroszynski, 1999; Arbel *et al.*, 2000, 2001; Neuman, Graves, and O'Shea, 2000; Faatz *et al.*, 2001; Pinhasi and Lurie, 2002; Neumann *et al.*, 2003; Huang, 2007; Lurie and Pinhasi, 2007; Watanabe *et al.*, 2007; Hama *et al.*, 2011; Kuroda *et al.*, 2011; Musumeci *et al.*, 2013; Seo, 2013a; Huang *et al.*, 2014, 2015), and Compton scattering (Gover and Sprangle, 1981). Radiation can also be emitted by currents that are induced by free electrons in polarizable structures and materials, such as in Cherenkov radiation (Cherenkov, 1934; Neighbors, Buskirk, and Saglan, 1984; Wiggins *et al.*, 2000), transition radiation (Piestrup and Finman, 1983; Happek, Blum, and Sievers, 1991; Shibata *et al.*, 1994; Lihn *et al.*, 1996; Orlandi, 2002; Leemans *et al.*, 2003; Geloni *et al.*, 2009), and Smith-Purcell radiation (Smith and Purcell, 1953; Brownell, Walsh, and Ducas, 1998; Korbly *et al.*, 2005; Shin *et al.*, 2007; Ginzburg *et al.*, 2013). Currently, most interesting are free-electron lasers (FELs), most potent intense coherent radiation sources that can operate in a wide range of radiation wavelengths from microwaves to x rays [see recent reviews by Bostedt *et al.* (2016), Pellegrini, Marinelli, and Reiche (2016), and Feng and Deng (2018)].

Here we use the laser physics terminology of stimulated interaction and spontaneous emission by atomic radiators, namely, stimulated emission or absorption is the radiation field amplification or attenuation of an incident radiation field, and spontaneous emission is the radiation emission of the particulate radiators in the absence of incident radiation field. The laser physics quantum description of free-electron radiation sources reduces to the classical point-particle description of radiation emission by electrons in acceleration or deceleration structures, including analogous fundamental (Einstein) relations between spontaneous and stimulated emission (Madey, 1979; Friedman *et al.*, 1988; Pan and Gover, 2018). In the present context, both spontaneous and stimulated interactions of electrons with radiation are treated in the classical point-particle limit of force equations and Maxwell equations.

Contrary to a FEL, that by its definition as a laser is a stimulated radiation emission device and is based on a continuous stream of accelerated electrons, the first focus of the present review is free-electron radiation devices that emit intense coherent spontaneous (superradiant) radiation without the fundamental process of stimulated emission. This is possible in all the previously mentioned radiation schemes, if the electron beam is prebunched before entering the radiative interaction region (in the case of a prebunched beam FEL—a magnetic undulator). Namely, such radiation sources emit coherent radiation without a coherent input radiation field (as required in a laser). However, as discussed later on, the coherent spontaneous radiation field can still be further amplified by stimulated emission if an external coherent input radiation field is inserted.

The condition for the generic coherent spontaneous superradiance process is

$$2\sigma_{tb} < T = 2\pi/\omega, \tag{1}$$

where ω is the radiation emission frequency, and $2\sigma_{tb}$ is the duration of the electron beam bunch. The process is visualized in Fig. 1 as a time interference of a train of radiation waves emitted by the electrons in a bunch, and observed, with some retardation and Doppler shift, at a long distance away from the emission point. Each electron emits in any specific direction radiation wave packets of frequency $\omega = 2\pi/T$ and duration $N_w T$, where N_w is the number of wiggling oscillations in the interaction length. The spontaneously emitted radiation fields of the different electrons add coherently in phase if the electron beam bunch is shorter than the emitted radiation period [Fig. 1(b), Eq. (1)], and the resultant field is proportional to the number of electrons in the bunch, N. Consequently, the intensity of the radiation of a prebunched beam is proportional to N^2. This is in contrast to spontaneous

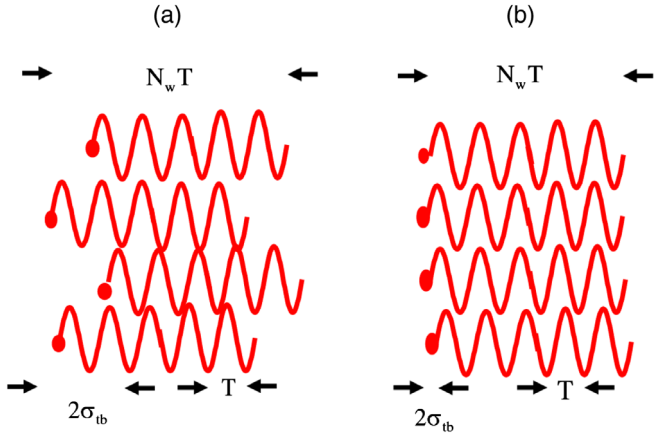

FIG. 1. (a) Spontaneous radiation emission. (b) Superradiant emission (coherent spontaneous emission).

emission from a randomly distributed beam in a long pulse [Fig. 1(a), opposite of Eq. (1)], where the radiation intensity is proportional to the number of electrons in the beam (N). This coherent radiation process is analogous to Dicke's superradiance from an ensemble of stationary atoms located within a volume smaller than their spontaneous emission radiation wavelength and excited so that their dipole moments emit in phase with each other (Dicke, 1954; Gross and Haroche, 1982). While Dicke's analysis started from a fundamental quantum-electrodynamics (QED) formulation, he showed that this process is valid also in the classical limit. The difference between a bunched electron beam and Dicke's ensemble of oscillating dipoles is only the movement of the electron bunch in the axial dimension. This provides, in the relativistic beam velocity limit, a large Doppler frequency shift of the radiation emitted in the forward direction.

As mentioned, superradiant emission from a single electron bunch beam takes place when the beam enters the interaction region of the radiative emission scheme with duration shorter than the period of the radiation wave [Eq. (1)]. Superradiance of a periodically bunched beam takes place when a train of tightly bunched electron bunches enters the interaction region at a rate equal to the radiation wave frequency. This generic coherent spontaneous radiation process can take place in any kind of free-electron radiation emission scheme (Schnitzer and Gover, 1985; Dattoli *et al.*, 1997; Gover, 2005b; Gover *et al.*, 2005; Penn, Reinsch, and Wurtele, 2006), including synchrotron radiation [where it is also termed coherent synchrotron radiation (CSR) or edge radiation] (Nodvick and Saxon, 1954; Green, 1976; Michel, 1982; Krinsky, 1983; Hirschmugl, Sagurton, and Williams, 1991; Tamada *et al.*, 1993; Berryman *et al.*, 1996; Wang, Krafft, and Sinclair, 1998; Giovenale *et al.*, 1999; Andersson, Johnson, and Nelander, 2000; Arp, 2001; Carr *et al.*, 2001, 2002; Abo-Bakr *et al.*, 2002; Byrd *et al.*, 2002, 2004; Geloni *et al.*, 2003; Adams, 2004; Sannibale *et al.*, 2004), coherent transition radiation (CTR) (Piestrup and Finman, 1983; Happek, Blum, and Sievers, 1991; Shibata *et al.*, 1994; Lihn *et al.*, 1996; Orlandi, 2002; Leemans *et al.*, 2003; Geloni *et al.*, 2009), undulator radiation (Bonifacio, Pellegrini, and Narducci, 1984b; Gover, Friedman, and Luccio, 1987; Jeong *et al.*, 1992; Ciocci *et al.*, 1993; Doria *et al.*, 1993; Jaroszynsky *et al.*, 1993; Asakawa *et al.*, 1994; Gover *et al.*, 1994; Cohen *et al.*, 1995; Mayhew *et al.*, 1997; McNeil, Robb, and Jaroszynski, 1999; Arbel *et al.*, 2000, 2001; Neuman, Graves, and O'Shea, 2000; Faatz *et al.*, 2001; Pinhasi and Lurie, 2002; Neumann *et al.*, 2003; Huang, 2007; Lurie and Pinhasi, 2007; Watanabe *et al.*, 2007; Hama *et al.*, 2011; Kuroda *et al.*, 2011; Musumeci *et al.*, 2013; Seo, 2013a; Huang *et al.*, 2014, 2015), Smith-Purcell radiation (Brownell, Walsh, and Ducas, 1998; Korbly *et al.*, 2005; Shin *et al.*, 2007; Ginzburg *et al.*, 2013), Cherenkov radiation (Neighbors, Buskirk, and Saglan, 1984; Wiggins *et al.*, 2000), dielectric waveguide radiation, and more.

Another interesting related coherent emission effect is exhibited by the same kind of single or periodically bunched electrons when they are subjected to a coherent radiation field of a copropagating wave in any kind of radiation emission scheme. If such a beam is tightly bunched relative to the wave period, or periodically bunched at the wave frequency, and if properly phased, then all electrons would experience the same deceleration force and emit in phase stimulated-superradiance radiation. This process is analogous to the same process of enhanced coherent radiation emission by an ensemble of two-quantum-level atoms that are subjected to a strong coherent radiation field. In the nonlinear regime all atoms undergo phase correlated Rabi oscillation between the two quantum levels and simultaneously can emit coherent stimulated-superradiance radiation (Ismailov and Kazakov, 1999; Brooke, 2008; Svidzinsky, Yuan, and Scully, 2013). The analog of the quantum Rabi oscillation, in the case of a bunched electron beam, is the synchrotron oscillation of a trapped bunched electron beam under the time harmonic force of a synchronous coherent radiation wave (ponderomotive wave in the case of undulator radiation).

Superradiant emission from a bunched beam may have important application in the development of coherent radiation sources at wavelength regimes and operating conditions where a stimulated emission radiation source is not practical, because the accelerated beam current is too low to provide sufficient gain within a practicable interaction length. We identify the THz frequency regime as a range where compact superradiant radiation sources are being developed (Ciocci *et al.*, 1993; Gover *et al.*, 1994, 2005; Faatz *et al.*, 2001; Shibata, Sasaki, and Ishi, 2002; Korbly *et al.*, 2005; Shin *et al.*, 2007; Yasuda *et al.*, 2008; Huang, 2010; Hama *et al.*, 2011; Ginzburg *et al.*, 2013; Huang *et al.*, 2015; Lurie, Friedman, and Pinhasi, 2015; Su *et al.*, 2018) based on moderately accelerated subpicosecond bunched beams, generated in photocathode injector electron guns (Akre *et al.*, 2008). We also assert that future compact coherent extreme ultraviolet (EUV) radiation sources based on dielectric laser accelerator (DLA) schemes (Peralta *et al.*, 2013) are likely to be developed as superradiant sources because of the low current and short interaction length expected to be attainable with such schemes. Beam bunching at the femtosecond and subfemtosecond duration ranges was demonstrated (Hommelhoff *et al.*, 2006; Zholents and Zolotorev, 2008; Hilbert *et al.*, 2009; Marceau *et al.*, 2013, 2015; Hoffrogge *et al.*, 2014; Wong *et al.*, 2015) and may be useful for superradiant radiation emission in the optical to EUV range. Various schemes for microprebunching the electron beam, including high gain harmonic generation (HGHG), echo-enabled harmonic generation (EEHG), or phase-merging enhanced harmonic generation (PEHG), have been developed for the superradiant generation of coherent UV and x-ray radiation (Yu, 1991; L. Yu *et al.*, 2000; Jia, 2008; Reiche *et al.*, 2008; Stupakov, 2009; Freund, Nguyen, and Carlsten, 2012; Graves *et al.*, 2013; Feng *et al.*, 2014; Qika, 2017). Most interestingly, recently tens of attoseconds duration of e-beam bunching was demonstrated at the electron quantum wave function level (Feist *et al.*, 2015; Kozák, Schönenberger, and Hommelhoff, 2018; Vanacore *et al.*, 2018), and it may exhibit superradiant emission in the modulated quantum electron wave packet level.

In the first part of this review, Secs. II and III, we present an analysis of superradiant emission in a general radiation emission scheme, but subsequently specify particularly to the case of undulator radiation. In general, the analysis of a radiative emission process requires a simultaneous solution of Maxwell equations for a particulate charge current source together with the force equations that govern the particles trajectories. However, in

the case of spontaneous emission (contrary to stimulated emission), the effect of the emitted radiation on the electron that had generated it is usually neglected (namely, a self-radiative interaction effect is not considered).

In this case, superradiant emission can be calculated based on solution on solving Maxwell equations alone, after evaluating the trajectories of the bunched beam in a force field in the absence of radiation. This is presented in Secs. II and III as follows: in Sec. II we derive the general expressions for random spontaneous emission, superradiant emission, and stimulated-superradiant emission from either single bunch or finite duration pulse of periodic bunches ("bunches train"). This analysis is carried out in a general spectral (Fourier transform) presentation of Maxwell equations. In both cases the current source is finite in time, the emitted radiation has finite energy, and therefore the continuous multifrequency spectral formulation is proper. In Sec. III we reiterate the analysis of spontaneous superradiance (SP-SR) and "zero-order" (in terms of the radiation field) stimulated superradiance (ST-SR) (namely, the effect of the radiation on the electron trajectories is negligible) for the case of an infinite (long) periodically bunched beam. The analysis is carried out in a single frequency (phasor) formulation for the steady-state case of undulator radiation (UR) by a periodically bunched electron beam (namely, an infinite train of bunches). In this case the radiation is composed only of the fundamental bunching frequency and its harmonics, and a single frequency model is proper. In this section we still use the approximation of negligible energy loss of the interacting e beam, namely, the radiation field is not intense enough to modify the electron trajectories, and explicit zero-order expressions for SP-SR and ST-SR emission are derived from Maxwell equations only. Using this zero-order approximation, we analytically evaluate the contribution of these two terms for the case of undulator radiation, and weigh the ratio between them and its scaling.

Confining the analysis to undulator radiation schemes, we extend in Sec. IV the zero-order analysis of superradiance and stimulated superradiance to a nonlinear interaction regime (namely, the effect of the radiation on the electron trajectories is non-negligible) in a uniform and tapered wiggler. This is the case where an intense radiation wave is injected externally into the interaction region together with a bunched e beam, and the interaction between the radiation and the beam is strong enough to produce non-negligible e-beam energy loss and a consequent slowing down of the beam. We review there the bunched beam dynamics qualitatively in terms of the mathematical pendulum equation and tilted pendulum equation models for the uniform and tapered wiggler, respectively. The characteristics of the pendulum equations are outlined in Appendix A.

A nonlinear analysis is required for studying the dynamics of the bunched beam interaction with a strong radiation field that can trap the electrons and for understanding the role of the fundamental processes of SP-SR, ST-SR in this regime, and the process of tapering-enhanced stimulated-superradiant amplification (TESSA) in a tapered wiggler. For this purpose we present in Sec. V a simple model for the beam-radiation interaction. This model is a self-consistent, energy-conserving formulation for the simultaneous solution of Maxwell equations and the force equations. The conservation of the energy relation is proved for general free-electron radiation schemes in Appendix C. The formulation is employed for the idealized case of an infinite, periodically tightly bunched cold beam, interacting with a single transverse radiation mode in a uniform or tapered wiggler. Expectedly, this model is consistent with the tilted pendulum equation model of KMR (Kroll, Morton, and Rosenbluth, 1981) for FEL saturation, but rather than starting from a random beam, we assume a beam with initial conditions of tight electron bunches and study their full nonlinear dynamics in the ponderomotive wave traps of the radiation mode as they evolve along the wiggler.

InSec. VI we present the solution of the coupled bunched-beam-radiation interaction equations based on numerical solutions of normalized master equations of the model for a uniform and tapered wiggler. The nonlinear dynamics of the fundamental SP-SR, ST-SR, and TESSA processes are presented by numerical examples and video simulations and are checked for consistency with the zero-order limits of the earlier sections. Interestingly enough, we identify there a special case of "self-interaction" (discussed in detail in Sec. VI.G), where a periodically bunched beam interacts nonlinearly with the spontaneous superradiant radiation it had generated in the first place.

In Sec. VII, the rigorous but ideal model of a perfect tightly bunched e beam is replaced by an approximate but more practical multiparticle model of arbitrary beam bunching and energy spread. This model is used for estimating limits of efficiency enhancement in a tapered wiggler in realizable configurations.

In Sec. VIII we review the applications of superradiant radiation sources in different realizations. These include a review of the development of various superradiant sources in the THz regime, new concepts of energy efficient schemes of TESSA and tapering-enhanced stimulated-superradiant oscillator (TESSO), and the relation to simulation and design work for optimization of energy extraction in a tapered wiggler FEL.

A. Superradiance in the wide sense

In the simplified model of superradiance processes presented in this review, we refer to processes in which the bunching amplitude of the electron beam is fixed. Whether we refer to a single short bunch beam or to an infinitely long periodically bunched beam, the assumption is that the bunch shape and bunching amplitude is constant throughout the interaction. The radiation emission is then characterized in the zero-order regime by the scaling $\propto N^2$ as in Dicke's superradiance. Also in the nonlinear regime, discussed from Sec. IV on, the model assumption is of tight full bunching: The bunches have dynamic processes of energy exchange with an intense radiation wave, but they do not spread and remain tightly bunched.

Of course, this model is a simplified idealization of more elaborate processes in real free-electron radiation sources. There are two main reasons that elaborate any clear-cut distinction between the processes of seeded FEL (FEL amplifier), self-amplified spontaneous emission (SASE) FEL and superradiant FEL, and lead to alternative wider sense definitions of superradiance (beyond superradiance in Dicke's sense). We explain and briefly review here the alternative definitions but will keep the terminology of

superradiance in the rest of the review in the narrow sense of Dicke's superradiance.

The first reason that breaks the distinction between a superradiant undulator radiation source and a FEL amplifier is the fact that while a superradiant source is based on a prebunched e beam, the conventional FEL radiation process also involves bunching. The stimulated emission process that is the fundamental radiation process in any laser is carried out in the FEL through a bunching process of a random electron beam by an externally injected coherent radiation field that bunches the beam at its frequency. Thus, in the case of a FEL amplifier there is no coherent radiation emission in the first sections of the interaction region (wiggler), but as the random electron beam gets bunched by the external radiation field, it starts radiating "superradiantly" in phase with the "seed-injected" radiation field. As the bunching and radiation emission processes continue along the interaction length, the radiation field starts growing exponentially by stimulated interaction, until the beam bunching saturates. The bunching stage in the FEL amplifier is the linear (low or high) gain regime of FEL theory. This stage is skipped in a prebunched superradiant FEL.

The situation is somewhat similar in SASE-FEL. In this case, there is no external radiation field that establishes coherent bunching in the beam, but the partially coherent spontaneous synchrotron undulator radiation emitted in the first section of the undulator can produce bunching of short coherence length in the beam that can still lead to a linear (field) exponential stimulated emission gain. In single path interaction, this process is enabled owing to the establishment of partial coherence in the beam through the "optical slippage effect": the light wave packets, emitted by the electrons, are faster than the electrons that generate them (propagating one wavelength λ relative to the electron during any wiggling period λ_w path of the electron in the wiggler). Consequently, partial coherence is established between electrons within the so-called "cooperation length" l_c which is the accumulated slippage $\lambda(l_g/\lambda_w)$ of the electrons, where l_g is the exponential gain length of the SASE-FEL.

Even though some bunching and superradiance processes are involved in the exponential light generation and amplification process of the FEL amplifier and the SASE-FEL, they would not usually be considered superradiant radiation sources. There are however some mixed cases of superradiance and stimulated emission gain. Such is the case of the microwave klystron, where the bunching of a continuous beam and the radiation process take place in separate cavities (Collin, 2007). The emission of the prebunched beam in the second cavity is superradiance in the narrow sense. A similar example is the "optical klystron oscillator" (Girard *et al.*, 1984). Here at steady-state oscillation the energy of the electron beam is bunched in an undulator by an input radiation field, after a process of density bunching in a dispersive magnetic section (chicane), the bunched beam is injected into a second undulator within the resonator together with the circulating radiation wave that interacts in phase with the bunched beam and enhances the oscillation gain. The interaction in this second step is certainly stimulated superradiance in the narrow sense.

Another case of mixed superradiance and stimulated emission is when the electron beam is partially bunched and then, at short interaction lengths, it emits superradiantly in the narrow sense ($\propto b_n^2 N^2$), where $b_n < 1$ is the bunching factor of harmonic n. However, before saturation, if the beam is not fully bunched, it can continue to increase exponentially its bunching and radiation emission by stimulated emission in the linear gain regime as in a regular FEL amplifier (Schnitzer and Gover, 1985; Qika, 2017). This principle is used in the HGHG process (L.-H. Yu *et al.*, 2000) in which a beam is energy bunched by an intense laser at optical (IR) frequency, and after passage through a dispersive magnet (chicane) it gets tightly bunched spatially, and its density contains high harmonics at small amplitude. The beam is then injected into a second undulator, synchronous with this small amplitude high harmonic current, where it radiates and gets amplified in an exponential "stimulated-superradiant" process, producing coherent radiation at extreme UV frequencies (Yu, 1991; Allaria *et al.*, 2012a).

Another case where the superradiance and stimulated emission processes are mixed and lead to alternative wider-sense definitions of radiation is the case of a finite pulse beam. In this case the SASE exponential growth process gets mixed with the short pulse superradiance process when the random beam pulse length l_b is shorter or near equal to the cooperation length $l_b \lesssim l_c$. In this case, the partially coherent SASE process may eventually yield a "single spike" coherent radiation pulse that may be termed "superradiant" in a wider sense, but the scaling of the radiation with the beam density is not always ($\propto N^2$) as in Dicke's superradiance because of the involvement of the exponential SASE processes. These kinds of wider sense superradiance processes were thoroughly studied mostly by Bonifacio *et al.* and others (Bonifacio, Pellegrini, and Narducci, 1984a; Bonifacio, Piovella, and McNeil, 1991; Bonifacio *et al.*, 1994; Krinsky, 1999; Watanabe *et al.*, 2007) who also identified similar superradiance processes in the leading and trailing regions of a long pulse ($l_b > l_c$) (Bonifacio *et al.*, 1990; Bonifacio, Piovella, and McNeil, 1991). Also numerous publications of Ginzburg and co-workers operating at the long wavelength (THz) regime (Ginzburg *et al.*, 2015) may be considered in this same category of superradiance in the wider sense.

As indicated, in the remainder of this review we will use the term of superradiance in the narrow (Dicke's) sense.

II. SUPERRADIANCE AND STIMULATED SUPERRADIANCE OF BUNCHED ELECTRON BEAM

As a starting point we present the theory of SP-SR and ST-SR emission from free electrons in a general radiative emission process (Gover, 2005b). In this section we use a spectral formulation, namely, all fields are given in the frequency domain as Fourier transforms of the real time-dependent fields:

$$\breve{A}(r,\omega) = \int_{-\infty}^{\infty} A(r,t) e^{i\omega t} dt. \tag{2}$$

We use the radiation modes expansion formulation of Gover (2005b), where the radiation field is expanded in terms of an orthogonal set of eigenmodes in a waveguide structure or in free space (e.g., Hermite-Gaussian modes):

$$\{\tilde{\boldsymbol{E}}_q(\mathbf{r}),\tilde{\boldsymbol{H}}_q(\mathbf{r})\}=\{\tilde{\boldsymbol{\mathcal{E}}}_q(\mathbf{r}_\perp),\tilde{\boldsymbol{\mathcal{H}}}_q(\mathbf{r}_\perp)\}e^{ik_{qz}z}, \tag{3}$$

$$\check{\mathbf{E}}(\mathbf{r},\omega)=\sum_{\pm q}\check{C}_q(z,\omega)\tilde{\boldsymbol{\mathcal{E}}}_q(\mathbf{r}_\perp)e^{ik_{qz}z}, \tag{4}$$

$$\check{\mathbf{H}}(\mathbf{r},\omega)=\sum_{\pm q}\check{C}_q(z,\omega)\tilde{\boldsymbol{\mathcal{H}}}_q(\mathbf{r}_\perp)e^{ik_{qz}z}. \tag{5}$$

The electric and magnetic fields representing the structure of the mode are named $\tilde{\boldsymbol{\mathcal{E}}}_q$ and $\tilde{\boldsymbol{\mathcal{H}}}_q$ and are usually nearly frequency independent. Their units are [V/m] and [A/m], respectively. The actual fields $\check{\mathbf{E}}$ and $\check{\mathbf{H}}$ are Fourier transforms and hence are in units of [s V/m] and [s A/m], respectively. Therefore, the amplitude coefficients $\check{C}_q$ have dimensions of time, hence units of [s].

The excitation equation of the mode amplitudes is

$$\frac{d\check{C}_q(z,\omega)}{dz}=\frac{-1}{4\mathcal{P}_q}\int\check{\mathbf{J}}(\mathbf{r},\omega)\cdot\tilde{\boldsymbol{\mathcal{E}}}_q^*(\mathbf{r}_\perp)e^{-ik_{qz}z}d^2\mathbf{r}_\perp, \tag{6}$$

where the current density $\check{\mathbf{J}}(\mathbf{r},\omega)$ is the Fourier transform of $\mathbf{J}(\mathbf{r},t)$.

Equation (6) is formally integrated and given in terms of the initial mode excitation amplitude and the currents

$$\check{C}_q(z,\omega)-\check{C}_q(0,\omega)=-\frac{1}{4\mathcal{P}_q}\int\check{\mathbf{J}}(\mathbf{r},\omega)\cdot\tilde{\boldsymbol{\mathcal{E}}}_q^*(\mathbf{r}_\perp)e^{-ik_{qz}z}dV, \tag{7}$$

where $\mathcal{P}_q$ is the power normalization parameter:

$$\mathcal{P}_q=\frac{1}{2}\mathrm{Re}\iint(\tilde{\boldsymbol{\mathcal{E}}}_q\times\tilde{\boldsymbol{\mathcal{H}}}_q^*)\cdot\hat{e}_z d^2\mathbf{r}_\perp=\frac{|\tilde{\boldsymbol{\mathcal{E}}}_q(\mathbf{r}_\perp=0)|^2}{2Z_q}A_{em\,q}, \tag{8}$$

where Z_q is the mode impedance (in free space $Z_q=\sqrt{\mu_0/\epsilon_0}$), and for a narrow beam, passing on axis near $\mathbf{r}_\perp=0$, Eq. (8) defines the mode effective area $A_{em\,q}$ in terms of the field of the mode on axis $\tilde{\boldsymbol{\mathcal{E}}}_q(\mathbf{r}_\perp=0)$.

For the Fourier transformed fields we define the total spectral energy (per unit of angular frequency) based on Parseval theorem as

$$\frac{dW}{d\omega}=\frac{2}{\pi}\sum_q\mathcal{P}_q|\check{C}_q(\omega)|^2. \tag{9}$$

This definition corresponds to positive frequencies only: $0<\omega<\infty$. Considering now one single mode q,

$$\frac{dW_q}{d\omega}=\frac{2}{\pi}\mathcal{P}_q|\check{C}_q(\omega)|^2. \tag{10}$$

For a particulate current (an electron beam):

$$J(\mathbf{r},t)=\sum_{j=1}^{N}-e\mathbf{v}_j(t)\delta(\mathbf{r}-\mathbf{r}_j(t)). \tag{11}$$

The field amplitude increment appears as a coherent sum of contributions (energy wave packets) from all the electrons in the beam:

$$\check{C}_q^{\mathrm{out}}(\omega)-\check{C}_q^{\mathrm{in}}(\omega)\equiv\sum_{j=1}^{N}\Delta\check{C}_{qj}(\omega)=-\frac{1}{4\mathcal{P}_q}\sum_{j=1}^{N}\Delta\check{\mathcal{W}}_{qj}, \tag{12}$$

$$\Delta\check{\mathcal{W}}_{qj}=-4\mathcal{P}_q\Delta\check{C}_{qj}=-e\int_{-\infty}^{\infty}\mathbf{v}_j(t)\cdot\tilde{\boldsymbol{\mathcal{E}}}_q^*(\mathbf{r}_j(t))e^{i\omega t}dt. \tag{13}$$

The contributions can be split into a spontaneous part (independent of the presence of the radiation field) and a stimulated (field dependent) part:

$$\Delta\check{\mathcal{W}}_{qj}=\Delta\check{\mathcal{W}}_{qj}^0+\Delta\check{\mathcal{W}}_{qj}^{st}. \tag{14}$$

We do not deal in this section with stimulated emission, but indicate that in general the second term $\Delta\check{\mathcal{W}}_{qj}^{st}$ is a function of $\check{C}_q(z)$ through $\mathbf{r}_j(t)$ and $\mathbf{v}_j(t)$; therefore the integral in Eq. (13) cannot be calculated explicitly. Its calculation requires solving the electron force equations and the differential equation (6). In the context of the linear gain regime of conventional FEL, $\Delta\check{C}_{qj}^{st}$ is proportional to the input field, i.e., proportional to $\check{C}_q^{\mathrm{in}}$, and in this case the solution of Eq. (6) results in the exponential gain expression of conventional FEL (Gover and Sprangle, 1981).

Assuming a narrow cold beam where all particles follow the same trajectories, we can write $\mathbf{r}_j(t)=\mathbf{r}_j^0(t-t_{0j})$ and $\mathbf{v}_j(t)=\mathbf{v}_j^0(t-t_{0j})$, change variable $t'=t-t_{0j}$ in Eq. (13) (Ianconescu *et al.*, 2015), so that the spontaneous emission wave packet contributions are identical, except for a phase factor corresponding to their injection time t_{0j}:

$$\Delta\check{\mathcal{W}}_{qj}^0=\Delta\check{\mathcal{W}}_{qe}^0e^{i\omega t_{0j}}, \tag{15}$$

where

$$\Delta\check{\mathcal{W}}_{qe}^0=-e\int_{-\infty}^{\infty}\boldsymbol{v}_e^0(t)\cdot\tilde{\boldsymbol{\mathcal{E}}}_q^*(\boldsymbol{r}_e^0(t))e^{i\omega t}dt. \tag{16}$$

The radiation mode amplitude at the output is composed of a sum of wave packet contributions including the input field contribution (if any):

$$\begin{aligned}\check{C}_q^{\mathrm{out}}(\omega)&=\check{C}_q^{\mathrm{in}}(\omega)+\Delta\check{C}_{qe}^0(\omega)\sum_{j=1}^{N}e^{i\omega t_{0j}}+\sum_{j=1}^{N}\Delta\check{C}_{qj}^{st}\\&=\check{C}_q^{\mathrm{in}}(\omega)-\frac{1}{4\mathcal{P}_q}\Delta\check{\mathcal{W}}_{qe}^0\sum_{j=1}^{N}e^{i\omega t_{0j}}-\frac{1}{4\mathcal{P}_q}\sum_{j=1}^{N}\Delta\check{\mathcal{W}}_{qj}^{st}\end{aligned} \tag{17}$$

so that the total spectral radiative energy from the electron pulse is

$$\frac{dW_q}{d\omega}=\frac{2}{\pi}\mathcal{P}_q|\check{C}_q^{\rm out}(\omega)|^2=\frac{2}{\pi}\mathcal{P}_q\left\{|\check{C}_q^{\rm in}(\omega)|^2+|\Delta C_{qe}^{(0)}(\omega)|^2\left|\sum_{j=1}^{N}e^{i\omega t_{oj}}\right|^2+\left[\check{C}_q^{\rm in}(\omega)\Delta C_{qe}^{(0)}(\omega)\sum_{j=1}^{N}e^{i\omega t_{oj}}+\text{c.c.}\right]\right.$$
$$\left.+\left[\check{C}_q^{\rm in}(\omega)\sum_{j=1}^{N}\Delta C_{qj}^{st}(\omega)+\text{c.c.}\right]+\left|\sum_{j=1}^{N}\Delta C_{qj}^{st}(\omega)\right|^2\right\}$$
$$\equiv\left(\frac{dW_q}{d\omega}\right)_{\rm in}+\left(\frac{dW_q}{d\omega}\right)_{\rm SP/SP\text{-}SR}+\left(\frac{dW_q}{d\omega}\right)_{\rm ST\text{-}SR}+\left(\frac{dW_q}{d\omega}\right)_{\rm st}. \tag{18}$$

The first term in the { }represents the input wave spectral energy, given the subscript "in." The second term is the spontaneous emission SP, which may also be spontaneous superradiant in the case that all contributions add in phase, hence given the subscript "SP-SR." The third term has a very small value (averages to 0) if the contributions add randomly. Thus it is relevant only if the electrons of the beam enter in phase with the radiated mode. It is therefore dependent on the coherent mode complex amplitude $\check{C}_q^{\rm in}$, and hence it is marked by the subscript "ST-SR," i.e., "zero-order"stimulated superradiance. The last two terms in the { } represent stimulated emission.

Figures 2(a) and 2(b) represent in the $\check{C}_q$ complex plane the conventional spontaneous emission and superradiant emission that correspond to the second term in Eq. (18), where in Fig. 2(a) the wave packets interfere randomly and in Fig. 2(b), constructively in phase. Figure 2(d) represents the third term in Eq. (18), where the coherent constructive interference of a prebunched beam interferes with the input field with some phase offset. When the electrons in the beam are injected at random in a long pulse, then in averaging the second term in Eq. (18), the uncorrelated mixed terms cancel out, and one obtains the conventional shot-noise driven spontaneous emission (Gover, 2005b; Ianconescu *et al.*, 2015):

$$\left(\frac{dW_q}{d\omega}\right)_{sp}=\frac{1}{8\pi\mathcal{P}_q}|\Delta\check{\mathcal{W}}_{qe}^{(0)}|^2N. \tag{19}$$

Only when the electrons are bunched into a pulse shorter than an optical period $\omega|t_{0i}-t_{0j}|\ll\pi$ does one get enhanced superradiant spontaneous emission, in which case all the terms in the bracket of the third term of Eq. (18) add up constructively in phase $\sum_{j=1}^{N}e^{i\omega t_{oj}}=Ne^{i\omega t_o}$ resulting in

$$\left(\frac{dW_q}{d\omega}\right)_{\rm SP\text{-}SR}=\frac{1}{8\pi\mathcal{P}_q}|\Delta\check{\mathcal{W}}_{qe}^{(0)}|^2N^2=\left\langle\left(\frac{dW_q}{d\omega}\right)\right\rangle_{sp}N. \tag{20}$$

Figure 2(d) displays a process of stimulated superradiance: all electrons oscillate in phase, but because a radiation mode of distinct phase is injected in, the third term in Eq. (18) will

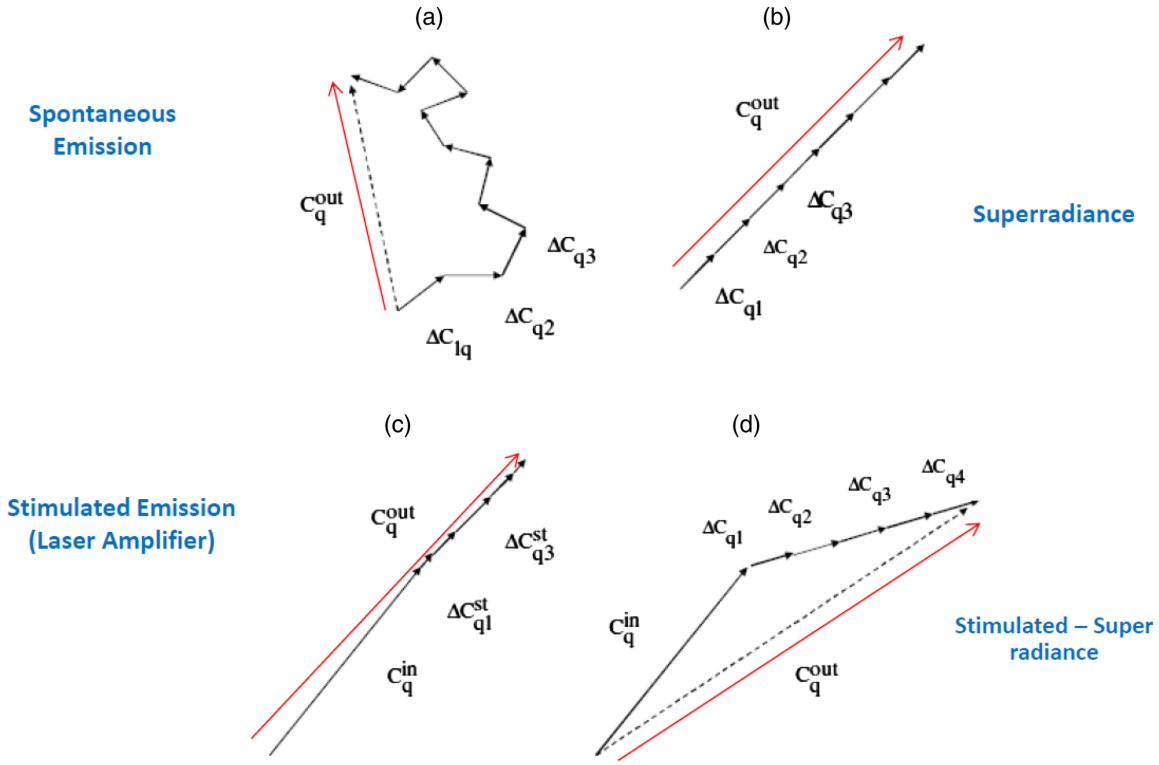

FIG. 2. Different cases of radiation: (a) spontaneous emission, (b) superradiance, (c) stimulated emission, and (d) stimulated superradiance.

contribute positive or negative radiative energy, depending whether the electron bunch oscillates in phase or out of phase with the input radiation field. If the phase of the electron bunch relative to the wave is φ, then the third term in Eq. (18) represents stimulated-superradiance spectral energy (Gover, 2005b):

$$\left(\frac{dW_q}{d\omega}\right)_{\text{ST-SR}} = -\frac{1}{\pi}|\check{C}_q^{\text{in}}||\Delta\check{\mathcal{W}}_{qe}^{(0)}|N\cos\varphi. \tag{21}$$

For purpose of comparison, we also display in Fig. 2(c) the process of conventional stimulated emission [fourth term in Eq. (18)], e.g., for the case of the FEL amplifier that we do not further consider here.

At this point we extend the analysis to include partial bunching, namely, electron beam bunches of finite duration and arbitrary bunch-shape function. One can characterize the distribution of electron entrance times t_{0j} of the electron bunch by means of a normalized bunch-shape function $f(t_0'-t_0)=i(t_0'-t_0)/eN$, where $i(t)$ is the e-beam bunch current, and t_0 is the bunch center entrance time:

$$\int_{-\infty}^{\infty} f(t_0'-t_0)dt_0' = 1. \tag{22}$$

Then the summation over t_{0j} may be substituted by integration over entrance times t_0':

$$\sum_{j=1}^{N} e^{i\omega t_{oj}} = N\int f(t_0'-t_0)e^{i\omega t_0'}dt_0' = Ne^{i\omega t_0}M_b(\omega), \tag{23}$$

where

$$M_b(\omega) = \frac{1}{N}\left\langle\sum_{j=1}^{N} e^{i\omega t_{0j}}\right\rangle = \int f(t)e^{i\omega t}dt \tag{24}$$

is the Fourier transform of the bunch-shape function, i.e., the bunching amplitude at frequency ω. It modifies Eqs. (20) and (21) to

$$\left(\frac{dW_q}{d\omega}\right)_{\text{SP-SR}} = \frac{1}{8\pi\mathcal{P}_q}|\Delta\check{\mathcal{W}}_{qe}^{(0)}|^2|M_b|^2N^2 \tag{25}$$

and

$$\left(\frac{dW_q}{d\omega}\right)_{\text{ST-SR}} = -\frac{1}{\pi}|\check{C}_q^{\text{in}}||\Delta\check{\mathcal{W}}_{qe}^{(0)}||M_b|N\cos\varphi. \tag{26}$$

In conditions of perfect bunching $f(t)=\delta(t)$ (and consequently $M_b=1$), Eqs. (20) and (21) are restored. For a finite size bunch, modeled by a Gaussian electron beam bunch distribution

$$f(t) = \frac{1}{\sqrt{2\pi}\sigma_{tb}}e^{-t^2/(2\sigma_{tb}^2)}, \tag{27}$$

the bunching factor is

$$M_b(\omega) = \int_{-\infty}^{\infty} e^{i\omega t}f(t)dt = e^{-\omega^2\sigma_{tb}^2/2}. \tag{28}$$

The zero-order analysis so far is valid for any interaction scheme for which the electron trajectories in the radiating structure are known explicitly to zero order, namely, in the absence of a radiation field, or where the change in the particles velocity and energy due to interaction with an external radiation field or their self-generated radiation field is negligible.

A. Superradiant undulator radiation

For the case of interest of undulator radiation we specify for each electron:

$$\mathbf{v}_i(t) = \text{Re}[\tilde{\mathbf{v}}_{\perp i}e^{-ik_w z_i(t)}], \tag{29}$$

where

$$\tilde{\mathbf{v}}_{\perp i} = \frac{c\tilde{\mathbf{a}}_w}{\gamma_i} = \frac{e\hat{z}\times\tilde{\mathbf{B}}_w}{\gamma_i mk_w}, \tag{30}$$

where $\tilde{\mathbf{B}}_w$ is the complex amplitude of the undulator periodic magnetic field $\mathbf{B}(z)=\text{Re}[\tilde{\mathbf{B}}_w e^{-ik_w z}]$. Assume that the electron beam is narrow enough so that all electrons experience the same field when interacting with the mode

$$\tilde{\boldsymbol{E}}_q(\mathbf{r}_j^0(t)) = \tilde{\boldsymbol{\mathcal{E}}}_q(\mathbf{r}_\perp=0)e^{ik_{qz}z_j^0(t)}, \tag{31}$$

where $z_j^0(t)=v_z(t-t_{0j})$, and $\mathbf{r}_\perp$ is the transverse coordinates vector of the electron beam, then substituting this and Eq. (29) into Eq. (16) one obtains

$$\Delta\check{\mathcal{W}}_{qj}^0 = -e\frac{\tilde{\mathbf{v}}_{\perp 0}\cdot\tilde{\boldsymbol{\mathcal{E}}}_q^*}{2v_z}L_w\,\text{sinc}(\theta L_w/2)e^{i\theta L_w/2}e^{i\omega t_{0j}}, \tag{32}$$

where $L_w=N_w\lambda_w$ is the interaction length ($\lambda_w=2\pi/k_w$), $\text{sinc}(x)=\sin x/x$, and $\theta(\omega)$, the detuning parameter, is defined by

$$\theta(\omega) = \frac{\omega}{v_z} - k_{zq}(\omega) - k_w. \tag{33}$$

The detuning function $\text{sinc}(\theta L/2)$ attains its maximum value at the synchronism frequency ω_r defined by

$$\theta(\omega_r) = \frac{\omega_r}{v_z} - k_{zq}(\omega_r) - k_w = 0. \tag{34}$$

Near synchronism

$$\theta(\omega)L_w \simeq (\omega-\omega_r)t_s = 2\pi\frac{\omega-\omega_r}{\Delta\omega}, \tag{35}$$

where

$$t_s = \frac{2\pi}{\Delta\omega} = \frac{L_w}{v_z} - \frac{L_w}{v_{gq}} \tag{36}$$

is the wave packet slippage time and $v_{gq} = d\omega/dk_{zq}$ at ω_r is the group velocity of the mode. In free space $k_{zq} = \omega/c$, $v_{gq} = c$, and the solution of Eq. (34) results in

$$\omega_r = \frac{ck_w}{1/\beta_z - 1} \simeq 2\gamma_z^2 ck_w, \tag{37}$$

$$\Delta\omega = \frac{\omega_r}{N_w}, \tag{38}$$

where the second part of Eq. (37) applies for an ultrarelativistic beam ($\beta \simeq 1$), and

$$\gamma_z^2 = \frac{\gamma^2}{1 + \bar{a}_w^2}, \tag{39}$$

where $\bar{a}_w \equiv e\bar{B}_w/mck_w$ is the one period rms average of $a_w(z)$. It is equal to the amplitude a_w in the case of a helical (circularly polarized) wiggler and to $a_w/\sqrt{2}$ in a linear (linearly polarized) magnetic wiggler.

When substituting Eqs. (30) and (32) into Eqs. (20) and (21) one obtains the expressions of UR superradiance and stimulated superradiance from a tight single bunch into a single mode q (Gover, 2005b)

$$\left(\frac{dW_q}{d\omega}\right)_{\text{SP-SR}} = \frac{N^2 e^2 Z_q}{16\pi}\left(\frac{\bar{a}_w}{\beta_z\gamma}\right)^2 \frac{L_w^2}{A_{em\,q}} \sin c^2(\theta L_w/2), \tag{40}$$

$$\left(\frac{dW_q}{d\omega}\right)_{\text{ST-SR}} = \frac{N}{\pi}\left(\frac{\bar{a}_w}{\beta_z\gamma}\right) e|\breve{E}(0,\omega)|L_w \sin c(\theta L_w/2) \times \cos(\varphi_{qb0} - \theta L_w/2), \tag{41}$$

where $\breve{E}(0,\omega) = \breve{C}_q(0,\omega)\tilde{\boldsymbol{\mathcal{E}}}_q(\mathbf{r}_\perp = 0)$ is the Fourier transform of the input injected radiation mode [Eqs. (2) and (4)] and $\varphi_{qb0}(\omega)$ is the phase between the radiation field and the bunch at the entrance to the wiggler.

While in the present paper we stay, for transparency, with a single radiation mode analysis, we point out that the general expression for radiation into all modes is found from summation over the contributions of all modes [Eq. (9)]. This expression can also be extended to the case of free-space radiation (Ianconescu *et al.*, 2015), where the far field spectral energy intensity is found to have a similar frequency functional dependence as Eq. (40) with the substitution $k_z = (\omega/c)\cos\Theta$ in the detuning parameter $\theta(\omega)$ [Eq. (33)], where Θ is the far field observation angle off the wiggler axis.

We now extend the analysis to the case of spontaneous emission from a finite train of bunches. Following the formulation of Gover (2005b), we consider a train of N_M identical bunches (neglecting shot noise) separated in time $T_b \equiv 2\pi/\omega_b$ apart. The arrival times of bunch k is

$$t_{0k} = [k - (N_M/2)]2\pi/\omega_b. \tag{42}$$

The summation of the phasors $e^{i\omega t_{0j}}$ in the second term of Eq. (17) is now reorganized into summation over the N_M bunches and summation over the N_b particles in each bunch as shown in Fig. 3. Given that electron n (n is between 1 to $N = N_M N_b$) is the electron j of bunch k, and $|\Delta t_{0i}| < T_b$, we have $t_{0n} = t_{0k} + \Delta t_j + t_0$ (t_0 being a pulse origin reference, e.g., the arrival time of the center of the train pulse), we can write

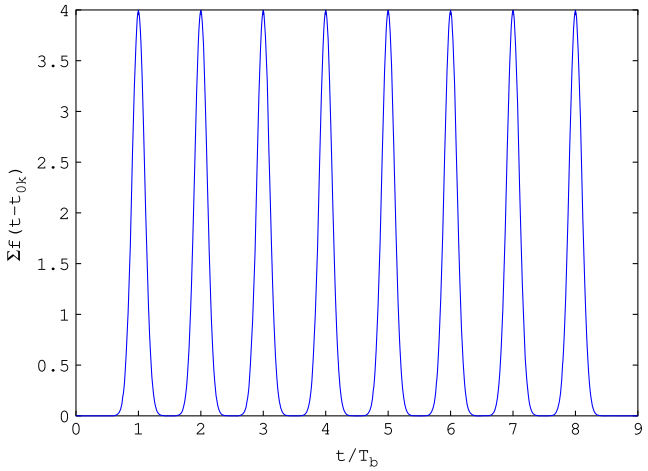

FIG. 3. The charge distribution function of a "macropulse" finite train of bunches arriving at times t_{0k}, with period $T_b = 2\pi/\omega_b$. Each bunch is a normalized Gaussian [Eq. (27)] with $\sigma_{tb} \ll T_b$.

$$\sum_{n=1}^{N} e^{i\omega t_{0n}} = \sum_{n=1}^{N} e^{i\omega t_{0k}} e^{i\omega\Delta t_j} e^{i\omega t_0} = e^{i\omega t_0} \sum_{k=1}^{N_M}\sum_{j=1}^{N_b} e^{i\omega t_{0k}} e^{i\omega\Delta t_j} = e^{i\omega t_0}\left(\sum_{k=1}^{N_M} e^{i\omega t_{0k}}\right)\left(\sum_{j=1}^{N_b} e^{i\omega\Delta t_j}\right). \tag{43}$$

We define the microbunch bunching factor:

$$M_b(\omega) = \frac{1}{N_b}\left\langle \sum_{j=1}^{N_b} e^{i\omega\Delta t_j} \right\rangle, \tag{44}$$

where $\langle\,\rangle$ mean averaging on the random Δt_j. We also define the macrobunch (pulse) form factor:

$$M_M(\omega) = \frac{1}{N_M}\sum_{k=1}^{N_M} e^{i\omega t_{0k}}. \tag{45}$$

Setting Eqs. (44) and (45) into (43) we obtain

$$\left\langle \sum_{n=1}^{N} e^{i\omega t_{0n}} \right\rangle = N M_b(\omega) M_M(\omega) e^{i\omega t_0}. \tag{46}$$

Note that the assumption that all microbunches in the macrobunch have an equal number of particles N_b amounts to neglecting shot noise due to a random variance of particles along the macrobunch. If one assumes that the distribution of the electron particles within the bunches is tight enough

$|\Delta t_{0j}| \ll T_b$, Eq. (44) can be written in terms of the particles distribution function within one period

$$M_b(\omega) = \frac{\omega_b}{2\pi}\int_{-\pi/(2\omega_b)}^{\pi/(2\omega_b)} f_b(\Delta t_0)d(\Delta t_0)$$

and approximated by Eq. (24). For a Gaussian distribution (27), M_b is then given by Eq. (28). The macrobunching form factor (42) is calculated using Eq. (45), as a geometric series sum:

$$M_M(\omega) = \frac{\sin(N_M\pi\omega/\omega_b)}{N_M\sin(\pi\omega/\omega_b)}. \tag{47}$$

This form factor contains the basic bunching frequency ω_b peak and an infinite number of high harmonics, as shown in Fig. 4. Consequently the superradiant spectral energy of the bunch train [the second term in Eq. (18)] is

$$\left(\frac{dW_q}{d\omega}\right)_{\text{SP-SR}} = \frac{N^2}{8\pi\mathcal{P}_q}|\Delta\check{\mathcal{W}}_{qe}^{(0)}|^2|M_b(\omega)|^2|M_M(\omega)|^2, \tag{48}$$

and the stimulated superradiance at zero-order approximation [the third term in Eq. (18)] is

$$\left(\frac{dW_q}{d\omega}\right)_{\text{ST-SR}} = \frac{N}{\pi}|\check{C}_q^{\text{in}}(\omega)||\Delta\check{\mathcal{W}}_{qe}^{(0)}||M_b(\omega)| \times |M_M(\omega)|\cos\varphi_{qb0}(\omega), \tag{49}$$

where $\varphi_{qb0}(\omega)$ is the phase between the radiation field and the periodically bunched beam, determined at the entrance to the wiggler.

For the case of interest of UR we substitute Eq. (32) into Eqs. (48) and (49) and obtain the general expression for spontaneous SP-SR and ST-SR spectral energy of a finite train of periodic bunches:

$$\left(\frac{dW_q}{d\omega}\right)_{\text{SP-SR}} = \frac{N^2e^2Z_q}{16\pi}\left(\frac{\bar{a}_w}{\beta_z\gamma}\right)^2\frac{L_w^2}{A_{em\,q}}|M_b(\omega)|^2|M_M(\omega)|^2 \times \sin c^2(\theta L_w/2) \tag{50}$$

and the stimulated-superradiant term is

$$\left(\frac{dW_q}{d\omega}\right)_{\text{ST-SR}} = \frac{N}{\pi}\left(\frac{\bar{a}_w}{\beta_z\gamma}\right)e|\check{E}(0,\omega)|L_w \times |M_b(\omega)||M_M(\omega)|\sin c[\theta(\omega)L_w/2] \times \cos[\varphi_{qb0}(\omega) - \theta L_w/2]. \tag{51}$$

The spectrum of superradiant and stimulated-superradiant UR is composed of harmonics of narrow linewidth $\Delta\omega \simeq \omega_b/N_M$ (Fig. 4) within the low frequency filtering band of the bunching factor $\omega < 1/\sigma_{tb}$ [Eq. (28)] and the finite interaction length bandwidth (38).

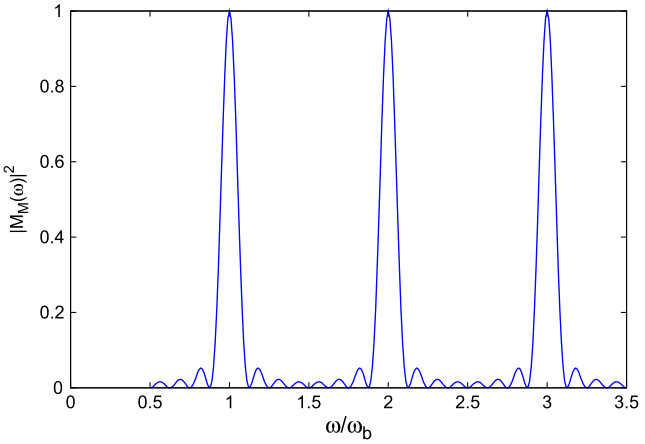

FIG. 4. The absolute square of the macropulse form-factor function in Eq. (47) for $N_M = 8$.

III. SINGLE FREQUENCY FORMULATION

In the limit of a continuous train of microbunches or a long macropulse $N_M \gg 1$, the macropulse form factor $M_M(\omega)$ behaves like a comb of delta functions and narrows the spectrum of the prebunched beam SP-SR and ST-SR undulator radiation to harmonics of the bunching frequencies $\omega = n\omega_b$. Instead of spectral energy, one can then evaluate the average radiation power output within the macropulse by integrating the spectral energy expressions (48) and (49) over frequency and dividing the integrated spectral energy by the pulse duration $T_M = N_M 2\pi/\omega_b$. Alternatively, one may have analyzed the continuous bunched beam problem from the start in a single frequency model using "phasor" formulation, concentrating for now on a single frequency ω_0:

$$A(\mathbf{r},t) = \text{Re}[\tilde{A}(\mathbf{r},\omega_0)e^{-i\omega_0 t}]. \tag{52}$$

Note that in this case the radiation frequency ω must be equal to the bunching frequency or one of its harmonics $\omega = \omega_0 = n\omega_b$, otherwise there will not be any steady-state interaction between them. The radiation mode excitation equations in the phasor formulation of the radiation fields $\{\tilde{\mathbf{E}}(\mathbf{r}), \tilde{\mathbf{H}}(\mathbf{r})\}$ are the same as Eqs. (3)–(6) with $\tilde{C}_q(z,\omega_0) \equiv \tilde{C}_q(z)$ replacing $\check{C}_q(z,\omega)$, and the spectral energy radiance expression (9) replaced by the total steady-state radiation power

$$P = \sum_q \mathcal{P}_q|\tilde{C}_q|^2. \tag{53}$$

As in Schnitzer and Gover (1985), Arbel *et al.* (2014), and Schneidmiller and Yurkov (2015), we take a model of a periodically modulated e-beam current of a single frequency ω_0:

$$I(z,t) = I_0\{1 + \text{Re}[\tilde{M}e^{-i\omega_0(t-z/v_z)}]\}. \tag{54}$$

This current represents one of the harmonics of a periodically bunched beam $\omega_0 = n\omega_b$.

The parameter $\tilde{M}$ can be calculated for each of the harmonics $\omega_n = n\omega_b$ from the Fourier series expansion of an infinite train of identical microbunches (shot noise is neglected):

$$I(z,t) = I_0 T_b \sum_{n=-\infty}^{\infty} f(t - z/v_z - nT_b), \tag{55}$$

where $T_b = 2\pi/\omega_b$ and the bunch profile is normalized according to $\int_{-T_b/2}^{T_b/2} f(t)dt = 1$. The Fourier expansion is

$$I(z,t) = I_0\{1 + 2\mathrm{Re}[b_n e^{in\omega_b(t-z/v_z)}]\}, \tag{56}$$

where

$$b_n = \int_{-T_b/2}^{T_b/2} f(t) e^{-in\omega_b(t-z/v_z)} dt. \tag{57}$$

Thus, Eq. (54) represents one of the harmonic components of frequency $\omega_0 = \omega_{bn} = n\omega_b$ and phasor amplitude $\tilde{M} = 2b_n$.

The bunching parameter b_n depends on the profile function of the microbunch. If the microbunches can be represented by the Gaussian function (27), such that $\sigma_{tb} \ll T_b/n$, then the integration in Eq. (57) can be carried to infinity, and then [see Eq. (28)]

$$b_n = M_b(\omega_n) = e^{-\omega_n^2\sigma_{tb}^2/2}. \tag{58}$$

The Gaussian approximation is not always most fitting to describe the bunch distribution function. A most useful scheme of bunching a continuous or long pulse beam is modulating its energy with a high intensity laser beam in a wiggler (or another interaction scheme), and then turning its energy modulation to density modulation by passing it through a dispersive section (DS), such as a "chicane" (see Appendix B). This scheme of bunching is useful for a variety of short wavelength radiation schemes, including HGHG (Yu, 1991; L. Yu *et al.*, 2000), EEHG (Stupakov, 2009; Xiang and Stupakov, 2009), PEHG (Jia, 2008; Feng *et al.*, 2014), and enhanced SASE (eSASE) (Zholents, 2005). Following the notation of Stupakov (2009), the bunching parameter after the DS is determined in this case by the initial energy spread of the beam $\sigma_{\gamma 0}/\gamma_0$, the compression parameter $B = \omega_b\sigma_t = \omega_b(R_{56}/c)(\sigma_{\gamma 0}/\gamma_0)$, and the energy modulation parameter $A = \Delta\gamma_{\mathrm{mod}}/\sigma_{\gamma 0}$, where $\sigma_{\gamma 0}$ is the intrinsic energy spread of the beam before modulation. For optimized bunching of harmonic n (given $n > 4$), the dispersion is adjusted so that $AB = 1$. In this case a useful expression for the bunching coefficient is (see Appendix B)

$$b_n = \frac{0.67}{n^{1/3}} e^{-n^2B^2/2}. \tag{59}$$

Assuming the beam has a normalized transverse profile distribution $f(\mathbf{r}_\perp)$, the transverse current density in the wiggler is

$$\mathbf{J}_\perp(\mathbf{r},\omega_0) = \frac{\tilde{I}_{m\perp}\hat{\mathbf{e}}_\perp}{2} f(\mathbf{r}_\perp) e^{i(\omega_0/v_z - k_w)z}, \tag{60}$$

where

$$\tilde{I}_{m\perp}\hat{\mathbf{e}}_\perp = I_0\tilde{M}\frac{\tilde{\boldsymbol{\beta}}_w}{\beta_z}. \tag{61}$$

Writing now the excitation equation in phasor formulation:

$$\tilde{C}_q(z) = \tilde{C}_q(0) - \frac{1}{4\mathcal{P}_q}\int \tilde{\mathbf{J}}_\perp(\mathbf{r},\omega_0)\cdot\tilde{\boldsymbol{\mathcal{E}}}_q^*(\mathbf{r}_\perp)e^{-ik_{zq}z}dV, \tag{62}$$

one obtains

$$\tilde{C}_q(z) = \tilde{C}_q(0) - \frac{\tilde{I}_{m\perp}}{8\mathcal{P}_q}|\tilde{\boldsymbol{\mathcal{E}}}_q(0)|F_q z e^{i\theta z/2}\sin c(\theta z/2), \tag{63}$$

where

$$\tilde{I}_{m\perp} = |\tilde{I}_{m\perp}|e^{i\varphi_{b0}} \tag{64}$$

and F_q is a field "filling factor":

$$F_q = \frac{1}{|\tilde{\boldsymbol{\mathcal{E}}}_q(0)|}\left|\int_{-\infty}^{\infty}\hat{\mathbf{e}}_\perp\cdot\tilde{\boldsymbol{\mathcal{E}}}_q^*(\mathbf{r}_\perp)f(\mathbf{r}_\perp)d^2r_\perp\right|. \tag{65}$$

This parameter is close to 1 when the beam is narrow relative to the transverse variation of the mode and the diffraction effect is negligible, or in the case of a transversely uniform beam and radiation field (1D model).

The time averaged radiation power will then be given by

$$P_q(z) = \mathcal{P}_q|\tilde{C}_q(z)|^2 = P_q(0) + P_{\text{SP-SR}}(z) + P_{\text{ST-SR}}(z). \tag{66}$$

With the definition (8) for the effective area of the radiation mode $A_{em\,q}$, the superradiant and stimulated-superradiant powers are

$$P_{\text{SP-SR}}(z) = \frac{1}{32}Z_q|\tilde{I}_{m\perp}|^2F_q^2\frac{z^2}{A_{em\,q}}\sin c^2(\theta z/2) \tag{67}$$

and

$$P_{\text{ST-SR}}(z) = \tfrac{1}{4}E(0)|\tilde{I}_{m\perp}|F_q z\cos(\varphi_{qb0} - \theta z/2)\sin c(\theta z/2), \tag{68}$$

where

$$E(0) = |\tilde{C}_q(0)||\tilde{\boldsymbol{\mathcal{E}}}_q(0)| \tag{69}$$

and

$$\varphi_{qb0} = \varphi_{q0} - \varphi_{b0} \tag{70}$$

is the phase difference between the radiation field phase φ_{q0} and the bunching current phase φ_{b0} at the entrance to the wiggler.

Maximal power generation is attained for $\theta = 0$ and $\varphi_{qb0} = 0$ (phase matching between the bunched current and radiation field):

$$P_{\text{SP-SR}}(z) = \frac{1}{32} Z_q |\tilde{I}_{m\perp}|^2 F^2 \frac{z^2}{A_{em\,q}} \tag{71}$$

and

$$P_{\text{ST-SR}}(z) = \frac{1}{4} |\tilde{I}_{m\perp}| \sqrt{\frac{2Z_q}{A_{em\,q}}} \sqrt{P_{\text{in}}} F_q z. \tag{72}$$

The ratio between the two contributions to the radiation power is

$$\frac{P_{\text{ST-SR}}}{P_{\text{SP-SR}}} = 8 \frac{A_{emq}}{Z_q \tilde{I}_{m\perp} F_q z} \sqrt{\frac{2Z_q}{A_{emq}}} \sqrt{P_{\text{in}}} = 8 \frac{A_{emq}}{Z_q \tilde{I}_{m\perp} F_q z} E(0). \tag{73}$$

In Fig. 5 we show the ratio of zero-order ST-SR to SP-SR for different initial power levels at $z = z_0$. Initially the ST-SR power dominates the SP-SR power, but evidently, for long interaction length the SP-SR power that grows like z^2 exceeds the ST-SR power that grows like z. At the beginning stages of interaction in the wiggler the ST-SR power may be significantly higher than the SP-SR power if the initial radiation power P_{in} injected is large enough. This balance is demonstrated in Fig. 5 for the parameters of the Linac Coherent Light Source (LCLS) (Emma *et al.*, 2014) (without tapering).

We point out that in the case of a long wiggler, diffraction effects of the radiation beam become significant (see Sec. VIII.C), and a single mode analysis would be relevant only in the initial part of the wiggler up to a distance of a Rayleigh length. The superradiant part of the radiation emission was analyzed, including diffraction effects, based on a Gaussian model for the radiation beam in Schneidmiller and Yurkov (2015). The contribution of the stimulated superradiance to the radiation emission has usually been ignored in analytic modeling. Our conclusion on the dominance of this contribution in the initial section of the wiggler is valid at least up to the distance of a Rayleigh length, within which the single radiation mode model is valid and would be valid then only if tight bunching is realizable. A more complete review of the modeling of radiation in the tapered wiggler section of an FEL and the limitations of the 1D modeling is postponed to Sec. VIII.C.

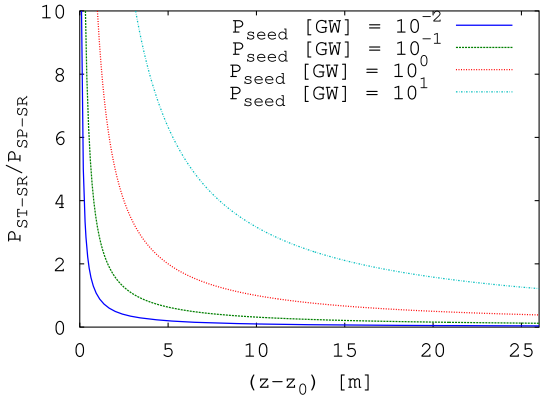

FIG. 5. Ratio of zero-order ST-SR to SP-SR generated power for different initial input power.

IV. SUPERRADIANCE AND STIMULATED SUPERRADIANCE IN THE NONLINEAR REGIME

The underlying assumption in the calculation of spontaneous emission, superradiant spontaneous emission, and zero-order stimulated-superradiant emission is that the beam energy loss as a result of radiation emission is negligible. When this is not the case, the problem becomes a nonlinear evolution problem. We now extend our model to the case of a continuously bunched electron beam interacting with a strong radiation field in an undulator, so that the electron beam loses an appreciable portion of its energy in favor of the radiation field. In this case, the electrons experience the dynamic force of the radiation wave and change their energy according to the force equation (C14) in Appendix C. As derived in the conventional theory of a FEL (Kroll, Morton, and Rosenbluth, 1981; Pellegrini, Marinelli, and Reiche, 2016) the scalar product of the radiation field $\mathbf{E}(r,t)$ and the wiggling velocity $\mathbf{v}_i(t)$ [Eq. (29)] produces a periodic "beat wave" force (the "ponderomotive force"), propagating with phase velocity

$$v_{ph} = \frac{\omega_0}{k_{zq} + k_w}. \tag{74}$$

This force wave can be synchronous with the electron beam near the synchronism condition of Eq. (34) or (37).

Near synchronism, electrons interact efficiently with the sinusoidal ponderomotive force. The dynamics of this interaction is analyzed and presented in Sec. V. In this section we discuss qualitatively the conceptual transition from the zero-order regime (no e-beam dynamics) to the nonlinear regime. For this we use the "pendulum" model that had been developed earlier for FEL theory (Colson, 1977; Kroll, Morton, and Rosenbluth, 1981; Pellegrini, Marinelli, and Reiche, 2016). According to this model, the incremental energy of the electron (off the synchronism energy) and its phase (relative to the sinusoidal ponderomotive wave) satisfy the "pendulum equations." The characteristics of the solution of this well-known mathematical equations and of the "tilted pendulum equations" are presented briefly in Appendix A. In analogy to the physical pendulum, the dynamics of the electron in the ponderomotive wave potential is described in terms of its trajectories in the phase space of its detuning parameter θ [Eq. (33)] and its phase ψ relative to the ponderomotive wave. The nonlinear regime saturation process of a FEL is explained in Appendix A in terms of the phase-space trajectories of Fig. 29 that consist of two kinds of trajectories: open and closed (trapped). The maximal loss of energy of an electron within the trap (and, respectively, its maximal deviation off synchronism $\Delta\theta$ due to the interaction) depends on the height of the trap $\Delta\theta = 2\theta_m$. A well-bunched electron beam will release maximum energy (transformed to radiation), if inserted into the trap near synchronism at phase $\psi = 0$ and detuning parameter near $-\theta = \theta_m$ corresponding to the top of the trap (Fig. 29), and winds up at the bottom of the trap at the end of the interaction length (the wiggler).

Extending the technology of a uniform wiggler FEL, a scheme of a "tapered wiggler" has been developed in the field of FELs for extracting higher radiation energy from the beam (Kroll, Morton, and Rosenbluth, 1981) beyond the maximal

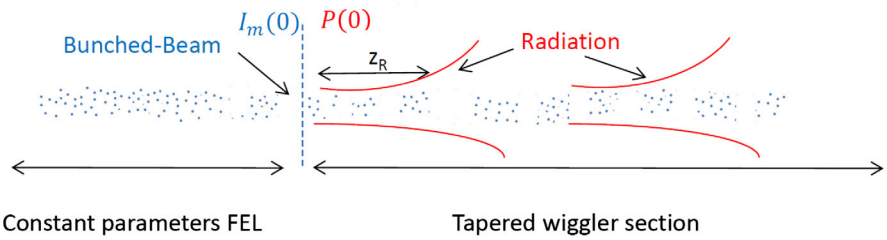

FIG. 6. Schematics of a seed-injected FEL followed by a tapered wiggler: at the end of the constant parameters wiggler, the partially bunched e beam and the amplified radiation wave are injected into a tapered wiggler section, where further radiation energy is extracted out of the bunched beam.

energy extraction efficiency of a uniform FEL. The experimental realization of this scheme is described schematically in Fig. 6 for the case of a tapered wiggler FEL. After providing linear gain in a uniform wiggler, the wasted beam that is partly bunched due to the interaction in the first section continues to interact along a tapered wiggler with the coherent radiation wave that was generated in the first section and is further amplified in the second section. In such a scheme, the wiggler wave number $k_w(z)$ is increased along the tapered wiggler section, so that the ponderomotive phase velocity v_{ph} [Eq. (74)] decreases gradually, keeping synchronism with the correspondingly slowing down electrons, trapped in the ponderomotive wave, so that the synchronism condition in Eq. (34) can be kept all along:

$$\theta(z) = \int_0^z \left[\frac{\omega_0}{v_z(z')} - k_{zq}(\omega_0) - k_w(z')\right] dz' \simeq 0. \quad (75)$$

The trapped electrons dynamics and the energy extraction process in this scheme can be presented in terms of the tilted pendulum model (Appendix A). They are described quantitatively in terms of their trajectories in phase space in Fig. 32 that shows that the electrons can stay trapped (although the trap is somewhat shrinked) and still keep decelerating along the tapered wiggler, keeping near synchronism with the slowing down ponderomotive wave. Note that in Eq. (75) v_z is the axial velocity of the beam averaged over the wiggler period. In a linear wiggler with $\bar{a}_w \gg 1$ the linear transverse wiggling gives rise to the longitudinal periodic quiver of $v_z(z)$ and a consequent radiative interaction at odd harmonic frequencies (Gover, 2005a; Pellegrini, Marinelli, and Reiche, 2016). For simplicity we ignore here these harmonic interactions. Also, in using the pendulum equation model to describe the dynamics of the electron inside the trap (synchrotron oscillation), it is implicitly assumed that the pendulum oscillation period (synchrotron period λ_S) is much longer than the wiggler period $\lambda_S \gg \lambda_w$.

For completion of this short review of a tapered wiggler FEL, we point out that besides tapering the wiggler wave number $k_w(z)$, enhanced energy extraction efficiency of saturated FEL is also possible in an alternative scheme of magnetic field wiggler parameter tapering. In this scheme, the period of the tapered wiggler stays constant, but the strength of the magnetic field and correspondingly the wiggler parameter $a_w(z) = |\tilde{\mathbf{a}}_w(z)|$ [Eq. (30)] is reduced gradually along the wiggler so that $\gamma_z^2(z) = \gamma^2(z)/[1 + a_w^2(z)]$ remains constant in Eq. (39). Since $\beta_z = [1 - 1/\gamma_z^2]^{1/2}$, the detuning synchronism condition (34) or (37) can be maintained along the interaction length despite the decline of the beam energy.

For a free-space wave, propagating on axis $k_{zq} = k_0 = \omega_0/c$, and then from Eq. (33):

$$\theta(z) = k_0[\beta_z^{-1}(z) - 1] - k_w(z), \quad (76)$$

where $k_0 = \omega_0/c$. The synchronism condition $\theta(z) = 0$ defines an energy synchronism condition between the electron beam and the wave for a general case of either a period or a field tapered wiggler:

$$\gamma_r(z) = \sqrt{\frac{1 + \bar{a}_w^2(z)}{1 - [1 + k_w(z)/k_0]^{-2}}} \simeq \sqrt{\frac{1 + \bar{a}_w^2(z)}{2}\frac{k_0}{k_w(z)}}, \quad (77)$$

where we used the identities $\gamma_z = (1 - \beta_z^2)^{-1/2}$ and $\gamma_z = \gamma/(1 + \bar{a}_w^2)^{1/2}$, and the second part simplification of the equation corresponds to the ultrarelativistic beam limit.

Assuming that the electrons are trapped, so that in the presence of the radiation field they stay with energy close to the synchronism energy γ_r, we write

$$\gamma = \gamma_r + \delta\gamma \quad (78)$$

and therefore the connection between the dynamic energy exchange of the electron within the trap $\delta\gamma(z)$ and the detuning parameter relative to the slowing down ponderomotive wave $\theta(z)$ is

$$\theta = \left.\frac{d\theta}{d\gamma}\right|_{\gamma_r} \delta\gamma = -\frac{k_0}{\beta_{zr}^3\gamma_{zr}^2\gamma_r}\delta\gamma \simeq -2k_w(z)\frac{\delta\gamma}{\gamma_r(z)} \quad (79)$$

[the approximate expression is for the ultrarelativistic case where $\beta_{zr} \simeq 1$, $k_w = k_0/(2\gamma_{zr}^2)$]. The synchronism energy $\gamma_r(z)$ is the energy of an electron moving at exact synchronism with the ponderomotive wave phase velocity ("fully trapped").

In the following sections we analyze the dynamic processes of a tightly bunched electron beam trapped in the ponderomotive potential of a uniform or tapered wiggler. Tight bunching of the beam relative to the period of the ponderomotive wave allows determination of the bunching phase relative to the ponderomotive phase and corresponding optimization of superradiant and stimulated-superradiant

processes. However, such tight bunching is hard to obtain in the present technological state of the art.

The tight bunching model presented in the next section can describe quite well recent experiments of TESSA and inverse FEL (IFEL) bunched beam acceleration demonstrated on the Rubicon and Nocibur setups at the Accelerator Test Facility (ATF) at Brookhaven National Laboratory (Tremaine *et al.*, 2011; Sudar *et al.*, 2016) that are described in Sec. VIII.B. Here very tight prebunching was attained using a high intensity 10.6 μm CO_2 laser. In the case of a seed-injected tapered wiggler FEL the tight bunching model is presently only partly relevant for describing the dynamics in the tapered wiggler section. In this case (see Fig. 6), both the coherent radiation field and a bunched e beam are inserted into the tapered wiggler section from the uniform wiggler (linear gain) section. Both SP-SR and ST-SR radiation would have been emitted from the tapered section, if the bunching produced in the uniform wiggler section of the FEL is tight enough. If phase-shifter technology (Ratner *et al.*, 2010; Mak, Curbis, and Werin, 2017) can be harnessed then to adjust the phase of the bunching relative to the radiation field, it could be used to enhance the ST-SR emission process. However, tight bunching is hard to get, and the input field intensity and phase of the bunching are not independently controlled in present day tapered wiggler x-ray FEL facilities, as is necessary for optimizing ST-SR. These, as well as the maintenance of small enough energy spread of the bunched beam when it enters the tapered section, are hard to control in present x-ray FEL facilities. Furthermore, transverse effects, primarily wave diffraction (see Fig. 6), are significant in the long section of the tapered undulator, despite the short wavelength of the radiation: they require extension of the single mode analysis to a multimode formulation or full 2D or 3D solution of Maxwell equations (Chen *et al.*, 2014; Emma and Pellegrini, 2014; Tsai *et al.*, 2018). These limitations are discussed in more detail in Sec. VIII.C. Thus the presented ideal model of the distinct SP-SR and ST-SR radiation extraction schemes serve in this case only for qualitative identification of tapering optimization strategies.

V. FORMULATION OF THE DYNAMICS OF A PERIODICALLY BUNCHED ELECTRON BEAM INTERACTING WITH RADIATION FIELD IN A GENERAL WIGGLER

In this section we extend the analysis of SP-SR and ST-SR in undulator radiation of a periodically bunched beam that was presented in Sec. III based on radiation mode excitation and phasor formulations, and we add the dynamics of the electrons under interaction with the radiation wave. Beyond the qualitative introduction of the pendulum equation in Sec. IV, we develop here master equations for the coupled radiation field and periodically bunched beam.

Solving now for the axial (z coordinate) evolution of the bunched beam in steady state, we assume that the infinite periodically bunched beam is composed of all identical bunches (namely, shot noise and finite pulse effects are neglected). The bunches are tightly bunched, hence they can be modeled as Dirac delta functions [see Appendix C, Eqs. (C1) and (C2)]. They all experience the same force equation and have the same trajectories as macroparticles of charge $Q_b = -eN_b$, and the time interval between two consecutive injected bunches is $T_b \equiv 2\pi/\omega_0$, therefore

$$\mathbf{J}(\mathbf{r},t) = Q_b \mathbf{v}_e(t) f(\mathbf{r}_\perp) \sum_{n=-\infty}^{\infty} \delta[z - z_e(t - nT_b - t_0)], \tag{80}$$

where we use $f(\mathbf{r}_\perp)$ in order to represent a beam of finite transverse distribution, as in Eq. (60).

With these simplifying assumptions, the phasor mode excitation equation (6) can be employed to any harmonic frequency of the radiation emitted by the current (80) for calculating the radiation power (53). As we show in Appendix C, this radiation power expression, combined with the beam energy exchange rate, derived from the force equation on the bunches

$$N_b mc^2 \frac{d\gamma}{dt} = Q_b \mathbf{v} \cdot \mathbf{E}(\mathbf{r},t), \tag{81}$$

results in exact conservation of power exchange between the radiation power $P(z)$ and the beam power $P_e = N_b mc^2(\gamma - 1)/T_b$, so that

$$\frac{dP}{dz} = -\frac{dP_e}{dz}. \tag{82}$$

Quite remarkably, this result is shown in generality for a bunched beam interaction with the radiation field (either external or self-generated by the beam) in any kind of radiation mechanism. It demonstrates the rigor of the mode expansion formulation of Maxwell equation [Eqs. (3)–(5)] and its consistency with the simplified bunched beam dynamics model.

The excitation equation for interaction of a tightly bunched periodic beam [Eq. (80)] interacting in a wiggler is derived in Appendix C [Eq. (C30)] (for simplicity we assume from now on $F_q = 1$):

$$\frac{d\tilde{C}_q(z)}{dz} = -\frac{Q_b \omega_0 \tilde{\boldsymbol{\beta}}_w(z) \cdot \tilde{\boldsymbol{\mathcal{E}}}_q^*(0)}{8\pi \mathcal{P}_q \beta_{zr}} e^{i\varphi_b(z)}, \tag{83}$$

where the beam bunching phase relative to the ponderomotive wave dynamically changes as a function of z because of the tapering and because of the energy change in the nonlinear regime:

$$\varphi_b(z) = \int_0^z \left(\frac{\omega_0}{v_z(z')} - k_w(z') - k_{zq} \right) dz' + \varphi_{b0}. \tag{84}$$

We define the dynamic detuning parameter, consistent with Eq. (33) (Gover, 2005a)

$$\theta(z) \equiv \frac{d\varphi_b}{dz} = \frac{\omega_0}{v_z(z)} - k_w(z) - k_{zq}. \tag{85}$$

The rate of change of the bunches energy is found in generality based on Appendix C by substituting

$$\mathbf{E}(\mathbf{r}, t_e(z)) = \mathrm{Re}[\tilde{C}_q(z) \tilde{\boldsymbol{\mathcal{E}}}(\mathbf{r}_\perp) e^{-i\int_0^z [\omega_0/v_z(z') - k_z] dz' - i\varphi_{b0}}], \tag{86}$$

and (C24) in Eq. (C15), which for a thin beam ($\mathbf{r}_\perp = \mathbf{0}$) results in

$$mc^2\frac{d\gamma}{dz} = \frac{1}{2\beta_{zr}}(-e)\eta_p|\tilde{\boldsymbol{\beta}}_w||\tilde{\boldsymbol{\mathcal{E}}}_q(0)||\tilde{C}_q(z)|\cos[\varphi_{qb}(z)], \tag{87}$$

where

$$\varphi_{qb}(z) = \varphi_q(z) - \varphi_b(z). \tag{88}$$

It is evident that the rate of beam energy change (87) depends both on the amplitude of the field $|\tilde{C}_q(z)|$ and on the z-dependent relative phase $\varphi_{qb}(z)$, which is the dynamic phase of the radiation field relative to the bunching current [consistent with Eq. (70)]. The phase $\varphi_b(z)$ is defined in Eq. (C29) and $\varphi_q(z)$ is the z-dependent phase of the radiation complex amplitude, so that

$$\tilde{C}_q(z) = |\tilde{C}_q(z)|e^{i\varphi_q(z)}. \tag{89}$$

The polarization match factor η_p is defined by

$$\eta_p = \frac{|\tilde{\boldsymbol{\beta}}_w^* \cdot \tilde{\boldsymbol{\mathcal{E}}}_q(0)|}{|\tilde{\boldsymbol{\beta}}_w||\tilde{\boldsymbol{\mathcal{E}}}_q(0)|}. \tag{90}$$

It is useful at this point to redefine the interaction coordinate z-dependent varying phase of the ponderomotive wave relative to the varying phase of the bunches as

$$\psi \equiv \varphi_{qb}(z) + \pi/2 = \psi(0) + [\varphi_q(z) - \varphi_q(0)] - \int_0^z \theta(z')dz', \tag{91}$$

so that $\psi(0) = \varphi_{qb0} + \pi/2$, where $\varphi_{qb0} = \varphi_{q0} - \varphi_{b0}$ is the phase of the radiation mode relative to the bunching at $z = 0$ [see Eq. (70)]. The $\pi/2$ phase shift corresponds to relating the bunches to the phase of the radiation vector potential or the ponderomotive wave potential, rather than to the electric field phase $\varphi_q(z)$ ($\tilde{\mathbf{E}} = -i\omega\tilde{\mathbf{A}}$).

Since at present we confine the analysis to interaction with a single mode, we simplify the notation for the field amplitude:

$$\tilde{E}(z) = \tilde{C}_q(z)|\tilde{\boldsymbol{\mathcal{E}}}_q(0)|, \tag{92}$$

where $\tilde{E}(z)$ is the complex radiation field amplitude on and along the beam axis. This results in, similarly to KMR (Kroll, Morton, and Rosenbluth, 1981), the following coupled beam and wave equations:

$$\frac{d\gamma}{dz} = -a|\tilde{E}(z)|\sin\psi, \tag{93}$$

$$\frac{d\tilde{E}(z)}{dz} = be^{i\varphi_b(z)} = ibe^{i[\varphi_q(z)-\psi]}, \tag{94}$$

where

$$a = \frac{e\eta_p}{2\beta_{zr}\gamma_r mc^2}\bar{a}_w(z), \tag{95}$$

$$b = \frac{|Q_b|\omega_0\eta_p\bar{a}_w(z)|\tilde{\boldsymbol{\mathcal{E}}}_q(0)|^2}{8\pi\mathcal{P}_q\beta_{zr}\gamma_r} = \frac{I\eta_p\bar{a}_w(z)Z_q}{2A_{em\,q}\beta_{zr}\gamma_r}, \tag{96}$$

where we used $|\tilde{\boldsymbol{\beta}}_w| = \bar{a}_w(z)/\gamma$, $|Q_b| = eN_b$ and I is the current. Here $\psi(z)$ [Eq. (91)] is the phase of the bunch relative to the vector potential of the wave $\mathbf{A}(t)$ (or relative to the electric field of the wave with $\pi/2$ phase shift), and $\varphi_q(z)$ is the phase of the radiation wave (89) that may also change dynamically due to the interaction.

The complex equation (94) can be broken into two equations for the modulus and the phase of the radiation mode:

$$\frac{d|\tilde{E}|}{dz} = b\sin\psi, \tag{97}$$

$$\frac{d\varphi_q}{dz} = \frac{b}{|\tilde{E}|}\cos\psi. \tag{98}$$

The detailed solution of the problem includes an iterative calculation of the beam energy (γ) [Eq. (93)] and the radiation mode amplitude $|\tilde{E}|$ [Eq. (97)] that are coupled to each other through the phase $\psi(z)$ [Eq. (91)] and the definition of the detuning parameter $\theta(z)$ [Eqs. (78) and (79)].

Note that only the initial phase of the mode relative to the bunching $\varphi_{qb0} = \varphi_q(0) - \varphi_b(0)$ is required for the determination of the initial condition $\psi(0) = \varphi_{qb0} + \pi/2$. After the solution of the two coupled equations [Eqs. (91) and (97)] the phase variation of the mode can always be calculated by integration of Eq. (98)

$$\varphi_q(z) = \phi_q(0) + \int_0^z \frac{b}{|\tilde{E}(z')|}\cos\psi(z')dz'. \tag{99}$$

A. Uniform wiggler

In this section we specify to a uniform wiggler, and therefore γ_r [see Eq. (77)] is independent of z, so that

$$\frac{d\theta}{dz} = -\frac{k_0}{\beta_{zr}^3\gamma_{zr}^2\gamma_r}\frac{d\delta\gamma}{dz} = -\frac{k_0}{\beta_{zr}^3\gamma_{zr}^2\gamma_r}\frac{d\gamma}{dz}. \tag{100}$$

The total power of the electron beam can be expressed as

$$P_{el} = \frac{1}{T_b}N_b mc^2(\gamma - 1) \simeq \frac{1}{T_b}N_b mc^2\gamma, \tag{101}$$

and using $\gamma = \gamma_r + \delta\gamma$, it is written as

$$\begin{aligned} P_{el} &= \frac{1}{T_b}N_b mc^2\gamma \\ &= \frac{1}{T_b}N_b mc^2(\gamma_r + \delta\gamma) \\ &= \frac{1}{T_b}N_b mc^2\left(\gamma_r - \frac{\beta_{zr}^3\gamma_{zr}^2\gamma_r}{k_0}\theta\right). \end{aligned} \tag{102}$$

Using Eq. (100), the energy equation (93) can be written in terms of the detuning parameter:

$$\frac{d\theta}{dz} = K_s^2(z)\sin\psi, \tag{103}$$

where

$$K_s^2(z) = \frac{k_0 e\eta_p}{2\beta_{zr}^4\gamma_{zr}^2\gamma_r^2 mc^2}\bar{a}_w|\tilde{E}(z)| \tag{104}$$

is the synchrotron oscillation wave number.

We summarize here the equations to be solved in terms of $\theta(z)$ or $\delta\gamma(z)$:

$$\frac{d|\tilde{E}|}{dz} = b\sin\psi, \tag{105}$$

$$\frac{d\theta}{dz} = K_s^2(z)\sin\psi \quad \text{or} \quad \frac{d\delta\gamma}{dz} = -\frac{\beta_{zr}^3\gamma_{zr}^2\gamma_r}{k_0}K_s^2(z)\sin\psi, \tag{106}$$

$$\frac{d\psi}{dz} = -\theta + \frac{b}{|\tilde{E}|}\cos\psi \quad \text{or} \quad \frac{d\psi}{dz} = \frac{k_0}{\beta_{zr}^3\gamma_{zr}^2\gamma_r}\delta\gamma + \frac{b}{|\tilde{E}|}\cos\psi. \tag{107}$$

Equations (98) and (107) seem to be singular for the special case of $\tilde{E}(0) = 0$, corresponding to a case of spontaneous emission and self-interaction of the e-beam bunch train with its own generated radiation. As explained in Sec. VI.G, this singularity is removable, and the formulation is valid also for the case of spontaneous emission and self-interaction.

Note that in the case in which $\tilde{E}(z) \simeq$ const these equations reduce to regular pendulum equations for the bunches (see Appendix A).

B. Tapered wiggler

In the case of a tapered wiggler, the synchronism energy γ_r is a function of z [Eq. (77)]. Using Eqs. (78) and (79), one obtains for the dynamics of the detuning parameter:

$$\begin{aligned}\frac{d\theta}{dz} &= -\frac{k_0}{\beta_{zr}^3\gamma_{zr}^2\gamma_r}\left[\frac{d\gamma}{dz} - \frac{d\gamma_r}{dz}\right] - \delta\gamma\frac{d}{dz}\left[\frac{k_0}{\beta_{zr}^3\gamma_{zr}^2\gamma_r}\right] \\ &\simeq -\frac{k_0}{\beta_{zr}^3\gamma_{zr}^2\gamma_r}\left[\frac{d\gamma}{dz} - \frac{d\gamma_r}{dz}\right],\end{aligned} \tag{108}$$

where the last equality is obtained by assuming that the energy tapering rate is slow relative to the synchrotron oscillation dynamics near synchronism, hence neglecting the second term in Eq. (108). Using Eq. (87) we obtain

$$\frac{d\theta}{dz} = K_s^2(z)\sin\psi + \frac{k_0}{\beta_{zr}^3\gamma_{zr}^2\gamma_r}\frac{d\gamma_r}{dz}. \tag{109}$$

Hence Eqs. (105)–(107) remain unchanged, except for Eq. (106) which becomes

$$\frac{d\theta}{dz} = K_s^2(z)\left[\sin\psi + \frac{k_0}{\beta_{zr}^3\gamma_{zr}^2\gamma_r K_s^2}\frac{d\gamma_r}{dz}\right]. \tag{110}$$

The second term in Eq. (110) adds a slope to the pendulum equation potential, and if this slope is too large then there cannot be trapped trajectories. This puts a limit on the tapering strength, so that the absolute value of the term which adds to $\sin\psi$ in Eq. (110) must be smaller than 1, and therefore it is useful to define it as

$$\sin\psi_r \equiv -\frac{k_0}{\beta_{zr}^3\gamma_{zr}^2\gamma_r K_s^2}\frac{d\gamma_r}{dz}. \tag{111}$$

With the simplifying assumptions β_{zr}, $\eta_p = 1$ and using Eq. (104) with $|\tilde{E}(z)| = E = \text{const}$, the tapering resonant phase can be expressed as

$$\sin\psi_r \equiv -2\frac{mc^2}{eE}\frac{\gamma_r}{\bar{a}_w}\frac{d\gamma_r}{dz}. \tag{112}$$

Hence we need only to add a term to Eq. (106) and we rewrite here the master equations for the tapering case

$$\frac{d|\tilde{E}|}{dz} = b\sin\psi, \tag{113}$$

$$\begin{aligned}\frac{d\theta}{dz} &= K_s^2(z)[\sin\psi - \sin\psi_r] \quad \text{or} \\ \frac{d\delta\gamma}{dz} &= -\frac{\beta_{zr}^3\gamma_{zr}^2\gamma_r}{k_0}K_s^2(z)[\sin\psi - \sin\psi_r],\end{aligned} \tag{114}$$

$$\frac{d\psi}{dz} = -\theta + \frac{b}{|\tilde{E}|}\cos\psi \quad \text{or} \quad \frac{d\psi}{dz} = \frac{k_0}{\beta_{zr}^3\gamma_{zr}^2\gamma_r}\delta\gamma + \frac{b}{|\tilde{E}|}\cos\psi. \tag{115}$$

In a radiation emitting wiggler (as opposed to an accelerator scheme) (Musumeci, Pellegrini, and Rosenzweig, 2005), the electrons lose energy; hence one will usually design $d\gamma_r/dz < 0$, so that $0 < \psi_r < \pi/2$.

Except for Eq. (106) that is replaced by Eq. (114), the other master equations to be solved are unchanged, but note that the coefficients of $|\tilde{E}|$ in Eq. (104) [$\gamma_r(z)$, $\gamma_{zr}(z)$, $\beta_{zr}(z)$, and $\bar{a}_w(z)$] are z dependent in the case of tapering, and so is the parameter b [Eq. (96)] if $\bar{a}_w = \bar{a}_w(z)$.

The power of the electron bunches is still given by Eq. (102), but here γ_r is a function of z; therefore the kinetic power exchanged is composed of the contribution of the tapered deceleration of the trap (first term) plus the contribution of the dynamics of the bunch within the trap (second term):

$$\begin{aligned}\frac{dP_{el}}{dz} &= \frac{N_b}{T_b}mc^2\frac{d\gamma}{dt} = \frac{1}{T_b}N_b mc^2\frac{\beta_{zr}^3\gamma_{zr}^2\gamma_r}{k_0}\left[\frac{k_0}{\beta_{zr}^3\gamma_{zr}^2\gamma_r}\frac{d\gamma_r}{dz} - \frac{d\theta}{dz}\right] \\ &= -\frac{1}{T_b}N_b mc^2\frac{\beta_{zr}^3\gamma_{zr}^2\gamma_r}{k_0}\left[K_s^2\sin\psi_r + \frac{d\theta}{dz}\right].\end{aligned} \tag{116}$$

VI. ANALYSIS OF THE INTERACTION DYNAMICS OF A BUNCHED ELECTRON BEAM WITH RADIATION IN THE TRAPPING REGIME

A. The fundamental radiation processes in phase space

We analyze in this section the phase-space dynamics of the bunched electron beam that come out of the solution of the coupled equations of Sec. V and relate them to the fundamental coherent spontaneous radiation emission processes presented in Secs. II and III. Qualitatively, we expect specific phase-space dynamic processes as depicted in Figs. 7 and 8. For a uniform wiggler the trap height in the $\theta-\psi$ plane is $2\theta_m = 4K_s$ [see Appendix A, Fig. 29 and Eq. (A5)]. The generalization for a tapered wiggler is $2\theta_m = 4K_s\sqrt{\cos\psi_r + (\psi_r - \pi/2)\sin\psi_r}$ [see Appendix A, Fig. 31 and Eq. (A13)].

Using Eq. (104) for K_s^2 and the connection between θ and $\delta\gamma$ in Eq. (79) one finds $\delta\gamma_m$ at the wiggler's entrance:

$$\delta\gamma_m = \sqrt{2\frac{e\eta_p\beta_{zr}^2\gamma_{zr}^2\bar{a}_w E(0)}{mc^2k_0}}\sqrt{\cos\psi_r + (\psi_r - \pi/2)\sin\psi_r}$$
$$\simeq \sqrt{\frac{e\eta_p\bar{a}_w E(0)}{mc^2k_w}}\sqrt{\cos\psi_r + (\psi_r - \pi/2)\sin\psi_r} \qquad (117)$$

and the second part simplification of the equation corresponds to the ultrarelativistic beam limit.

In Sec. VI.B we formulate a normalized version of the bunched beam–radiation coupled equations, and in the subsequent sections we demonstrate the phase-space evolution dynamics of these processes in a uniform and tapered wiggler, by presenting the z dependent numerical computation solutions of the normalized coupled mode equations and via the linked video displays [see the Supplemental Material (207)].

B. Simulation of the dynamics and radiation of a perfectly periodically bunched beam in the saturation regime

To demonstrate the fundamental dynamic processes of SP-SR and ST-SR in a uniform and tapered wiggler, described in the previous section, we present simulation results and video displays based on the numerical solution of the master equations (105)–(107) and for the case of a tapered wiggler (113)–(115) that we normalized in Appendix D. The normalized equations (D2)–(D9) can be solved for a general case of wiggler amplitude and period tapering with arbitrary varying beam parameters: $\bar{a}_w(z)$, $\gamma_r(z)$, and $\sin\psi_r(z)$, and for general initial conditions of the bunches and the radiation $\psi(0)$, $\theta(0)$, and $|\tilde{E}(0)|$. The development of the radiation wave power and

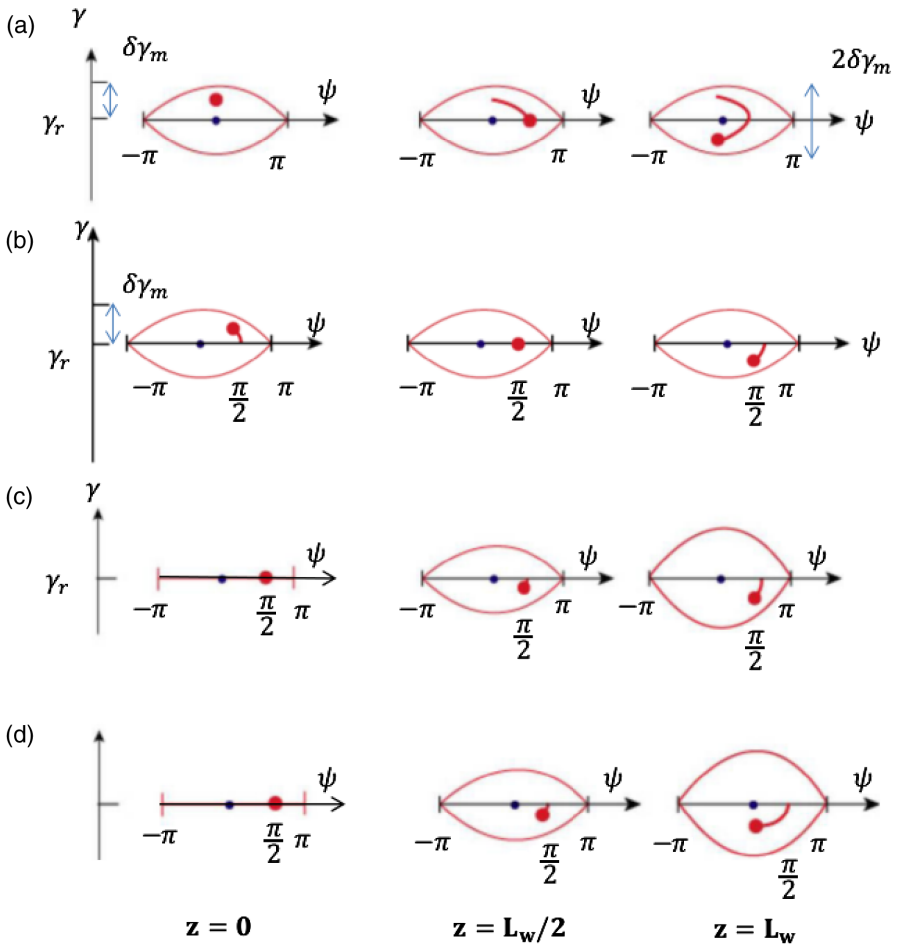

FIG. 7. SP-SR and ST-SR phase-space diagrams of trap dynamics for a uniform wiggler: (a) trapped bunch—maximum energy extraction, (b) zeroth-order ST-SR—high gain, (c) superradiance SP-SR, and (d) saturated superradiance (self-interaction).

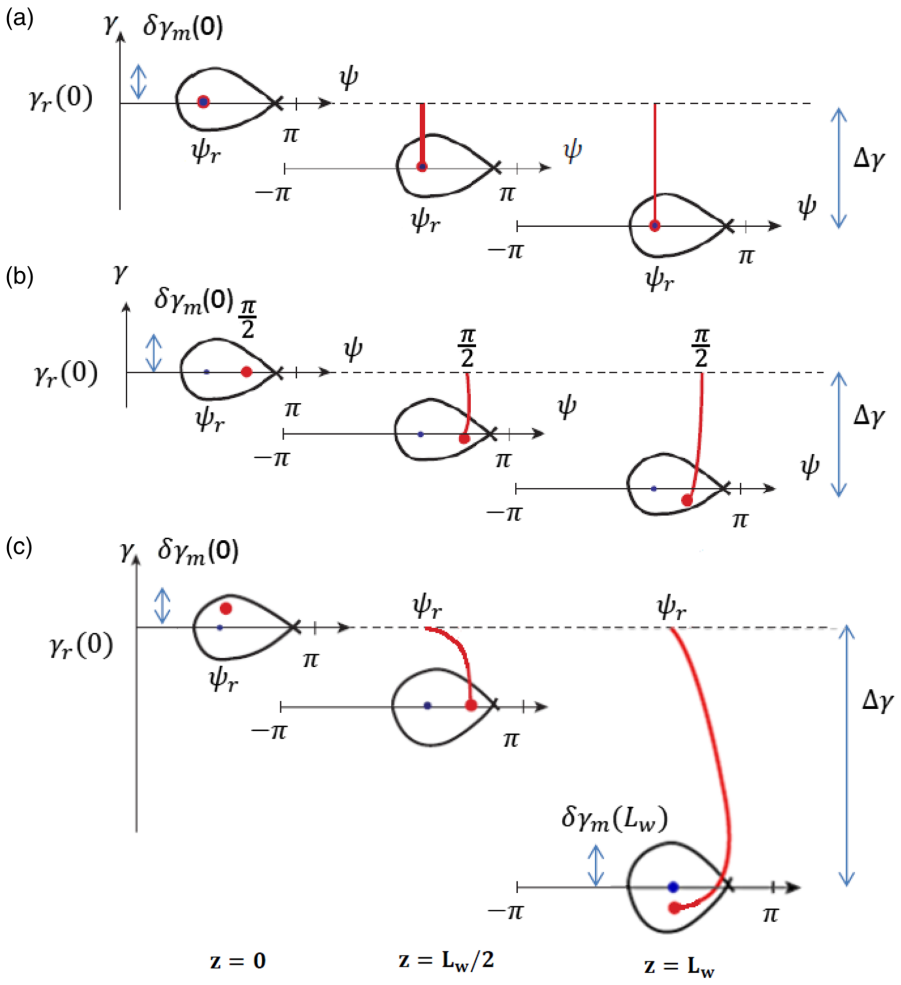

FIG. 8. TES and TESSA phase-space diagrams of trap dynamics for a tapered wiggler: (a) TES (resonant trapping), (b) TESSA (maximum gain), and (c) TESSA (maximum energy extraction).

the beam power along the interaction length are then calculated explicitly from Eqs. (D12)–(D14).

In the absence of tapering and in the case of linear tapering ($\psi_r = \text{const}$), and also assuming moderate variation of the wiggler parameters along the interaction length, we can set the coefficients $f_B(u)$, $f_K(u) \simeq \text{const}$ [Eqs. (D8) and (D9)]. We use this model in the following computations for the purpose of illustrating the interaction processes discussed in the previous sections. In this case, the general equations (113)–(115) are cast into a simple compact form for the normalized field $\bar{E} \equiv |\tilde{E}|/b(0)L_w$, the phase ψ, and the normalized detuning parameter $\bar{\theta} \equiv \theta L_w$, in terms of a normalized interaction length $u = z/L_w$:

$$\frac{d\bar{E}}{du} = \sin\psi, \tag{118}$$

$$\frac{d\bar{\theta}}{du} = K_{s0}^2 \bar{E}[\sin\psi - \sin\psi_r], \tag{119}$$

$$\frac{d\psi}{du} = -\bar{\theta} + \frac{1}{\bar{E}}\cos\psi. \tag{120}$$

Remarkably, only one parameter K_{s0}^2 [Eq. (D7)] is required in addition to the initial conditions in order to solve the closed-form equations (118)–(120) as a function of the normalized axial coordinate u, and display its trajectories in the normalized phase space $(\bar{\theta}, \psi)$. Other laboratory parameters are needed only to calculate of the power exchange [see Appendix D, Eqs. (D12)–(D14)]:

$$\bar{P}_{em} = \bar{E}^2(u), \tag{121}$$

$$\Delta\bar{P}_{\text{el}} = \Delta\bar{P}_{\text{tap}} + \Delta\bar{P}_{\text{dyn}}, \tag{122}$$

where

$$\Delta\bar{P}_{\text{tap}} = -2\int_0^u \bar{E}(u')\sin\psi_r(u')du', \tag{123}$$

$$\Delta\bar{P}_{\text{dyn}} = -2[\bar{\theta}(u) - \bar{\theta}(0)]/K_{s0}^2, \tag{124}$$

where all overbar power parameters are normalized $\bar{P} = P/P_{\text{REF}}$, P_{REF} being defined in Eq. (D13) is

$$P_{\text{REF}} = \frac{1}{16\pi^2}\frac{\eta_p^2 \bar{a}_w^2(0)}{\beta_{zr}^2(0)\gamma_r^2(0)}\frac{Q_b^2\omega_0^2 L_w^2 Z_q}{A_{em\,q}}. \tag{125}$$

Under the simplifying assumptions leading to Eqs. (118)–(120) we arrive at the conclusion [Eq. (122)] that the electron energy loss is a sum of contributions due to the tapering ($\Delta P_{\rm tap}$) and the inner trap dynamics ($\Delta P_{\rm dyn}$).

In the following simulations (Figs. 9–12 and five videos [see the Supplemental Material (207)] we use a numerical value $K_{s0}^2 = 1.59$ (see Appendix D). This parameter (corresponding to the Nocibur experiment) (Sudar *et al.*, 2016) is sufficient for the $\bar{\theta} - \psi$ trajectories display. In order to display the $\gamma - \psi$ phase-space trajectories, we use in the following examples in Eq. (79) the laboratory parameters $\gamma_r = 127.2$, $N_w = L_w/\lambda_w = 11$ (Sudar *et al.*, 2016) assuming idealized tight bunching and moderate tapering.

C. Untrapped trajectories in a uniform wiggler

In order to show the consistency of the normalized nonlinear equations with the earlier results of SP-SR and ST-SR in the zero-order approximation of Secs. II and III [Eqs. (67) and (68)], we set $\psi_r = 0$ in Eq. (119), and for an untrapped electron we consider $\bar{\theta}$ to be almost constant, i.e., $\bar{\theta}(u) \simeq \bar{\theta}(0)$.

Expressing Eq. (94) in terms of the normalized parameters $u \equiv z/L_w$, $\bar{\theta} \equiv \theta L_w$, [using Eq. (91)], and defining $\tilde{E} \equiv \bar{E}e^{i\varphi_q} = (|\tilde{E}|/bL_w)e^{i\varphi_q}$, one obtains

$$\frac{d\tilde{E}}{du} = e^{i\varphi_b}. \tag{126}$$

Using the definition of φ_b from Eq. (C29) or (85), with $\bar{\theta}(u) \simeq \bar{\theta}(0)$, we obtain

$$\varphi_b \simeq \bar{\theta}(0)u + \varphi_{b0}. \tag{127}$$

Integrating Eq. (126) we obtain

$$\tilde{E}(u) = \tilde{E}(0) + ue^{i[\varphi_{b0}+\bar{\theta}(0)u/2]}\,\mathrm{sinc}[\bar{\theta}(0)u/2]. \tag{128}$$

With $\tilde{E}(0) = |\tilde{E}(0)|e^{i\varphi_q(0)}$, one gets

$$|\tilde{E}(u)|^2 = |\tilde{E}(0)|^2 + u^2\mathrm{sinc}^2[\bar{\theta}(0)u/2] + 2u|\tilde{E}(0)|\,\mathrm{sinc}[\bar{\theta}(0)u/2]\cos[\varphi_{qb0} - \bar{\theta}(0)u/2], \tag{129}$$

and using the definition of ψ in Eq. (91), it can also be written as

$$P_{em}/P_{\rm REF} = |\tilde{E}(u)|^2 = |\tilde{E}(0)|^2 + u^2\mathrm{sinc}^2[\bar{\theta}(0)u/2] + 2u|\tilde{E}(0)|\,\mathrm{sinc}[\bar{\theta}(0)u/2]\,\sin[\psi(0) - \bar{\theta}(0)u/2]. \tag{130}$$

This represents the normalized output power with full correspondence to the zero-order approximate expressions (66)–(68) derived in Sec. III for superradiance (SP-SR) (quadratic term) and stimulated superradiance (ST-SR) (linear term), respectively.

D. Maximal energy extraction from a bunched beam in a uniform wiggler

In Fig. 9 and the Supplemental Material (207) we display the dynamics of the electron beam in the case of maximal energy extraction from a bunched beam [Fig. 7(a)], which corresponds to the case of maximum power extraction from a perfectly bunched beam in a saturated FEL. Maximal energy extraction from the e beam ($2\delta\gamma_m$) is attained when the bunch enters the trap at phase $\psi(0) = 0$ with energy detuning $\delta\gamma(0) \simeq \delta\gamma_m$ and winds up at the end of the interaction length at the bottom of the trap $\delta\gamma(L_w) \simeq -\delta\gamma_m$, after performing half a period of synchrotron oscillation. Note that in this case of maximal extraction, the initial gain is null: $d\delta\gamma/dz|_{z=0} = 0$ [Eq. (105)] and the radiation buildup starts slow [quadratically as in Eq. (25)]; see Fig. 9(b).

E. Stimulated superradiance in a uniform wiggler

Of special interest is the stimulated superradiance [Fig. 7(b)] where maximum initial gain is expected when starting from $\delta\gamma(0) \simeq 0$ and $\psi(0) = \pi/2$. The simulation result of this case is shown in Fig. 10 and the Supplemental Material (207).

Note that direct differentiation of Eqs. (121), (122), and (124) results in

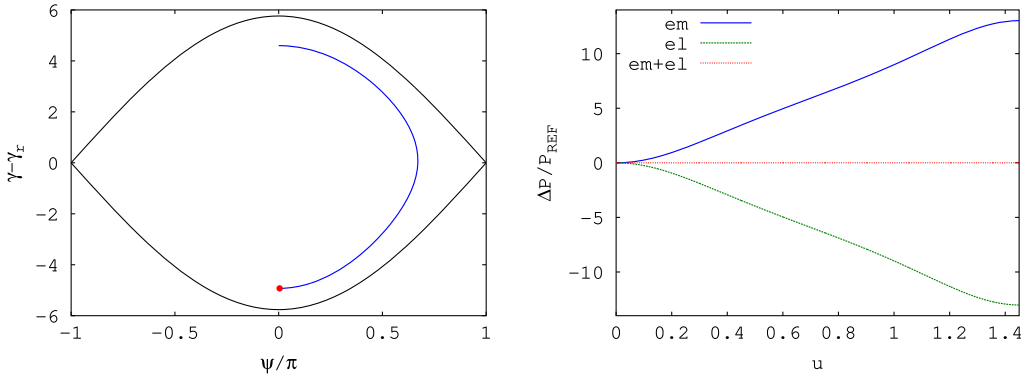

FIG. 9. Maximal energy extraction of a perfectly bunched beam in a uniform wiggler trap. Left panel: The phase-space diagram $\gamma - \gamma_r$, where the black line shows the separatrix at the end of the trajectory. Right panel: The radiation power change, the electron beam power change, and their sum, which stays at 0. See the Supplemental Material (207).

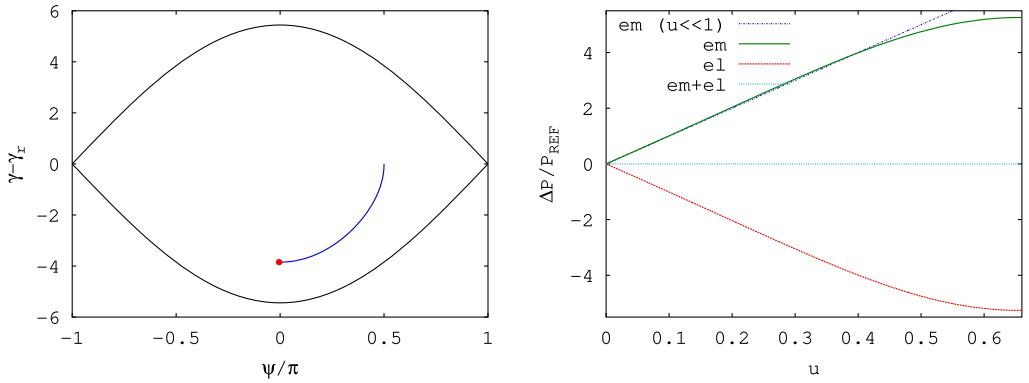

FIG. 10. Stimulated superradiance in a uniform wiggler with maximum gain bunching phase $\psi(0) = \pi/2$. Left panel: The phase-space diagram $\gamma - \gamma_r$, where the black line shows the separatrix at the end of the trajectory. Right panel: The radiation power change, the electron beam power change, and their sum, which stays at 0. The broken line shows the initially linear radiation power growth as in Eq. (132). See the Supplemental Material (207).

$$\frac{1}{P_{\mathrm{REF}}}\frac{dP_{em}}{du} = -\frac{1}{P_{\mathrm{REF}}}\frac{dP_{\mathrm{el}}}{du} = 2\bar{E}(u)\frac{d\bar{E}(u)}{du} = 2\bar{E}(u)\sin\psi(u) \tag{131}$$

and therefore the initial power growth (in a range $0 < u \ll 1$) is proportional to u (see the tangent dash-dotted line in Fig. 10, right panel):

$$\Delta P_{em} = -\Delta P_{\mathrm{el}} = 2P_{\mathrm{REF}}\bar{E}(0)u\sin\psi(0). \tag{132}$$

This is exactly consistent with the zero-order approximation of ST-SR power growth [Eq. (68)]. Also it is evident that the maximum initial gain is attained with $\psi(0) = \pi/2$.

In second order in u, the integration of Eq. (118) results in $\bar{E}(u) = \bar{E}(0) + u\sin\psi(0)$ and consequently from the integration of Eq. (131) or directly from the definition (121):

$$\begin{aligned}\Delta P_{em}/P_{\mathrm{REF}} &= \bar{E}^2(u) - \bar{E}^2(0) \\ &= 2u\bar{E}(0)\sin\psi(0) + u^2\sin^2\psi(0).\end{aligned} \tag{133}$$

We conclude that the initial emission process is always composed of both contributions of ST-SR (first term) and SP-SR (second term). When the field is strong enough $\bar{E}(0) \gg u\sin\psi(0)/2$ then the ST-SR term is dominant and the power starts growing linearly as in Fig. 10(b).

F. Tapered wiggler

As shown in Fig. 8, in case of a tapered wiggler, the main contribution to the radiated power extraction from the e beam comes usually from the tapering process, but there is contribution also from the phase-space evolution of synchrotron oscillation dynamics inside the decelerating trap. If the bunch is deeply trapped [$\psi(0) = \psi_r$, $\delta\gamma(0) = 0$] [Fig. 8(a)] the beam energy drops only with the trap deceleration. When the trapped bunch is not at the bottom of the trap potential as is the case in Fig. 8(b) [$\psi(0) = \pi/2$, $\delta\gamma(0) = 0$] and Fig. 8(c) [$\psi(0) = 0$, $\delta\gamma(0) = \delta\gamma_m(0)$], there is also contribution of the inner-trap synchrotron oscillation dynamics to the beam energy total drop. Maximal energy extraction is attained in the case of Fig. 8(c); however, the initial energy drop rate is zero in this case [$\psi(0) = \psi_r$] and is maximal in the case of Fig. 8(b) [$\psi(0) = \pi/2$]. This may play a role in optimal tapering and bunch phasing strategy.

In Fig. 11 and the Supplemental Material (207), we show a bunch initially trapped in the middle of the trap [at $\psi(0) = \psi_r$], and $\theta(0) = 0$ [i.e., $\gamma(0) - \gamma_r(0) = 0$] for normalized parameters example of initial input field $\bar{E}(0) = 2$, using $\psi_r = \pi/4$. Figure 11, left panel, shows the phase-space diagram ψ, $\gamma - \gamma_r(0)$ in which the upper black line shows the separatrix at the beginning of the trajectory and the lower black line shows the separatrix at the end of the trajectory. This shift in the separatrix location is due to the tapering and gives the major contribution to the e-beam power decrement (deceleration). Figure 11, right panel, shows the radiation power incremental growth (blue), the electron beam power decrement (green), and the sum of radiation and e-beam power increments which stays at 0. To get a better insight into the different phenomena, we show separately the contributions of the tapering ($\Delta P_{\mathrm{el}(\gamma_r)}$) (light blue) and the synchrotron oscillation dynamics ($\Delta P_{\mathrm{el}(\delta\gamma)}$) (red) to the total beam power drop (ΔP_{el}) (green); see Eq. (122). The tapering contribution here is around 9 times bigger than the synchrotron oscillation dynamics contribution.

Figure 12 [see Supplemental Material (207)] shows the same as Fig. 11, only the initial bunch phase is at $\psi(0) = \pi/2$, instead of ψ_r. We find that in this case the contribution of the tapering to the total e-beam power loss is still dominant, but less, being around 2.6 times bigger than the synchrotron oscillation dynamics contribution. This is due to the fact that the synchrotron oscillation contribution increased significantly in the case of $\psi(0) = \pi/2$, relative to the case $\psi(0) = \psi_r = \pi/4$. Therefore, the total radiation power enhancement is bigger in this case by 30% over the case of $\psi(0) = \psi_r = \pi/4$.

We draw attention to the initial power growth rate Eqs. (131)–(133) that were derived without the use of the ψ_r dependent Eq. (119), and therefore are also valid for the tapered wiggler case $\psi_r \neq 0$. To better illustrate the role of the tapering and inner trap dynamics, as well as the spontaneous superradiance and stimulated-superradiance processes

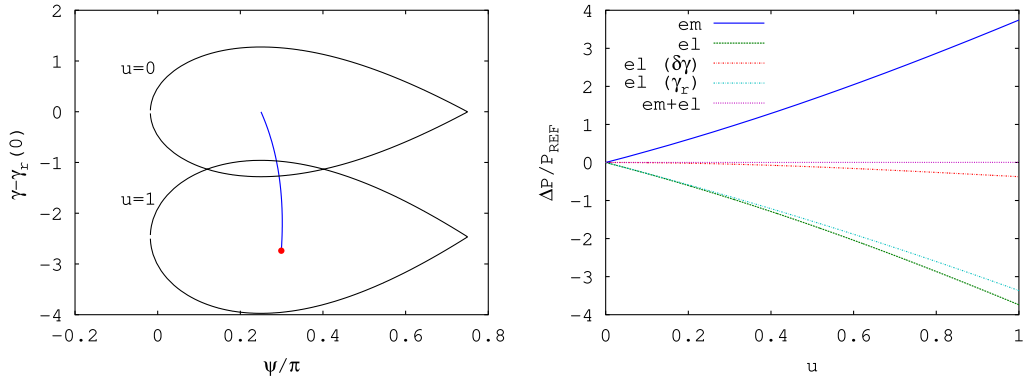

FIG. 11. Tapering-enhanced superradiance (TESSA) of a perfectly bunched beam starting at the bottom of the trap $\delta\gamma(0)=0$, $\psi(0)=\psi_r$. Left panel: The phase-space diagram ψ, $\gamma-\gamma_r(0)$, where the upper black line shows the separatrix at the beginning of the trajectory ($u=0$) and the lower black line shows the separatrix at the end of the trajectory ($u=1$). Right panel: The radiation power change, the electron beam power change, and their sum which stays at 0. We show separately the contributions of the tapering ($\Delta P_{\mathrm{el}(\gamma_r)}$) and the synchrotron oscillation dynamics ($\Delta P_{\mathrm{el}(\delta\gamma)}$) to the total beam power drop (ΔP_{el}). See the Supplemental Material (207).

in the initial interaction stage $u \ll 1$, it helps to rewrite Eq. (133) (that is valid also for a tapered wiggler $\sin\psi_r \neq 0$) in the following form:

$$\Delta P_{em}/P_{\mathrm{REF}} = 2u\bar{E}(0)\sin\psi_r + \{2u\bar{E}(0)[\sin\psi(0)-\sin\psi_r] + u^2\sin^2\psi(0)\}. \tag{134}$$

In Eq. (134) the terms in brackets (linear and square in u) represent the effect of the dynamics inside the trap (synchrotron oscillations): ST-SR (linear) and SP-SR (quadratic) processes. The first term (linear) is the effect of tapering [see Eq. (123)].

We therefore also conclude that in the tapering case, the highest gain is attained for initial phasing $\psi(0)=\pi/2$, a factor of $\sqrt{2}$ relative to the case of deep trapping $\psi(0)=\psi_r=\pi/4$ shown in Fig. 11.

However, the case of $\psi(0)=\psi_r$ is also important in practice, because the trapping is deeper, and it may be a preferred strategy for the case of imperfect bunching, where trapping efficiency is an issue (see Sec. VII). For $\psi(0)=\psi_r$ Eq. (134) reduces to

$$\Delta P_{em}/P_{\mathrm{REF}} = 2u\bar{E}(0)\sin\psi_r + u^2\sin^2\psi_r. \tag{135}$$

G. Superradiance and self-interaction

Of special interest is the case of pure superradiance where the radiation grows spontaneously in a uniform wiggler without any input field [$\bar{E}(0)=0$] [Fig. 7(c)]. If the built-up radiation grows up enough, the beam may saturate by its own radiation [Fig. 7(d)].

The second term in Eq. (133) is independent of $\bar{E}(0)$ and for $\bar{E}(0)=0$ it results in $\Delta P_{em}/P_{\mathrm{REF}} = u^2\sin^2\psi(0)$. The phase $\psi(0)$ is ill defined because the null radiation field has arbitrary phase. This is the reason for the seeming singularities in Eqs. (98) and (107) that can be removed only when $\psi(0)=\pi/2$. The physical explanation for this particular determination of the radiation phase is that in the absence of the initial radiation phase, the phase of the excited radiation mode is determined by the phase of the bunched beam φ_{b0}, as can be seen [Eqs. (63), (64), and (92)] by setting $z=\delta z \ll 2\pi/\theta$:

$$\tilde{E}(\delta z) = 0^+ + |\tilde{E}|e^{i\varphi_{b0}}. \tag{136}$$

Setting then $\varphi_q(0)=\varphi_{b0}$, and using Eqs. (C29) and (70), i.e., $\varphi(0)=\varphi_{b0}$, we get from the definition (91) $\psi(0)=\pi/2$ and therefore,

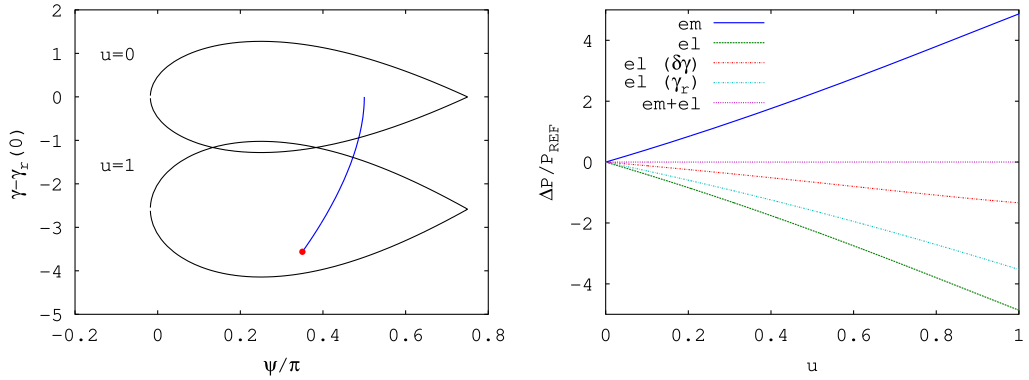

FIG. 12. TESSA radiation extraction by a perfectly bunched beam, phased initially at $\psi(0)=\pi/2$ for maximal initial radiation growth rate (gain). Note that the total radiation emission power in this case is 30% higher than in the case of $\psi(0)=\psi_r$ (Fig. 11). See the Supplemental Material (207).

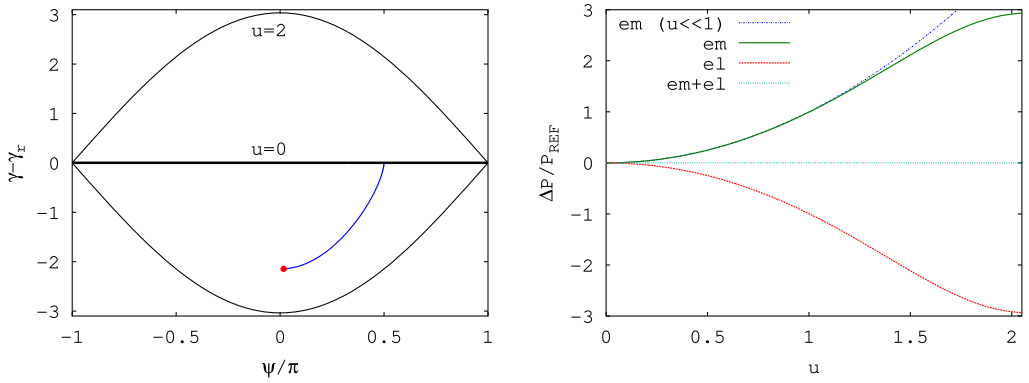

FIG. 13. Saturated self-interaction superradiance in a uniform wiggler. Left panel: The phase-space diagram $\gamma - \gamma_r$, where the thick middle black line shows the nonexistent separatrix at the beginning of the trajectory ($u = 0$) and the upper and lower black lines show the separatrix at the end of the trajectory ($u = 2$). Right panel: The radiation power change, the electron beam power change, and their sum which stays at 0. See the Supplemental Material (207).

$$P_{em}/P_{\mathrm{REF}} = u^2. \tag{137}$$

This is evidently a normalized parameters representation of the case of superradiance, where the power grows quadratically from 0 with the interaction length z; see Eq. (67).

In Fig. 13 and the Supplemental Material (207) we show the trajectories and power growth of the prebunched beam radiation in a uniform wiggler, starting from the zero input field. The quadratic approximation (137) is also shown in Fig. 13 by the dash-dotted line and matches well the power growth rate.

This case of radiation emission by the beam in a uniform wiggler when $\tilde{E}(0) = 0$ is of special interest. Although in the derivation of the quadratic growth of superradiance [Eq. (67)] it was assumed that the beam energy does not change, in the present energy-conserving nonlinear model we see that in the more complete energy-conserving analysis, the beam energy goes down as expected, in correspondence with the superradiant power growth. This case can be related to the problem of radiation emission due to charged particles acceleration in free space. In that case, the energy loss of the particle due to its radiation emission is explained in terms of the Abraham-Lorentz effective radiation reaction force that can be derived only indirectly from energy conservation considerations (Dirac, 1938; Wheeler and Feynman, 1945; Schwinger, 1949; Ianconescu and Horwitz, 1992, 2002, 2003; Gupta and Padmanabhan, 1998).

In contrast to the free-space self-interaction case, in the present case of periodic bunched beam radiation emission into a transversely confined single mode, the self-interaction problem is explicitly soluble. As seen in Fig. 13, the spontaneous emission of the undulator radiation field grows from 0 (at $u = 0$) with a distinct phase, so that the tight bunches are found initially automatically at phase $\psi(0) = \pi/2$ relative to the ponderomotive wave bucket. This happens to be exactly the phase of maximum stimulated superradiance, where the bunched beam experiences maximum deceleration by the electric field of the radiation mode that it had excited. Further tracing of the beam dynamics, as shown in Fig. 13, the periodic beam self-interacts with its own radiation and slows down, reaching a nonlinear self-absorption saturation regime at long interaction length u, and even can be reaccelerated after the maximal deceleration point $u = 2$, reabsorbing the radiation that is generated in the first part of the undulator.

Figure 14 displays an even more interesting case of tapering-enhanced superradiance (TES), showing that in the nonlinear regime, a periodically bunched beam that is trapped in its own generated radiation trap as in Fig. 13 can exhibit further enhanced radiation emission if the undulator becomes tapered after a long enough section of trap buildup along a uniform undulator section. In Fig. 14 and the Supplemental Material (207) the uniform undulator in the section $0 < u < 0.5$ turns adiabatically at $u = 0.5$ into a tapered undulator with $\psi_r = \pi/4$, extracting further beam energy in the tapered section $0.5 < u < 2$.

Note that contrary to the Abraham-Lorentz case of free-space emission into a continuum of modes and frequencies, here we consider emission into a single mode, and because the beam is infinitely periodically bunched, there is no issue of slippage effect. Note that a similar "self-interaction" nonlinear superradiance process has been predicted also with a single bunch interaction with a wave-guided THz beam in a tapered wiggler under conditions of zero slippage attained due to the wave-guide dispersion (Snively *et al.*, 2019). These schemes of self-interaction may have a practical advantage in development of future short wavelength radiation sources because they are not susceptible to jitter problems between the beam bunch (bunches) and the seed radiation, since the electrons are trapped in the tapered section at the right phase of the coherent radiation generated by themselves.

VII. TAPERED WIGGLER FEL WITH PREBUNCHED ELECTRON BEAM OF FINITE DISTRIBUTION

The ideal tight bunching model presented in the previous sections is good for identifying the fundamental processes of superradiance and stimulated superradiance in a tapered wiggler FEL. At the present state of the art of technology it is hard to satisfy the tight bunching condition $\sigma_{tb} n \omega_0 \ll 1$ required for attaining a nondiminishing bunching factor (58) and for taking advantage of bunch phasing optimization of inner-trap stimulated-superradiance dynamics [Eq. (132),

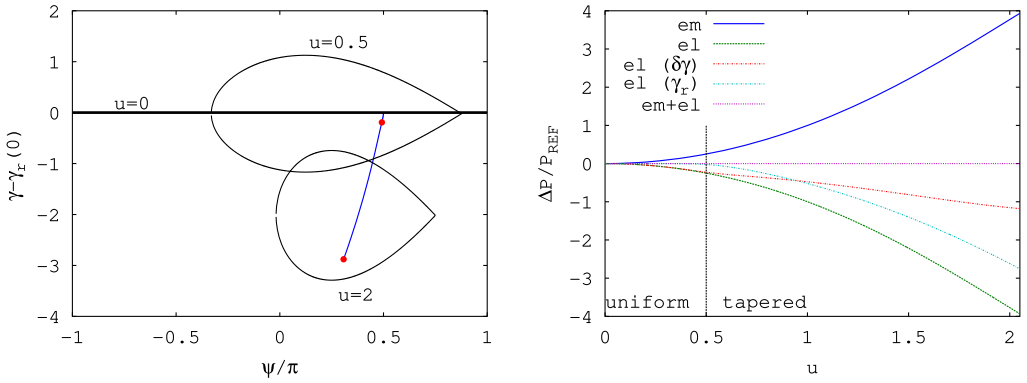

FIG. 14. Self-interaction tapering-enhanced superradiance (TES). Left panel: The phase-space diagram $\gamma - \gamma_r(0)$, where the thick horizontal black line shows the nonexistent separatrix at the beginning of the trajectory ($u = 0$), the upper "eye" separatrix shows the self-interaction built-up trap at the transition of the uniform wiggler into a tapered wiggler at $u = 0.5$ and the lower separatrix at the end of the trajectory ($u = 2$). Right panel: The radiation power change (em), the electron beam power change due to internal trap dynamics ($\delta\gamma$) and due to tapering (γ_r), and their sum (el). The sum of the generated radiation power (em) and the negative beam power increment (el) is null, keeping energy conservation. See the Supplemental Material (207).

Fig. 10] which is valid only in the tight bunch model. Short wavelength bunching techniques involve high harmonic energy modulation of a beam subjected to high-power IR lasers in a wiggler as in HGHG (Yu, 1991; L. Yu *et al.*, 2000), EEHG (Jia, 2008; Stupakov, 2009; Qika, 2017), and PEHG (Feng *et al.*, 2014). The energy bunching turns into tight density bunching when passed through a dispersive magnetic element (chicane) (Sudar, Musumeci, and Duris, 2017). However, obtaining significant harmonic current components at short wavelengths is still a challenging technical task. Furthermore, the model assumption of a cold beam often does not hold, and, in particular, in the case of efficiency enhancement in the postsaturation tapered wiggler section of a seeded FEL, the beam energy spread σ_γ is as large as the trap height $\delta\gamma_m$. However, a new concept of "fresh-bunch" input signal injection (where the first bunch is used to generate the modulation power and then discarded while a second bunch is overlapped with the seed) (Ben-Zvi, Yang, and Yu, 1992; Emma, Feng *et al.*, 2017; Emma, Lutman *et al.*, 2017) and further technological developments may make it possible to get closer to the ideal conditions of our model. We mention that the fresh-bunch technique can be applied to two different slices of the same electron bunch, in which case it is sometimes termed "fresh slice" (Lutman *et al.*, 2016; Emma, Lutman *et al.*, 2017). The cases discussed in Allaria *et al.* (2012) and the Shanghai deep-ultraviolet FEL tests (Zhao and Wang, 2016) are fresh-bunch results for HGHG schemes, and they also apply there the same principle (suppressing or enhancing lasing for different parts of the bunch in different portions of the undulator).

In this section we present a more general model for efficiency enhanced radiation emission in a FEL with energy spread and phase distribution of the prebunched beam and compare the simulation results to the case of no bunching at all.

Following the analysis by Emma, Sudar *et al.* (2017) we redefine the interpretation of Eqs. (93), (118), and (120) to correspond to individual electrons in the particle distribution of each bunch. We present the single radiation mode excitation (6) in terms of the absolute value of its transverse electric field on axis (92):

$$E(z) = |\tilde{C}_q(z)||\tilde{\boldsymbol{\mathcal{E}}}_q(\mathbf{r}_\perp(0))|. \tag{138}$$

These equations for the electron phase $\psi_j(z)$, energy $\gamma_i(z)$, and radiation field $E(z)$ are then recast correspondingly to the following:

$$\frac{d\psi_j}{dz} = k_w\left(1 - \frac{\gamma_j^2}{\gamma_r^2}\right), \tag{139}$$

$$\frac{d\gamma_j}{dz} = -\frac{\bar{a}_w eE}{\gamma_j mc^2}\sin\psi_j, \tag{140}$$

$$\frac{dE}{dz} = \chi\bar{a}_w\left\langle\frac{\sin\psi_j}{\gamma_j}\right\rangle, \tag{141}$$

with $\chi = Z_0 I/2A_{emq}$, $\bar{a}_w = e\bar{B}_w/mck_w$ is the undulator parameter [Eq. (30)], and $\gamma_r^2 = (1 + \bar{a}_w^2)k/2k_w$ [Eq. (77)] is the resonant energy.

In this transformation we used the relativistic beam approximation $\gamma_j \gg 1$, and used the definition of the normalization power in terms of the effective mode cross-section area [Eq. (8)] in the definitions of the parameters a and b [Eqs. (95) and (96)].

In the resonant particle approximation the efficiency can be written as

$$\eta(z) = \frac{1}{\gamma_0}\left|\sum_i \gamma_i(z) - \gamma_{i,0}\right| \simeq f_t\left|\frac{\gamma_r(z) - \gamma_0}{\gamma_0}\right| = f_t\left|\frac{\Delta\gamma_r}{\gamma_0}\right|, \tag{142}$$

where f_t is the fraction of trapped electrons which in general depends on the size of the bucket, i.e., the input seed power, the undulator field, and the resonant phase. We assume for simplicity that the trapping fraction is independent of z in the postsaturation regime. Different initial conditions for tapered

FELs result in different trapping fractions and different scaling of the output efficiency. Note that as we discuss in Sec. VIII.C, the assumption of the constant trapping fraction breaks down for long undulators due to diffraction and time-dependent effects as evidenced in 3D simulations (Emma *et al.*, 2016).

Integrating Eqs. (139)–(141) as shown by Emma, Sudar *et al.* (2017) we have an approximation for the power extraction efficiency for $\psi_j = \psi_r = \text{const}$:

$$\eta(z) = f_t \frac{e}{\gamma_0 mc^2}\left(E_0 \frac{\bar{a}_w(0)}{\gamma_0} z \sin\psi_r + \frac{f_t \chi}{2}\frac{\bar{a}_w^2(0)}{\gamma_0^2} z^2 \sin^2\psi_r\right) \tag{143}$$

and with $P_{\text{rad}}(z) = P_0 + \eta(z) P_{\text{beam}}$, after rearranging the constants we have [compare with Eq. (135)]

$$\begin{aligned} P_{\text{rad}}(z) &= P_0 + E_0 \frac{\bar{a}_w(0)}{\gamma_0} f_t I z \sin\psi_r \\ &\quad + \frac{Z_0}{4A_{em\,q}}\left(\frac{\bar{a}_w(0)}{\gamma_0}\right)^2 (f_t I z \sin\psi_r)^2 \\ &\equiv P_0 + P_{\text{TAPER}} + P_{\text{SR}}, \end{aligned} \tag{144}$$

where the seed field is given by $E_0 = \sqrt{Z_0 P_0 / A_{em\,q}}$. Equation (144) is identical to the normalized equation (135), after multiplication by the normalizing power P_{REF} [Eq. (D13)], and using $f_t = 1$. We also remark that in the ideal case of perfect bunching (Sec. VI) f_t can be either 0 or 1, so in case it is 1 (fully trapped bunch), instead of choosing initial phase $\psi(0) = \psi_r$, which is meant to maximize f_t, one would rather choose $\psi(0) = \pi/2$ [cf. Figs. 11 and 12 and discussion before Eq. (135)].

In the absence of an input seed we recover the familiar scaling for coherent emission from a bunched beam $P_{\text{rad}}(z) = P_{\text{SR}}(z) \propto (f_t I z)^2$ (Saldin, Schneidmiller, and Yurkov, 2005). This is also true for long undulators since the quadratic term P_{SR} dominates the radiation power scaling if the undulator length L_w satisfies

$$L_w \gg 10^6 \frac{\gamma_0}{\bar{a}_w(0)} \frac{\sqrt{A_{em\,q}}[\mu\text{m}]}{I[\text{kA}]} \frac{\sqrt{P[\text{MW}]}}{\sin\psi_r}.$$

At the same time for short undulators and intense seed pulses, the efficiency and output power are linearly proportional to the undulator length and the field strength. This is the low gain TESSA regime (Duris, Murokh, and Musumeci, 2015) discussed in the previous sections. We apply the power scaling law to a tapered FEL amplifier in two different scenarios: starting from a large seed with an unbunched and a prebunched electron beam (Emma, Sudar *et al.*, 2017).

The analytic power estimate from Eq. (144) is in good agreement with numerical integration of the 1D FEL equations (Emma, Sudar *et al.*, 2017). The scaling highlights the trade-off between fast energy extraction (large ψ_r) and large trapping fraction (small ψ_r), with the optimal value around $\psi_r \simeq 40°$, compared to $\psi_r = 90°$ which emerged from the single particle picture. This estimate recovers the well-known result of Brau and Cooper (1980) in the low gain (constant P_{rad}) high efficiency FEL in which the optimal resonant phase is also $\psi_r \simeq 40°$ for a cold beam with $f_t = f_b$. This occurs because the efficiency in the low and high gain cases scales as $\eta \propto f_t \sin\psi_r$ and $\eta \propto (f_t \sin\psi_r)^2$, respectively, and hence is maximized at the same value of ψ_r.

A. Scaling laws of tapering-enhanced superradiance and stimulated superradiance

It is instructive at this point to compare and distinguish the scaling laws of radiation emission derived in different parts of this review. The general nonlinear interaction regime was analyzed numerically and graphically for a tightly bunched beam in Sec. VII. However, examination of the initial power growth scaling, by first and second order expansion in terms of the axial propagation parameter $u = z/L_W$, provided insight into the different coherent spontaneous and stimulated-superradiance processes in a uniform and in a tapered undulator. We can now compare these scaling laws to the ones derived for a finite distribution beam [Eq. (144)].

In the ideal case of a cold tightly bunched beam [$\sigma_{tb} \ll 1/n\omega_0$, see Eq. (28)], the initial phase of the bunches $\psi(0)$ [Eq. (91)] is well defined, and the radiation power increment is given in terms of a linear term $2u\bar{E}(0)\sin\psi(0)$ and a quadratic term $u^2 \sin^2\psi(0)$ [Eq. (133)]. The linear term is due to the ST-SR radiation emission process and is maximized when $\psi(0) = \pi/2$; it represents the ST-SR in the high gain initial stage of a synchrotron oscillation process of a tight bunch in a built-up trap. The quadratic term is due to the SP-SR radiation emission process. It exists whether there is an input field $\bar{E}(0)$ or not. In the latter case [$\bar{E}(0) = 0$], the bunches determine the radiation field and its phase $\psi(0) = \pi/2$. The radiation fields and the trap bucket grow slowly ($\propto u^2$) around the bunch that eventually interacts with its self-generated radiation and saturates in a synchrotron oscillation process (Sec. VI.G).

Remarkably, Eq. (133) and the two terms of ST-SR (linear in u) and SP-SR (quadratic in u) also exist in the case of tapering, but here, for linear tapering, an additional energy extraction term, linear with u, is added in Eq. (134) $2u\bar{E}(0)\sin\psi_r$. The ST-SR term $2u\bar{E}(0)[\sin\psi(0) - \sin\psi_r]$ corresponds to the start of a synchrotron oscillation process around central phase ψ_r in a decelerating and somewhat shrunk trap, and the SP-SR term $u^2 \sin^2\psi(0)$ stays the same. In the case of $\psi(0) = \psi_r$, the synchrotron oscillation stimulated emission process diminishes and one is left only with a linear term due to tapering and a quadratic term due to SP-SR [Eq. (135)].

The extension to the finite distribution case Eq. (144) is fully consistent with Eq. (135) for the most practical case, where only a fraction f_t of the electrons in the beam gets trapped. The main consideration then for optimizing power extraction is maximizing f_t. It is then optimal to choose $\psi(0) \simeq \psi_r$. In this case one abandons any contribution from the synchrotron oscillation dynamic process and remains only with the linear term due to the tapering and the quadratic term due to SP-SR [second and third terms in Eq. (144)] that are proportional to $f_t I z$ and $(f_t I z)^2$, respectively.

The scaling of the term P_{TAPER} and P_{SR} in Eq. (144) in the TESSA interaction is the same as the scaling of the ST-SR [Eq. (72)] and SP-SR [Eq. (71)] expressions in the uniform

undulator with factors of $\sin\psi_r$ and $\sin^2\psi_r$, respectively. Similarly to Eq. (73), the ratio between the terms is

$$\frac{P_{\mathrm{TAPER}}}{P_{\mathrm{SR}}} = \frac{4A_{em\,q}E_0}{Z_0[\bar{a}_w(0)/\gamma_0]f_t I z \sin\psi_r}. \tag{145}$$

For a short interaction length the tapering power extraction P_{TAPER} is dominant if a strong input radiation field is exercised.

B. Unbunched beam

Even though prebunching is desirable, quite significant tapered wiggler energy extraction from an unbunched beam is possible if the slanted traps still capture enough particles.

Starting from a large seed with a cold unbunched beam, the trapping fraction is a function of the resonant phase only. It can therefore be approximated by the bucket width

$$f_t = f_b = \frac{\psi_2 - \psi_1}{2\pi}$$

(see Fig. 15, left) with $\psi_{1,2}$ the solutions of the equations

$$\psi_2 = \pi - \psi_r, \tag{146}$$

$$\cos\psi_1 + \psi_1 \sin\psi_r = \cos\psi_2 + \psi_2 \sin\psi_r \tag{147}$$

(see Appendix A, Fig. 31).

C. Bunched beam

From Eq. (144) for the power estimate, we can see that increasing the trapping fraction greatly increases the output power for the same resonant phase $P_{\mathrm{rad}}(z) \propto P_{\mathrm{SR}}(z) \propto f_t^2$. Figure 15 (right two panels) shows the significantly enhanced trapping fraction of particles trapped in the bucket with a prebunched electron beam considering also the effect of energy spread $\sigma_{\gamma 0}$ and the modulation strength

$$A \equiv \Delta\gamma_{\mathrm{mod}}/\sigma_{\gamma 0}, \tag{148}$$

where A is the modulation parameter, defined in Appendix B [Eq. (B6)]. Figure 15 shows the trapping fraction f_t computed for examples of a one-stage or two-stage prebuncher setup similar to that discussed by Sudar, Musumeci, and Duris (2017). Note that in the context of Fig. 15 it was assumed that the strength of the wiggler and the intensity of the radiation wave field are the same in the modulation and tapered wiggler sections, so that $\Delta\gamma_{\mathrm{mod}} = \delta\gamma_m$, where $\delta\gamma_m$ is given in Eq. (117). In the more general case these may be independent controllable parameters.

Experimental results demonstrating very high energy extraction from a prebunched electron beam in a tapered undulator have recently been reported by Sudar *et al.* (2016), and are discussed in Sec. VIII.B. The trapping fraction in this case is not only a function of the resonant phase but also of the initial laser seed power which sets the prebunching modulation strength A. Figure 16 displays comparison of [from Emma, Sudar *et al.* (2017)] the trapping fraction without prebunching to the analytic fit of the trapping fraction $f_t = f_t(\psi_r, A)$ for optimal buncher settings in a single or double buncher configuration (Sudar *et al.*, 2018) with a bucket height 10–30 times larger than the initial electron energy spread. The advantage of prebunching is clear in the increasing trapping fraction for both the single and double buncher cases at modest modulation strengths $A \sim 10$. As discussed in more detail by Emma, Sudar *et al.* (2017) the main challenge in this scheme is to generate the seed laser power capable to induce an $A = 10$ modulation which could be achieved, for example, in a fresh bunch configuration (Ben-Zvi, Yang, and Yu, 1992; Emma, Feng *et al.*, 2017; Emma, Lutman *et al.*, 2017).

Our analysis of the 1D physics of high gain–high efficiency tapered FELs, including the effects of energy spread and bunching, displays the advantage of prebunching in a high efficiency FEL due to the increased particle trapping in the postsaturation region. Prebunching not only increases the peak efficiency but exhibits optimal energy extraction at larger resonant phase compared to the unbunched case. This faster

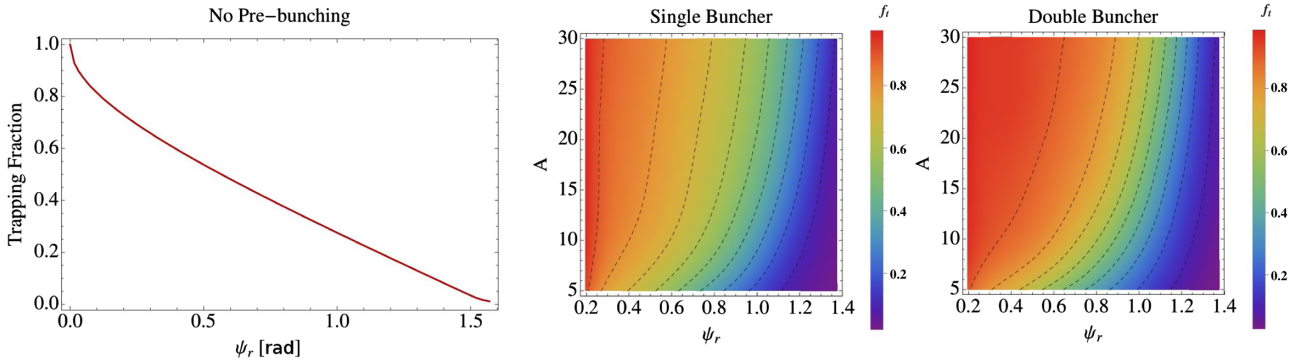

FIG. 15. Left: Trapping fraction for a cold unbunched beam and a large input seed, approximately given by the bucket width. Middle and right: The trapping fraction f_t as a function of the modulation parameter $A \equiv \Delta\gamma_{\mathrm{mod}}/\sigma_{\gamma 0}$ [see Eq. (148)] and the resonant phase ψ_r for a (middle) single buncher and a (right) double buncher (Sudar, Musumeci, and Duris, 2017; Sudar *et al.*, 2018). The broken lines are polynomial fitting curves of $f_t(\psi_r, A) = \mathrm{const}$. The color coded diagrams of f_t as a function of ψ_r and A were computed for the single and double buncher examples (Sudar, Musumeci, and Duris, 2017). The trapping fraction obtained with prebunching is larger than in the unbunched case. The advantage of the double buncher compared to the single buncher scheme is largest for large modulation parameter $A > 10$ and $\psi_r < \pi/4$. Adapted from Emma, Sudar *et al.*, 2017.

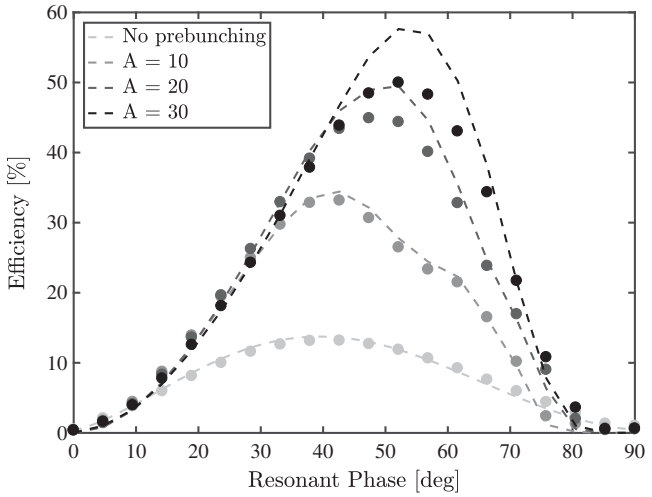

FIG. 16. Analytic estimate of the power extraction efficiency based on Eq. (B13) and on simulation [solution of Eqs. (139)–(141)] (dots) without prebunching and for three different values of the modulation strength A. The advantage of prebunching is clear in both the larger maximum efficiency and the peak efficiency occurring at larger resonant phase, allowing faster energy extraction. From Emma, Sudar *et al.*, 2017.

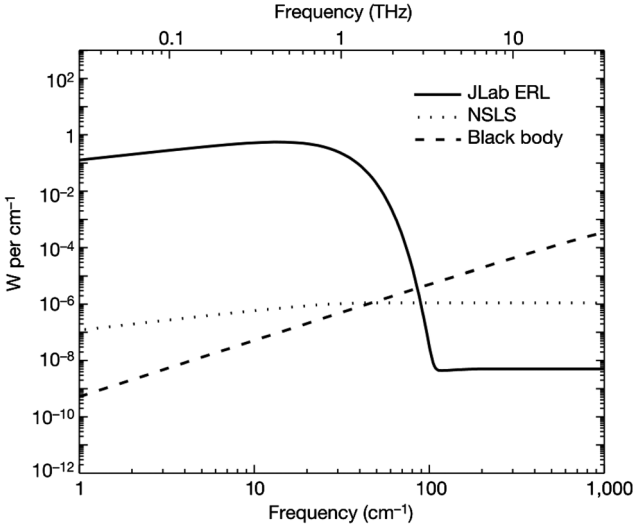

FIG. 17. Average power from multiple single-bunch superradiant (CSR) emission of wide bandwidth THz radiation in an ERL accelerator. An enhancement of the spontaneous emission radiation spectral power takes place at low frequencies due to superradiant CSR. From Carr *et al.*, 2002.

extraction of energy is important for reducing harmful 3D effects, specifically diffraction due to reduced optical guiding in tapered FELs with long undulators. Having a prebunched electron beam also allows more aggressive (larger resonant phase) tapered FEL designs, damping the time-dependent parasitic effects of the sideband instability (see Sec. VIII.C.2 (Kroll and Rosenbluth, 1980; Kroll, Morton, and Rosenbluth, 1981)), which can limit the output efficiency.

VIII. APPLICATIONS

A. Superradiant coherent radiation sources

A straightforward application of superradiance is in developing THz superradiant sources. This is quite expected, because the electron beam bunches generated in a common photocathode gun of modern rf linacs have a bunch duration of $\sigma_{tb} < 1$ ps. Consequently, a bunching factor of $M_b \simeq 1$ is attainable for radiation frequencies in the range of $f < 1$ THz.

Figure 17 shows an experimental demonstration of the transition of radiation power from spontaneous emission $\propto N$ [Eq. (19)] to superradiant emission $\propto N^2$ [Eq. (20)] that takes place with the cutoff condition $\omega\sigma_{tb} \simeq 1$. In this experiment, carried out at the Jefferson Lab energy retrieval linac (ERL) FEL (Carr *et al.*, 2002), a record high frequency-integrated THz power (20 W) was measured due to repetitive single bunch superradiant CSR emission from a bending magnet. The THz radiation was generated from a continuous stream of electron beam microbunches of duration 0.5 ps, circulating in a superconducting ERL at a repetition rate of 75 MHz. Figure 17 shows more than 7 orders of magnitude enhancement in the spectral power at the superradiance regime relative to the spontaneous emission regime. This corresponds to the large enhancement by a factor of N, which is the number of electrons in each bunch [Eq. (20)].

There are numerous SR experiments world-wide pursued or planned, mainly in the THz spectral regime (Ciocci *et al.*, 1993; Gover *et al.*, 1994, 2005; Faatz *et al.*, 2001; Shibata, Sasaki, and Ishi, 2002; Korbly *et al.*, 2005; Shin *et al.*, 2007; Yasuda *et al.*, 2008; Huang, 2010; Hama *et al.*, 2011; Ginzburg *et al.*, 2013; Huang *et al.*, 2015; Lurie, Friedman, and Pinhasi, 2015; Su *et al.*, 2018). More than 20 experiments of SR THz sources based on either undulator, CTR, or bending magnets (CSR or edge radiation) are listed in Gensch *et al.* (2013). We review several representative THz radiation facilities based on superradiance and refer the interested reader to review articles on this subject (Gensch *et al.*, 2013; Asgekar *et al.*, 2014; Green *et al.*, 2016). An example is the TELBE (Terahertzstrahlung Elektronen Linearbeschleuniger für strahlen hoher Brillanz und niedriger Emittanz) facility located in Helmholtz-Zentrum Dresden-Rossendorf (HZDR), shown schematically in Fig. 18 (Green *et al.*, 2016). This facility is based on superradiant enhancement of radiation from relativistic electron bunches in a compact superconducting linear accelerator. This prototype source generates high-field THz pulses at quasicontinuous-wave repetition rates up to the MHz regime and exceeds the power of state-of-the-art laser-based sources by more than 2 orders of magnitude.

Other facilities in design are the Ferninfrarot Linac Und Test Experiment (FLUTE) (Nasse *et al.*, 2013) located at the Karlsruhe Institute of Technology and the Photo Injector Test facility at Zeuthen (PITZ) (Boonpornprasert *et al.*, 2014) at Deutsches Elektronen-Synchrotron (DESY). The first one uses a 2.5 cell normal conducting photocathode rf gun to preaccelerate the electrons to an energy of 7 MeV. This gun was specially designed for very high bunch charge and operates at 2.998 GHz (European S band). This facility is designed to employ coherent synchrotron and edge radiation (CSR and CER) or superradiant coherent transition radiation (CTR).

Another notable planned facility (PITZ) is intended to develop THz radiation generation sources in two complementary

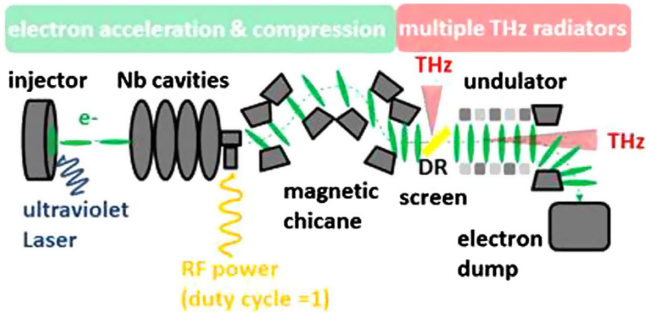

FIG. 18. Electron bunches are extracted from a solid, accelerated to relativistic energies and compressed to sub-ps duration in a compact superconducting radio-frequency linac with a chicane bunch compressor. The electron bunches can emit THz pulses in different types of radiators. At TELBE, repetition rates up to 13 MHz are feasible. THz pulses are generated by a diffraction radiator (DR) and one undulator. From Green *et al.*, 2016.

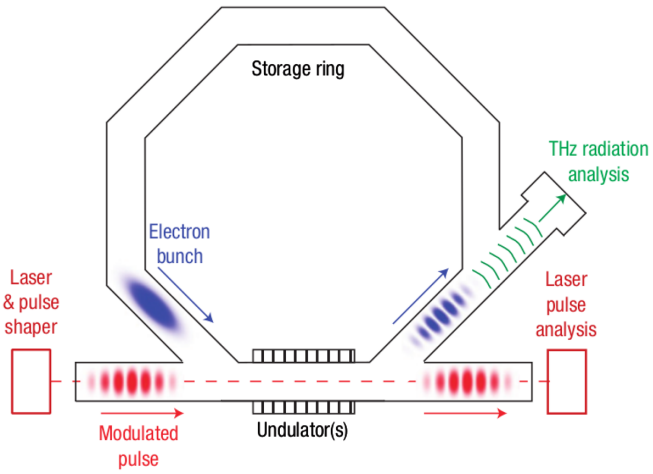

FIG. 19. Superradiant CSR narrow bandwidth THz radiation emission by trains of ps bunches generated in a storage ring by laser modulation in a wiggler. From Bielawski *et al.*, 2008.

schemes: (i) SASE FEL using an undulator and high charge electron bunches and (ii) CTR using an ultrashort electron bunch tightly compressed by a chicane. The SASE radiation is anticipated to cover a radiation short wavelengths range of 20–100 μm while radiation wavelengths above 100 μm for which the bunch duration is shorter than the wavelength will be generated by the superradiant CTR scheme.

A good experimental demonstration of narrow-band coherent THz superradiant emission in an undulator with a finite pulse train of bunches is shown in Fig. 19. Here the relatively long pulses of the UVISOR-II storage ring are periodically modulated in an undulator by a THz modulated laser beam and emit narrow-band superradiant CSR radiation [as in Eq. (48), Fig. 3] at the bending magnet (Bielawski *et al.*, 2008).

Another example of THz superradiance by a periodically bunched finite pulse train was recently demonstrated by Tsinghua University in China (Su *et al.*, 2018). In this scheme a bunch train is created by laser stacking using birefringent α barium borate crystal serials from a Ti:sapphire laser system, an energy chirp is introduced into the electron pulse which is then compressed with a magnetic chicane and entered into a permanent magnet undulator. The resulting narrow bandwidth radiation is tunable in the range of 0.4 to 10 THz.

Under construction in Ariel University is the Israeli THz FEL, a cooperation between Ariel University and Tel Aviv University (Friedman *et al.*, 2014). The device, depicted in Fig. 20, is designed to operate with a compact rf photocathode gun of up to 6.5 MeV. The gun introduces an energy chirp to the beam, thus resulting in a compression of the electron pulse. The compressed pulse then enters into a 2 cm period 80 cm long linear Halbach undulator, generating superradiant radiation at 1–4 THz. Tuning is carried out by varying the electron energy and/or the undulator gap. Another ultrashort (5 mm period) wiggler is under construction for operating in a mode of negative mass effect (Balal *et al.*, 2015; Lurie, Bratman, and Savilov, 2016; Bratman and Lurie, 2018).

The project is planned to be carried out in several phases. In the first phase the FEL will operate in a single bunch superradiance mode [Eq. (40)] with bunches compressed to less than 150 fs, generating 10 ps THz pulses of about 50 kW peak power. In a second phase, the FEL will operate in a periodic prebunching superradiant mode [Eq. (50)]. The THz prebunching will be produced by illuminating the photocathode with two optical beams, generated by splitting the naturally chirped ultrafast laser beam. With proper relative delay, the two beams will produce on the cathode a THz laser beat and thus modulate the emitted electron photocurrent. In a future phase of the project, it is intended to equip the facility with an additional tapered undulator (Duris *et al.*, 2014) in

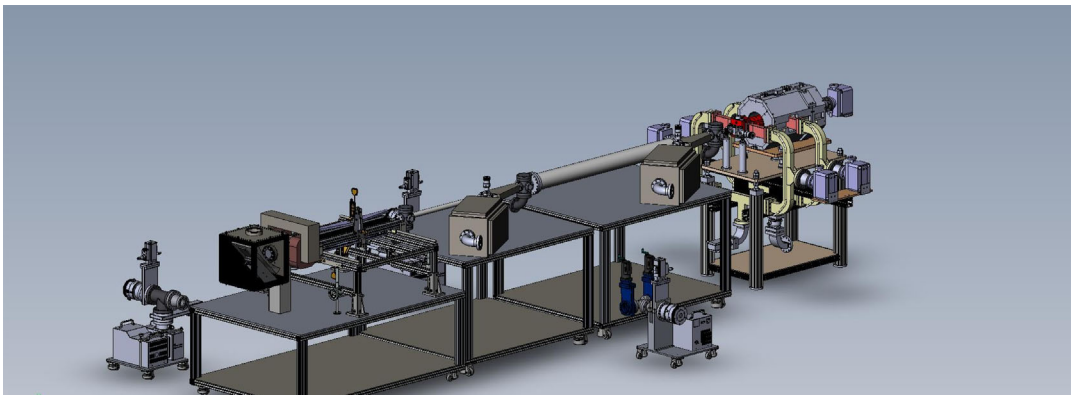

FIG. 20. Layout of the Israeli superradiant THz FEL.

order to demonstrate intense THz radiation in a zero-slippage waveguide TES operating mode (Sec. VI.G) and THz beam acceleration (Snively *et al.*, 2019).

Beside CSR and superradiant undulator radiation mechanisms, there have been numerous demonstrations of superradiant radiation in various radiation emission mechanisms, including CTR (Happek, Blum, and Sievers, 1991; Shibata *et al.*, 1994), diffraction radiation, Cherenkov dielectric structure radiation (Neighbors, Buskirk, and Saglan, 1984; Wiggins *et al.*, 2000) and Smith-Purcell radiation (Brownell, Walsh, and Ducas, 1998; Korbly *et al.*, 2005; Shin *et al.*, 2007; Ginzburg *et al.*, 2013; Bluem *et al.*, 2015). A demonstration of superradiant Smith-Purcell radiation by a finite pulse train of tight bunches was reported by Korbly *et al.* (2005). In this experiment a 100 ns macropulse beam, composed of a 17 GHz train of 1500 microbunches of 0.5 ps from a 15 MeV linac, was passed in proximity to a 1 cm period blazed grating of 10 periods. The experiment demonstrated extremely narrow bandwidth THz radiation at up to the 30th harmonic of the fundamental 17 GHz frequency in a comb pattern characterized by the macrobunching form factor [Eq. (47)]; see Fig. 4.

Superradiant THz sources are being developed in many advanced XUV FEL facilities taking advantage of the coherent radiation emitted by the spent electrons from the FEL undulators before being dumped. Coherent THz beams synchronous with the main XUV output pulses of the FEL are useful for pump-probe experiment applications such as using the high-power THz pulses as a pump in order to modulate structural properties of matter, thereby inducing phase transitions (Adams, 2004). The linear acceleration sections produce naturally THz radiation using dedicated undulators and bending magnets (CSR) in the free-electron laser in Hamburg (FLASH) (Gensch *et al.*, 2008) or a dedicated target foil (CTR) in FLASH (Hoffmann *et al.*, 2011) and FERMI (TeraFERMI (Svetina *et al.*, 2016). The quality of the beam after UV and XUV generation in the FEL is good enough for producing superradiant THz radiation that can be synchronized with some delay with the UV and XUV pulses of the same bunch for pump-probe experiments.

We point out that there are superradiant emission effects (in the narrow and wider sense) also in common IR and FIR FEL oscillators based on photocathode rf linacs,[1] e.g., the CLIO (Centre Laser Infrarouge d'Orsay) FEL in France (Ortega, 1996), the FELBE (Fel Elektronen Linearbeschleuniger für strahlen hoher Brillanz und niedriger Emittanz) in HZDR (Gabriel *et al.*, 2000b), the FELIX (Free Electron Lasers for Infrared eXperiments) (Gabriel *et al.*, 2000a), Radboud University (Zhaunerchyk *et al.*, 2010), and Novosibirsk FEL (Kulipanov *et al.*, 2015). These facilities, operating as FELs in oscillator configuration, provide tunable coherent narrow bandwidth radiation in the THz up to a mm-wavelength range. The rf accelerator bunches in such facilities are in the picosecond scale duration, so that in the shorter wavelength (IR) range of their operation, the pulse duration is longer than the slippage time along the wiggler, and therefore, their operation is primarily in a stimulated emission (laser) mode. However, when operating at the long wavelength range (FIR or THz), they exhibit pronounced slippage effects and superradiance in the wider sense. Even a stimulated-superradiance effect was observed by Zhaunerchyk *et al.* (2010) due to the presence of an intense circulating field in the resonator.

We would be amiss if we did not mention that long wavelength superradiance effects can be observed in synchrotron storage rings. The turn of the electron in the bends of a synchrotron light source generates a wide band radiation with frequencies ranging from zero frequency to the cutoff frequency. It is inevitable that due to the pulsed nature of the electron beam, superradiance would occur at wavelengths longer than the pulse length. The superradiant emission at the synchrotron bending magnets is termed "coherent synchrotron radiation.". The typical spectral range of CSR corresponding to the steady-state bunch duration in synchrotron storage rings is in the microwave to mm-wave range. However, there are numerous demonstrations of CSR emission with synchrotron storage rings also in the THz regime (Abo-Bakr *et al.*, 2002; Byrd *et al.*, 2004; Sannibale *et al.*, 2004; Wang *et al.*, 2006). Billinghurst *et al.* (2013) at the Canadian Light Source reported observation of superradiance at frequencies that were harmonics of the electron beam pulse train. Synchrotron storage rings employ rf frequencies of 500 MHz and lower. Therefore, their circulation bunch lengths, and consequently their CSR wavelength cutoffs, are in the mm-wavelength range (Abo-Bakr *et al.*, 2002). It is still possible to operate such a synchrotron storage ring at THz frequencies in a "burst mode" of fewer circulating bunches (Abo-Bakr *et al.*, 2002) at the expense of instability and a shorter circulating lifetime. Also worth mentioning is that in storage rings it is possible to get THz radiation in dedicated IR beam lines, and this requires a special mode of operation where the bunches are compressed (however, this has a negative effect on the synchrotron ring lifetime). FLUTE (Nasse *et al.*, 2013) used this special regime where the bunch is squeezed longitudinally to the picosecond range, offering THz radiation to its users. Alternatively, stable THz CSR emission can be demonstrated with dedicated storage rings, operating at high (S-band) frequency (Byrd *et al.*, 2004; Wang *et al.*, 2006).

Finally we mention the great interest in extending the concepts of superradiant emission to short wavelengths in the optical to x-ray regime. Several techniques have been proposed for attaining electron beam bunches in the femtosecond (Hommelhoff *et al.*, 2006; Zholents and Zolotorev, 2008; Hilbert *et al.*, 2009; Marceau *et al.*, 2013, 2015; Hoffrogge *et al.*, 2014; Wong *et al.*, 2015) and subfemtosecond range and may be used for optical XUV superradiant sources. Attosecond level bunching has been demonstrated even at the quantum electron wave function level (Feist *et al.*, 2015; Priebe *et al.*, 2017; Kozák, Schönenberger, and Hommelhoff, 2018). Spontaneous and stimulated superradiance have also been considered at the quantum wave function level (Pan and Gover, 2018).

An entire class by itself comprises the schemes of combined bunching and harmonic emission in undulators with ultrafast optical lasers (Appendix B). The interested reader is referred to reports on these processes of HGHG (Yu, 1991; L. Yu *et al.*, 2000), EEHG (Jia, 2008; Stupakov, 2009; Qika, 2017), and PEHG (Feng *et al.*, 2014).

[1]Europe, 2005, "European fel," https://www.fels-of-europe.eu.

B. TESSA and TESSO concepts

This section contains a summary of the recent activities in high extraction efficiency experiments taking advantage of the TESSA process. Using an intense seed pulse in conjunction with prebunched beams it becomes possible to initialize the system in a favorable initial state with particles deeply trapped in the ponderomotive bucket of a tapered undulator.

It is interesting here to note the reciprocal relation between the challenges of radiation emission and the quest for laser-driven accelerators. TESSA can be thought of as the reverse of an inverse free-electron laser accelerator (Palmer, 1972; Courant, Pellegrini, and Zakowicz, 1985) which among other laser-driven schemes has some unique advantages due to the lack of nearby boundaries, structure, or medium to couple the light to the electrons. These result in a direct coupling between an electromagnetic field and a relativistic electron beam with little irreversible losses enabling in principle very high conversion efficiencies. A long history of IFEL experiments (Marshall *et al.*, 1991; Kimura *et al.*, 2001; Musumeci, 2005) was recently followed by experimental results on IFEL (ATF Rubicon experiment) (Duris *et al.*, 2014) and the Lawrence Livermore National Laboratory (LLNL) IFEL experiment (Moody *et al.*, 2016) which showed the advantages of the helical geometry and the possibility to double the energy of a 50 MeV relativistic beam using < 200 GW peak power CO_2 laser and accelerating gradients up to 200 MeV/m. The experience gained over many years in developing a tapered undulator for acceleration purposes gives thanks to the TESSA mechanism direct application in the field of high efficiency coherent radiation sources.

A schematic of a TESSA amplifier is shown in Fig. 21. The strong seed pulse stimulates the emission of a large amount of radiation from prebunched superradiant electron beams. This emission of radiation causes the electrons to quickly lose their energy. If the undulator is tapered in order to maintain the resonant condition and sustain the interaction over long undulator section(s) with strong coupling to the fundamental laser mode, one can achieve very high conversion efficiency.

The scheme differs from a tapered FEL amplifier since using a very high initial intensity and an initially microbunched beam allows trapping the beam into a deep ponderomotive bucket (as oppose to a tapered FEL amplifier where the trapping potential well is always "full to the brim" with particles, see comparison in Fig. 22). A consequence of this important difference in the initial conditions of the system is that the TESSA undulator can be tapered more aggressively (hence the use of strongly tapered helical undulator) before suffering from particle detrapping as is usually the case for tapered FELs. This results in a higher decelerating gradient and energy extraction from the electron beam. Furthermore, the steeper tapering profile and higher radiation gain reduces the degrading effects of diffraction and sideband instability.

In order to better frame the experiments, it is helpful to distinguish two regimes of operation of TESSA.

1. Small gain regime

In this regime the electromagnetic radiation is assumed to be nearly constant along the interaction. In this case the amplifier behaves as a particle decelerator with an output signal only moderately larger than the input (gain close to unity). This regime can be useful to quickly estimate the efficiency for a low gain amplifier. In practice it can be useful in an optical cavity configuration where part of the output power is split and redirected at the input. This scheme implementation is discussed further in Sec. VIII.B.4 (see Fig. 28).

Using Eq. (77), assuming a constant period undulator ($\lambda_w = \text{const}$), and defining the normalized potential vector

$$K_l \equiv \frac{eE}{mc^2 k}, \tag{149}$$

one can integrate Eq. (112) and obtain the total change of the wiggler parameter, along the wiggler (Duris *et al.*, 2018):

$$\Delta \bar{a}_w = 4\pi N_w K_l \sin\psi_r. \tag{150}$$

In practice the contribution of internal dynamics to the power extraction efficiency is negligible in these experiments

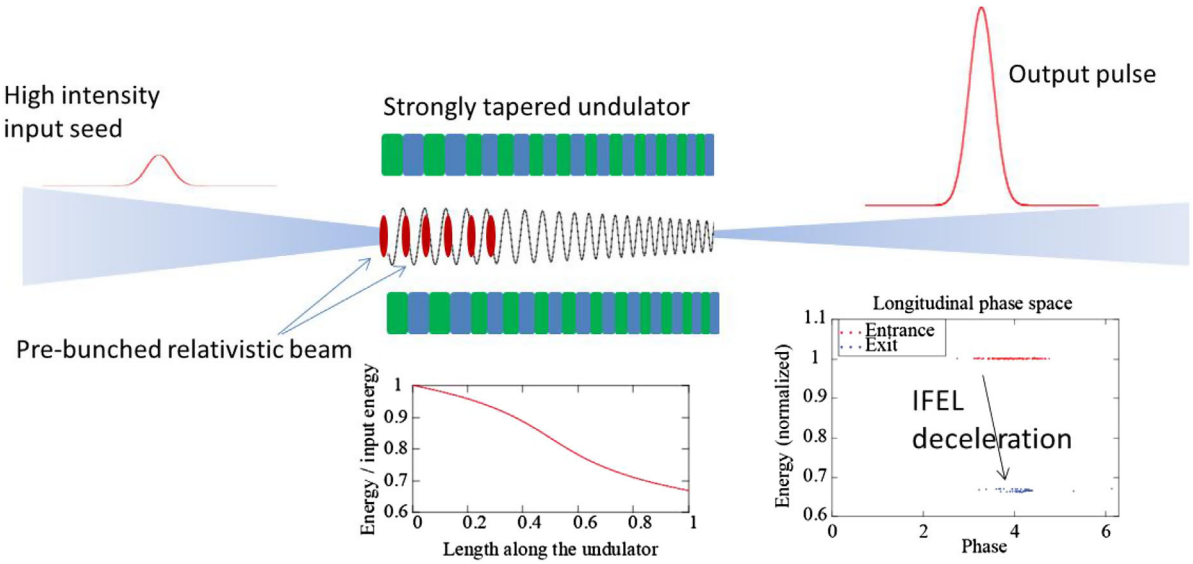

FIG. 21. Tapering-enhanced stimulated-superradiant amplifier.

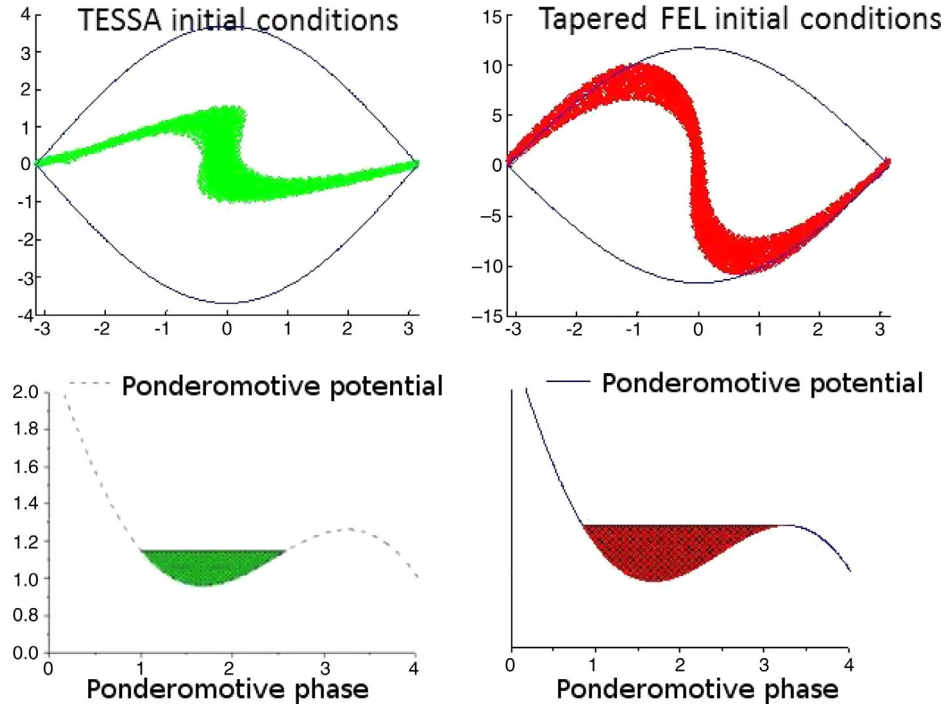

FIG. 22. (Left) Deeply trapped TESSA initial conditions. (Right) Full bucket tapered FEL initial conditions.

and the main contribution to the power generation is the wiggler tapering. The extraction efficiency is given by the ratio of the energy decrement $\gamma_r(0)-\gamma_r(L_w)$ and $\gamma_r(0)$ [Eq. (77)] times the trapping efficiency:

$$\eta = f_t\left(1-\frac{\gamma_r(L_w)}{\gamma_r(0)}\right) = f_t\left(1-\sqrt{\frac{1+(\bar{a}_w-\Delta\bar{a}_w)^2}{1+\bar{a}_w^2}}\right)$$
$$= f_t\left(1-\sqrt{1-\frac{2\bar{a}_w(0)\Delta\bar{a}_w}{1+\bar{a}_w^2(0)}+\frac{\Delta\bar{a}_w^2}{1+\bar{a}_w^2(0)}}\right)$$
$$\approx f_t\frac{\bar{a}_w(0)\Delta\bar{a}_w}{1+\bar{a}_w(0)^2}, \tag{151}$$

where $\Delta\bar{a}_w$ is given in Eq. (150), f_t is the fraction of particles trapped in the ponderomotive potential and ψ_r is the design resonant phase (typically ~45° to compromise optimum deceleration and maximum trapping). If one includes diffraction effects in the optimization, it is found that the input seed should be focused at the center of the undulator with a Rayleigh range about 1/6 of the undulator length. For large K_l and long undulator this number can easily approach 50%.

2. High gain regime

In the small signal gain regime, the conversion efficiency is independent of the beam current, since there we are not considering the fact that the radiation is increasing along the undulator. When one includes the growth of the signal amplitude, a steeper tapering can be allowed and stronger amplification can occur. In order for this to occur it is essential to develop a tapering optimization algorithm which can take advantage of the newly generated radiation intensity in the most efficient way. Duris, Murokh, and Musumeci (2015) obtained the optimization algorithm through fully three-dimensional computer simulations. The Genesis-informed tapering algorithm was developed to read off the on-axis intensity after solving the field propagation equations for a small section of the undulator and use this information to optimize the next period undulator parameter variations maximizing the energy extraction without compromising the trapping.

3. Nocibur experiment: Demonstration of small gain regime

The Nocibur experiment (Sudar *et al.*, 2016) demonstrated the low gain TESSA regime, converting up to 30% of a highly relativistic electron beam's energy to coherent 10.3 μm radiation. The experiment was performed at the Brookhaven National Laboratory's Accelerator Test Facility, utilizing a 200 GW seed from the high-power mid-IR CO_2 laser. The strongly tapered, helical Rubicon undulator that was used as an inverse FEL accelerator (Tremaine *et al.*, 2011) was reversed to decelerate up to 45% of a 100 pC, 65 MeV electron beam to 35 MeV; see Fig. 23.

Considering the initial beam energy of 6.5 mJ and defining the total electron beam energy after the interaction as

$$E_{\mathrm{tot}} = \frac{Q}{e}\int \frac{1}{N_{\mathrm{tot}}}\frac{dN}{dE}EdE \tag{152}$$

gives an average final electron beam energy of 4.5 ± 0.4 mJ and an extraction efficiency of 30%; see Fig. 24.

The Rubicon undulator consists of two 11 period planar Halbach undulators oriented perpendicular and shifted in phase by $\pi/2$ with a total interaction length of 0.54 m. The undulator period is tapered from 6 to 4 cm, allowing the undulator gap to remain approximately constant throughout the interaction. Undulator $\bar{a}_w(z)$ tapering was determined by matching the resonant gradient, determined by the undulator

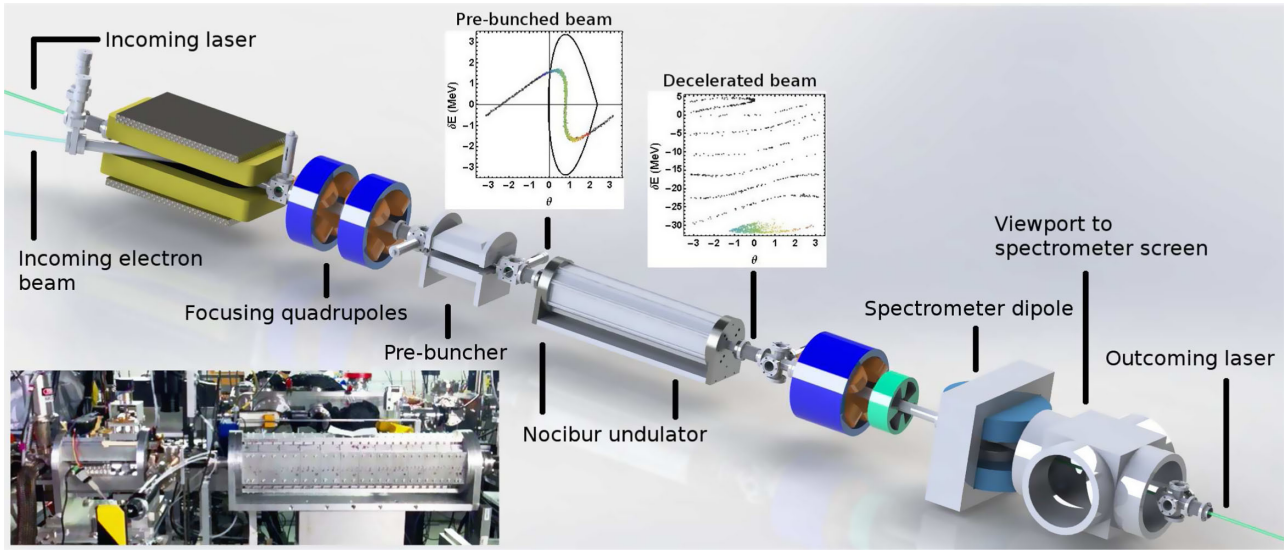

FIG. 23. Nocibur experiment beam line layout.

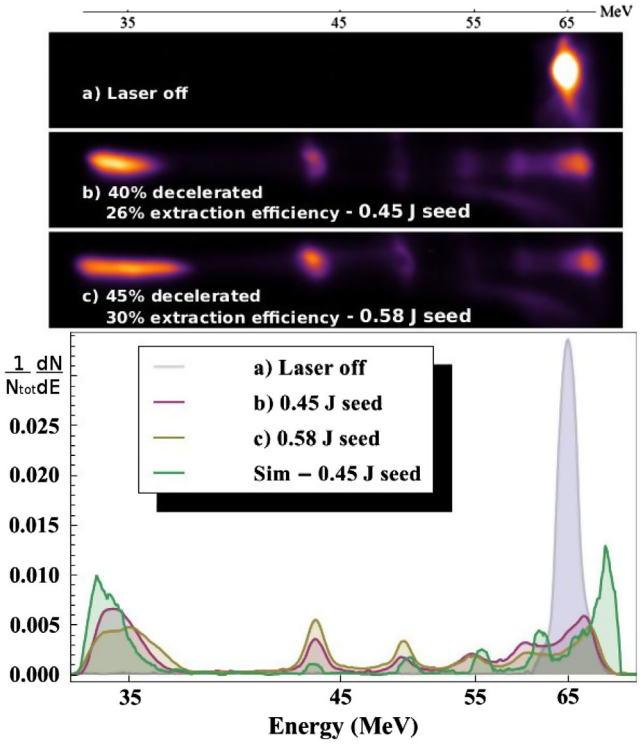

FIG. 24. Experimental spectra.

parameters, to the ponderomotive gradient (Fig. 25) asserting a resonant phase of $\pi/4$.

To increase the energy extraction efficiency further, the electron beam was prebunched to increase the fraction of particles trapped in the ponderomotive potential. The prebuncher consists of a single 5 cm period planar Halbach undulator followed by a permanent magnet chicane with a variable gap. As the electron beam passes through the short undulator section, interaction with the same laser seed used to drive the Nocibur interaction produces a sinusoidal energy modulation on the electron beam, periodic at the laser wavelength This modulation is now locked in phase with the Nocibur seed laser. The subsequent chicane provides dispersion, converting the energy modulation to density modulation. This produces a series of periodically spaced microbunches, while also introducing a phase delay between the microbunches and laser. The variable chicane gap allows for tunability of the dispersion and phase delay, allowing injection of the microbunches in the ponderomotive potential at the resonant phase; see Fig. 26. Prebunching increased the fraction of particles trapped from 17% without prebunching to 45% increasing the extraction efficiency by a factor of 3.

Direct measurement and characterization of the produced radiation was hindered by the presence of the 200 GW seed. However, experimental spectra are in excellent agreement with 3D time-dependent Genesis simulations which predict a

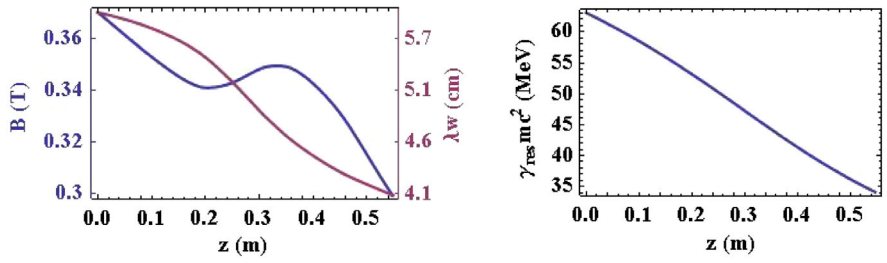

FIG. 25. (Left) Undulator period (red) and magnetic field amplitude (blue). (Right) Resonant energy.

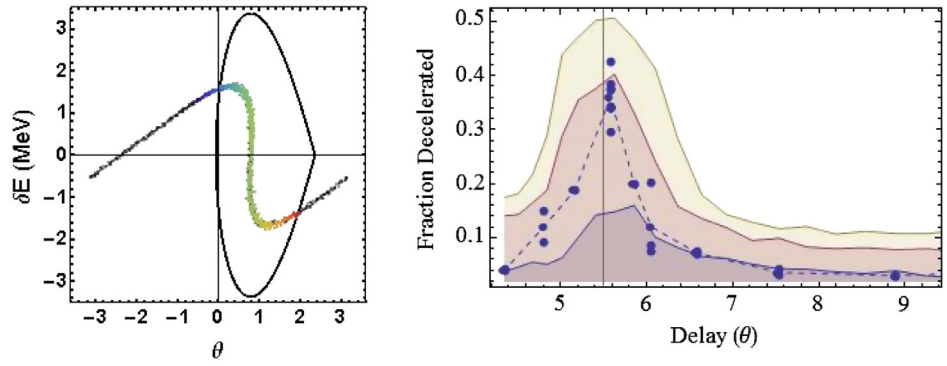

FIG. 26. (Left) Prebunched *e*-beam longitudinal phase space in the Nocibur initial ponderomotive potential. (Right) Fraction trapped data (points) vs injection phase controlled by a varying chicane gap compared with general particle tracer simulations with seed energy 0.55 J (yellow) 0.45 J (red), and 0.35 J (blue).

2 mJ increase in radiation energy. This is consistent with the previously defined total energy lost by the electron beam, validating the assumption that energy lost by the electron beam is converted directly to coherent radiation; see Fig. 27.

Note that the transverse distribution of the newly generated radiation is particularly interesting. The emission source in fact is the tightly focused electron beam current, which has a spot size much smaller than the seed radiation. Consequently the radiation has a much stronger divergence angle. We highlight this effect by showing in the right panel of Fig. 27(b) the intensity distribution difference between the seed mode and the amplified mode which exhibits a hole on axis due to diffraction.

Furthermore, Genesis simulations show an increase in the divergence angle of the produced radiation since it is emitted by the electron beam at a waist much smaller than the laser seed. This is important to account for when considering utilizing the low gain TESSA interaction in a recirculation scheme.

4. Outlook: TESSO

The features of the TESSA concept have naturally the potential for very high-power extraction efficiency. However, since the concept requires a high intensity coherent radiation signal input in order to form the traps for an injected prebunched beam, its optical amplification gain is low or moderate. It is reasonable in this case to consider a radiation recirculation approach, namely, an oscillator or a regenerative amplifier, as shown schematically in Fig. 28. Such a TESSO device may be an exceptionally energy efficient and high average power radiation source (Duris *et al.*, 2018).

The main challenge for realizing this concept is the requirement for a high intensity radiation seed "igniter" and a high repetition bunched beam train synchronous with the round-trip time of the resonator. Concepts of stimulated-superradiant FEL oscillator radiation with a uniform wiggler have been considered by Alexeev *et al.* (1989) and Seo (2013) and by Krongauz *et al.* (2000) and Gover *et al.* (2005), where

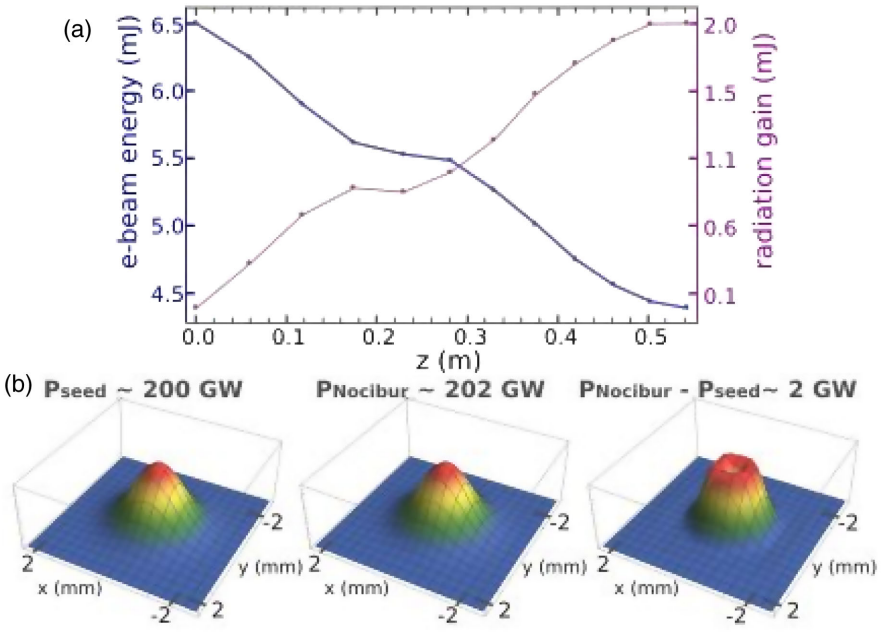

FIG. 27. (a) Total *e*-beam energy and radiation gain along the Nocibur interaction from Genesis simulation. (b) Output radiation transverse distribution from Genesis.

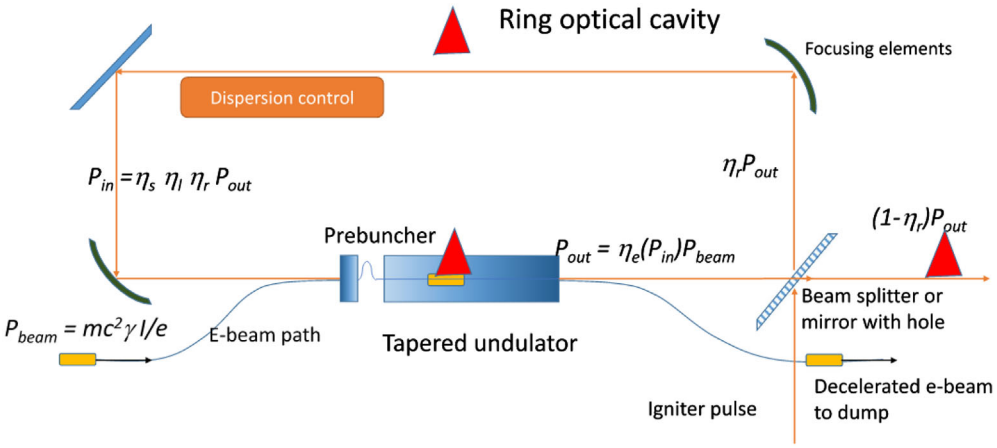

FIG. 28. TESSO scheme: The scheme requires the use of a high repetition rate electron bunch with temporal separation tuned to the cavity round-trip length. A fraction of the output radiation is redirected at the input to prebunch the beam and start the TESSA amplification for the next electron bunch.

a strategy of buildup in the resonator is considered starting from zero-order superradiance and stimulated superradiance. In this scheme the beam energy is temporally ramped in a process in which the bunched beam eventually gets trapped in the built-up radiation field and then continues in a steady-state saturated superradiant oscillation mode. However, such a strategy would not be efficient for a tapered wiggler oscillator concept, because in this case there is no gain in the small signal regime before saturation. On the other hand, concepts of tapered wiggler oscillators have been considered in the past with continuous beams (Saldin, Schneidmiller, and Yurkov, 1993; Dattoli *et al.*, 2012) and can be helpful to the case of bunched beam TESSO.

A high-power TESSO radiation source would be highly desirable especially in the UV regime. Such a scheme was considered theoretically for wavelength 266 nm (Duris *et al.*, 2018). This wavelength comfortably lies in the easily accessible region using cm period undulators and a moderate energy (375 MeV) beam energy (Murokh *et al.*, 2017). More recently it was studied in the high gain TESSA regime using numerical simulations showing the various trade-offs to optimize the efficiency as a function of the beam and laser parameters. In particular, the challenges associated with start-up from low power have been bypassed by assuming that a short pulse high-power laser source (low repetition rate) would be available to ignite the oscillator. Conversion efficiencies approaching 40% have been shown feasible in 3D simulations.

C. Efficiency enhancement in the tapered wiggler section of a seed-injected FEL

In real short wavelengths UV-XUV FELs (Fig. 6) the fundamental efficiency enhancement processes are not straightforwardly applicable. In the first place, as displayed in Fig. 6, diffraction effects are significant and the use of a single radiation mode model is not valid in a long interaction length. Furthermore, in present-day x-ray FEL facilities there is little control over the input field intensity and the bunching phase of the beam at the entrance to the tapered wiggler section, independently of the prior section of uniform wiggler amplification. Nevertheless, in the future, emerging new techniques may enable better control of the bunched beam and implementation of SR and ST-SR processes. Indeed, phase jump efficiency enhancement methods have been proposed based on small chicanes placed in the space between wiggler sections in short wavelength FEL (Ratner *et al.*, 2010; Mak, Curbis, and Werin, 2017; Tsai *et al.*, 2019). In such a scheme the bunched beam is made to go a longer path relative to the radiation wave, and after each section, the slowed down bunches can be reinserted into an optimized (downstream side) of the next (backstream) ponderomotive potential trap. It is thus conceivable that similar methods can be developed in the future to optimize the entrance phase of the bunches in the tapered wiggler to enhance the radiation power emission rate. Furthermore, new developments of fresh-bunch techniques (Ben-Zvi, Yang, and Yu, 1992; Emma, Feng *et al.*, 2017; Emma, Lutman *et al.*, 2017) make it possible to inject into the tapered wiggler traps bunches with energy spread smaller than the depth of the trap. Recent works also suggest that with such a fresh bunch, maintaining a high trapping efficiency along the interaction length may be possible with proper strategies of wiggler tapering (Tsai *et al.*, 2019). However, at the present state of the art of short wavelength FELs, the fundamental interaction processes of SR and ST-SR are complicated by many supplemental effects that do not enable use of simple analytic models.

Numerical simulations have played a key role in understanding the various physical mechanisms at work in high efficiency tapered wiggler FELs. The importance of numerical studies is due to the inherently nonlinear evolution of the electron beam and radiation emission in the postsaturation region of tapered FELs which makes analytic results difficult to obtain without resorting to approximation. As qualitatively discussed in the previous section, early numerical studies revealed the importance of two fundamental effects which limit the efficiency of tapered FELs: diffraction due to reduced radiation guiding (Prosnitz, Szoke, and Neil, 1981; Scharlemann, Sessler, and Wurtele, 1985) (see Fig. 6) and the sideband instability (Kroll and Rosenbluth, 1980; Kroll,

Morton, and Rosenbluth, 1981). These effects have been analyzed both separately and in combination via 1D and 3D codes, with multifrequency effects enabled or intentionally disabled (Quimby, Slater, and Wilcoxon, 1985; Hafizi *et al.*, 1989; Isermann and Graham, 1992; Fawley, 1995; Reiche, 1999; Fawley *et al.*, 2002; Jiao *et al.*, 2012; Emma *et al.*, 2014; Duris, Murokh, and Musumeci, 2015; Schneidmiller and Yurkov, 2015; Emma, Sudar *et al.*, 2017).

1. Transverse effects

The simple single mode model is not valid in the long wiggler FEL where diffraction effects dominate. One must then use a multimode analysis (Chen *et al.*, 2014; Emma and Pellegrini, 2014; Tsai *et al.*, 2018) or numerical solutions of Maxwell equations. Growth of the radiation spot size during the postsaturation region decreases the effective bucket area in which electrons are trapped and continue to lose energy to the radiation field. This effect becomes dominant for tapered wigglers of multiple Rayleigh lengths and sets a limit on the maximum achievable efficiency. This limit was first estimated analytically by Fawley (1996) and has subsequently been verified in numerical studies (Jiao *et al.*, 2012). To deter the expansion of the radiation it is necessary to maintain the refractive guiding as strong as possible in the tapered section of the undulator. The strength of the guiding (given by the electron beam refractive index) (Scharlemann, Sessler, and Wurtele, 1985) is proportional to the beam bunching which underscores the importance of maintaining a large fraction of the beam trapped and bunched in the tapered wiggler for maximum output efficiency. Recent numerical studies have suggested improving the effect of the guiding by varying the electron beam spot size in the tapered section (Jiao *et al.*, 2012) or shaping the electron transverse distribution from Gaussian to parabolic or uniform (Emma *et al.*, 2014b), yielding a relative improvement in the efficiency around 10%–40%. In particular, Jiao *et al.* (2012) developed an iterative optimization algorithm which optimizes the polynomial taper profile as well as the strength of the quadrupole focusing based on the evolution of the radiation spot size in different sections of the tapered undulator. Another recent study (Schneidmiller and Yurkov, 2015) examined the effect of diffraction on the optimization of a tapered FEL by parametrizing the z-dependent emission of radiation as a function of the Fresnel number $N = k\sigma^2/z$ where $k = 2\pi/\lambda$ is the radiation wave number. The two limits of a thin electron beam $N \gg 1$ and a wide electron beam $N \ll 1$ correspond to a quadratic and a linear growth in the radiation power and occur in the early and late stages of a tapered wiggler, respectively. As such, the tapering law determined is a hybrid of a quadratic taper at the start of the postsaturation section followed by a linear taper toward the end of the wiggler, with the exact form depending on the electron beam and undulator parameters. As we remark in the next section, the useful guidelines provided in these studies must be applied while also taking into account the impact of multifrequency effects, as they can prove crucial when coupled with transverse effects and can change the form of the optimal tapering profile for maximum output efficiency (Emma *et al.*, 2014).

2. Multifrequency effects

Multifrequency effects in the postsaturation regime can cause the amplification of undesired frequencies which can perturb the dynamics of the electron motion, disrupting the radiation gain and reducing the output efficiency. One of the most deleterious of these effects to the tapered FEL performance is the synchrotron sideband instability (Kroll and Rosenbluth, 1980; Kroll, Morton, and Rosenbluth, 1981). Sidebands are generated due to amplitude and phase modulations of the electric field which result from the trapped particles undergoing multiple synchrotron oscillations as they pass through the tapered section of the wiggler. From the 1D FEL field equation it is clear that as the electrons oscillate in the longitudinal phase space the gain and the phase shift of the radiation field will be different at different locations in the undulator and, due to shot noise and/or existing current modulations imprinted on the electron beam, at different locations along the bunch. This results in a temporal modulation of the radiation amplitude and phase giving rise to sidebands displaced from the central wavelength. Suppression of shot noise in the early stages of electron beam acceleration would be a way to deter the start of sideband instability out of noise. Theoretically the scaling of noise suppression schemes could reach x-ray frequencies (Nause, Dyunin, and Gover, 2014) but these have been demonstrated so far only at optical frequencies (Gover *et al.*, 2012; Ratner and Stupakov, 2012; Ratner *et al.*, 2015).

The resonance between sideband radiation frequencies and the electron synchrotron motion gives rise to the synchrotron sidebands displaced from the central wavelength by an amount $\Delta\lambda/\lambda_0 = \lambda_w/L_s$, where $L_s = 2\pi/K_s$ [Eq. (104)] is the synchrotron period. Since the resonance between the electron synchrotron motion and the ponderomotive wave is what causes the net energy transfer to the sidebands, we expect the sideband gain to be small in the regions in which the electric field, and thus the synchrotron frequency, are changing rapidly. For this reason in the original literature (Kroll, Morton, and Rosenbluth, 1981) it was thought that high gain FEL amplifiers (as opposed to the low gain FEL oscillators) would avoid the sideband problem due to the rapidly increasing radiation field in the tapered region causing a rapidly changing synchrotron frequency. Suppressing sideband growth in the FEL oscillator was therefore first studied in the 1D limit with a time-dependent FEL code, and it was shown that the instability could be suppressed by adding suitable frequency filters into the FEL optical cavity (Quimby, Slater, and Wilcoxon, 1985). While the 1D FEL theory predicts weak sideband growth for FEL amplifiers, as we have discussed, diffraction effects in tapered wiggler FELs cause the electric field growth to slow down and eventually saturate due to reduced optical guiding. As a result, the onset of sideband-induced detrapping is coupled to the limits on the electric field growth set by the reduction in guiding. As the electric field approaches its asymptotic value we expect the effect of the sidebands to be more pronounced and more significant detrapping to occur as a result. Eventually this process can lead to a second saturation of the tapered FEL power, as shown, for example, by Jiao *et al.* (2012) and Emma *et al.* (2014).

Suppressing the sideband instability therefore remains one of the key issues for tapered FEL amplifiers, particularly those which are multiple synchrotron periods in length. To that end, a number of sideband suppression schemes have been recently proposed for high efficiency FEL amplifiers. For example, it was shown in simulations that a large seed power in an FEL amplifier can offer a significant "head start" for the fundamental compared to the sidebands which start from noise. This allows the fundamental to reach high peak power before the sidebands grow to an appreciable amplitude (Emma *et al.*, 2014). In order to achieve a large enough seed for a tapered x-ray FEL while preserving the beam quality necessary for efficient amplification in the tapered wiggler, a technique termed "fresh-bunch self-seeding" was recently demonstrated at the LCLS, recording an increase in x-ray brightness by a factor of 2 compared to the state of the art (Emma, Lutman *et al.*, 2017). An alternative method making use of periodic delays between wiggler sections which introduce a $\pi/2$ phase shift for the sideband oscillations while preserving the phase of the resonant frequency was proposed by Duris, Murokh, and Musumeci (2015). Therein it was shown that a modest number of such delays could be used to recover the maximum efficiency achievable with multifrequency effects disabled. A similar technique has been suggested which introduces a modulation in the undulator magnetic field, effectively achieving a $\pi/2$ delay at the sideband frequency while maintaining resonance with the fundamental (Emma, Lutman *et al.*, 2017). This has been shown in simulations to reduce the sideband amplitude by more than an order of magnitude, improving the brightness of tapered wiggler FELs. Finally, a prebunched electron beam allows the FEL undulator tapering to be more rapid, thus leading to a faster-changing synchrotron frequency and consequently a reduction in the sideband growth. In conclusion note that, in addition to the previous analysis, the optimization of FEL efficiency via undulator tapering remains an active field of research with recent simulations and experiments revealing interesting results (Wu *et al.*, 2018). More experimental results can be found at the Sorgente Pulsata Auto-amplificata di Radiazione Coerente (SPARC) UV FEL (Giannessi *et al.*, 2013), the Shanghai Institute of Applied Physics (SINAP) (Li *et al.*, 2013), etc.

IX. CONCLUSIONS

Electron beams of small emittance and energy spread are in principle low entropy sources of radiative energy and therefore have the potential for ultimately high energy extraction efficiency and power. When the electron beam is prebunched at optical frequency, it is a good match with the coherent radiation wave at the corresponding six-dimensional volume in Liouville's phase space, and therefore a phase-space transformation of beam kinetic energy to optical power can take place with high energy extraction efficiency.

Based on this general principle, we identify radiation emission schemes of enhanced coherent spontaneous radiation: superradiance (SP-SR) and stimulated superradiance (ST-SR). In both schemes the enhancement is due to the constructive coherent interaction of the radiation wave with all electrons in a single or multiple bunched beam. For a short interaction length, the SP-SR emission is characterized by power generation scaling $\propto N^2L^2$, and the ST-SR power increment scales as $\propto NLE_0$, where N is the number of particles, L is the interaction length, and E_0 is the field strength at the entry to the interaction region. At longer interaction lengths, these scaling laws change due to a nonlinear process in which the beam energy drops and the electron dynamics during the interaction plays a role.

We used a simple model of ideally tightly bunched electron beams to describe the nonlinear interaction process for coherent radiative interaction in a magnetic wiggler (FEL). The model is applied to both uniform wiggler and tapered wiggler cases. In the case of tapering, the ponderomotive wave traps that are created by an intense input radiation wave and the tapered wiggler enable continued phase-matched stimulated interaction with the slowing down bunched beam (TESSA) and enhanced energy extraction from the beam.

The simplified nonlinear model presented is energy conserving and consistent with the zero-order analysis and scaling of SP-SR and ST-SR. At short distances (z) a bunched beam always exhibits SP-SR emission scaling as $\propto N^2z^2$, and ST-SR emission scaling as $\propto NzE_0$ if it is injected at a deceleration phase relative to the wave ($\psi = \pi/2$). It is then possible to get initially enhanced radiation extraction when the input radiation field and its relative bunching phase are controllable.

The nonlinear dynamics of the electrons in the potential traps of the ponderomotive potential is analogous to that of a mathematical pendulum, and in the case of a tapered wiggler—a titled pendulum. In the case of a tapered wiggler (TESSA) the analysis reveals that the electron beam energy drop (turned into radiation gain) is composed of two contributions: (a) an energy drop due to the reduced average kinetic energy of all electrons that stay trapped in the slowing down traps along the tapered wiggler, and (b) internal synchrotron oscillation dynamics of the tight bunches within the trap. If the bunching is tight there is an advantage to inject the beam at maximum ST-SR deceleration phase $\psi(0) = \pi/2$, but in practice the bunching efficiency is not perfect, and for maximum trapping efficiency one would prefer to inject the spread-phase bunch at the resonant particle center phase $\psi(0) = \psi_r$. In this case, the contribution of the internal trap dynamics and ST-SR emission are negligible.

Beyond the ideal tight bunching model that is useful for identifying the fundamental emission processes, we also presented for the TESSA case an approximate analysis and simulation results for the interaction with a beam of finite energy and phase spread. In this case, relevant to the present state of the art of TESSA and FEL technology, the contribution of the internal dynamics of synchrotron oscillation is washed out, and the dominant contribution is the resonant energy drop due to tapering $\Delta\gamma = \gamma_r(0) - \gamma_r(L_w)$. Also in this case there is an advantage in having high initial field E_0, tight bunching, and good control over the injection phase $\psi(0)$ in order to achieve high trapping efficiency and enable an aggressive tapering rate with deep enough traps. Future development of beam and laser technology, such as the fresh bunch technique (Emma, Lutman *et al.*, 2017), may lead to better control of these parameters and development of very high efficiency TESSA and TESSO radiation sources.

In the last part of this article we reviewed the applications and experimental demonstrations of radiation sources based on a bunched e beam: superradiant, stimulated superradiant, and

TESSA. Most of the superradiant radiation sources operate in the THz regime, because practically, modern rf accelerators are based on subps short electron bunches photoemitted using femtosecond ultrafast lasers. In the case of nonlinear interaction of a bunched beam in a tapered wiggler we reviewed the experimental demonstration of significant radiative energy transfer efficiency in TESSO experiments in Tremaine *et al.* (2011) and Sudar *et al.* (2016). We finally pointed out the relevance of SP-SR and ST-SR processes in considering optimized tapering strategy in tapered wiggler FEL. It was indicated, however, that in this case several processes of energy and phase spread radiation diffraction and multifrequency effects mask the fundamental radiation processes in a long wiggler, and they have been analyzed primarily with numerical computations.

LIST OF SYMBOLS AND ABBREVIATIONS

CSR	coherent synchrotron radiation
CTR	coherent transition radiation
EEHG	echo-enabled harmonic generation
ERL	energy retrieval linac
FEL	free electron laser
HGHG	high gain harmonic generation
IR	infrared
KMR	Kroll-Morton-Rosenbluth
linac	linear accelerator
PEHG	phase-merging enhanced harmonic generation
SASE	self-amplified spontaneous emission
SP-SR	spontaneous superradiance
ST-SR	stimulated superradiance
TES	tapering-enhanced superradiance
TESSA	tapering-enhanced stimulated-superradiant amplification
TESSO	tapering-enhanced stimulated-superradiant oscillator
THz	terahertz
UR	undulator radiation

Note that the terms "wiggler" and "undulator" are interchangeably used in this review, as are the terms "superradiance" and "coherent spontaneous radiation."

ACKNOWLEDGMENTS

This research was supported in part by a grant from the United States-Israel Binational Science Foundation (BSF), Jerusalem, Israel, the Israel Science Foundation (ISF), and the German-Israeli Project Cooperation (DIP).

APPENDIX A: PENDULUM EQUATION IN FEL CONTEXT

The classical pendulum equation is given by

$$\frac{d\theta}{dz} = K_s^2 \sin\psi, \tag{A1}$$

$$\frac{d\psi}{dz} = -\theta \tag{A2}$$

(in the case of a physical pendulum $K_s^2 = g/l$, where g is the gravitation constant and l is the length of the pendulum, ψ is the tilt angle and θ is the angular velocity, and the independent variable would be t and not z).

In the context of a periodically bunched electron beam, θ represents the detuning parameter between the velocity of the bunches and the phase velocity of the ponderomotive wave radiation field [see Eq. (33)], while ψ represents the phase of the bunch relative to the ponderomotive wave

$$\psi \equiv -[\varphi_b(z) - \varphi_q(z) - \pi/2]. \tag{A3}$$

The parameter K_s, called the synchrotron oscillation wave number, represents the small oscillation frequency of the bunches relative to the center of the trap. K_s is essentially the amplitude of the ponderomotive wave and is proportional to the wiggler strength and the radiation field amplitude [Eq. (104)].

Multiplying the left-hand side (lhs) of Eq. (A1) with the right-hand side (rhs) of Eq. (A2) and vice versa, and integrating, results in

$$\tfrac{1}{2}\theta^2 - K_s^2 \cos\psi \equiv T(\theta) + U(\psi) = C. \tag{A4}$$

Here we identify $T(\theta) = \frac{1}{2}\theta^2$ with the kinetic energy and $U(\psi) = -K_s^2 \cos\psi$ with the potential energy. C is an integration constant that is determined by the initial value of the electron trajectory $C = T(\theta(0)) + U(\psi(0))$. Inspecting Fig. 29 we observe two kinds of trajectories: for $C(\theta(0), \psi(0)) > K_s^2$ all trajectories are open, namely, electrons injected at phase and detuning initial conditions corresponding to this case propagate in open phase-space trajectories, bypassing the periodic traps without getting trapped. In the opposite case $C(\theta(0), \psi(0)) < K_s^2$ electrons follow closed trajectories, and if injected into the trap, they stay trapped, performing "synchrotron oscillations" around

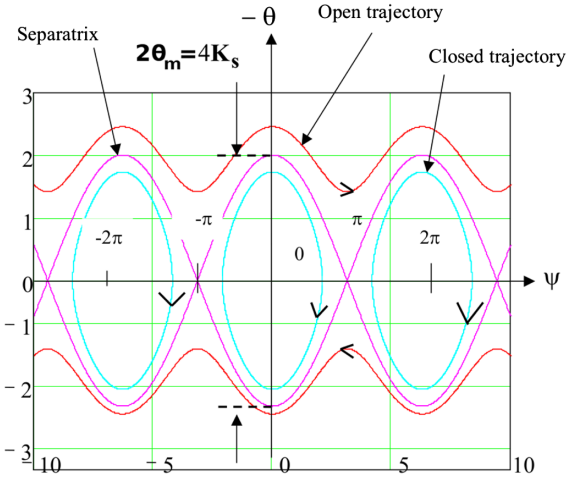

FIG. 29. The $\theta - \psi$ phase-space trajectories of the pendulum equation.

the center of the trap and moving on the average at the phase velocity of the ponderomotive force (74). The equality $C(\theta(0),\psi(0)) = K_s^2$ represents the separatrix—the borderline between open and closed trajectories. The separatrix represents a "trap" or a "bucket" in which electrons are trapped, executing synchrotron trajectories without escape. The height of the trap is

$$2\theta_m = 4K_s \tag{A5}$$

and its width is 2π, i.e., $-\pi < \psi < \pi$.

To describe the electron dynamics in a tapered wiggler we note that in this case the phase velocity of the ponderomotive wave (74) decelerates when the wiggler period gets shorter as a function of z. This can be envisioned as a physical situation where the electron in a decelerating frame experiences an imaginary acceleration force in addition to the restoring force of the pendulum. This can be shown to be equivalent to adding a term to the rhs of Eq. (A1). To make sure that the acceleration (tapering force) is smaller than the restoring force, and the electrons can still be trapped, we define this term as $-K_s^2 \sin\psi_r$:

$$\frac{d\theta}{dz} = K_s^2[\sin\psi - \sin\psi_r]. \tag{A6}$$

Since $\sin\psi_r < 1$, there is always a range of phases ψ around $\psi = \psi_r$ in which oscillatory dynamics around the resonant phase ψ_r is possible.

For the case $\sin\psi_r = \text{const}$ (linear wiggler tapering), the integration of Eq. (A6) with (A2) is straightforward (Kroll, Morton, and Rosenbluth, 1981):

$$\tfrac{1}{2}\theta^2 - K_s^2[\cos\psi + \psi\sin\psi_r] \equiv T(\theta) + U(\psi) = C, \tag{A7}$$

where the kinetic energy $T(\theta)$ is the same as before, but the potential energy $U(\psi)$ has an additional term:

$$U(\psi) = -K_s^2[\cos\psi + \psi\sin\psi_r] \tag{A8}$$

shown in Fig. 30 with $K_s = 1$ and $\sin\psi_r = 0.5$. $C = T(\theta(0)) + U(\psi(0))$ is an integration constant established by the initial values of θ and ψ.

To analyze the potential energy $U(\psi)$ in Eq. (A8), we find the maxima and minima by solving $dU/d\psi = 0$. This results in

$$\psi^n_{\max} = \pi - \psi_r + 2\pi n \equiv \psi^n_2, \tag{A9}$$

which is the right limit of the trap n, named ψ^n_2, and

$$\psi^n_{\min} = \psi_r + 2\pi n. \tag{A10}$$

We define the separatrix for the trap n by setting $C^n_{\rm sep} = U(\psi^n_2) = K_s^2[\cos\psi_r - (\pi - \psi_r + 2\pi n)\sin\psi_r]$, so that nonzero kinetic energy $T(\theta) \geq 0$ is possible for either $\psi > \psi^n_2$ (open trajectories) or $\psi^n_1 < \psi < \psi^n_2$ (closed trajectories). Here ψ^n_1 is the other (left boundary phase) of the equation $U(\psi) = C^n_{\rm sep}$ (see Fig. 30 and the phase space presentation of the separatrix for $n = 0$ in Fig. 31). Using $C = C^n_{\rm sep}$ in Eq. (A7), for $n = 0$ we obtain

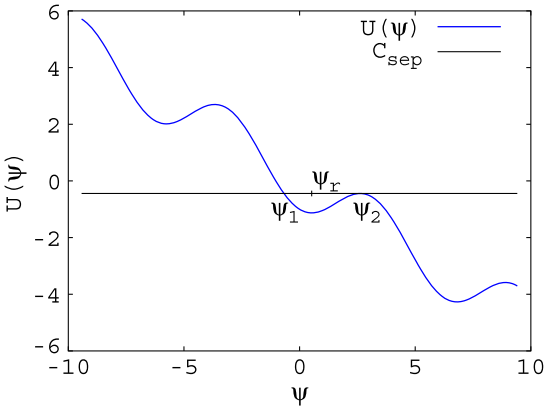

FIG. 30. The potential energy for a tapered wiggler with $K_s = 1$ and $\sin\psi_r = 0.5$. Shown are $C_{\rm sep}$ and the values of ψ_1 and ψ_2 for $n = 0$.

$$\tfrac{1}{2}\theta^2 = K_s^2[\cos\psi + \psi\sin\psi_r + \cos\psi_r - (\pi - \psi_r)\sin\psi_r] \tag{A11}$$

from which the curve of the separatrix in Fig. 31 is represented by

$$\theta = \sqrt{2}K_s\sqrt{\cos\psi + \psi\sin\psi_r + \cos\psi_r - (\pi - \psi_r)\sin\psi_r}. \tag{A12}$$

The height of the tilted pendulum separatrix is $2\theta_m$, where θ_m is the value of θ in Eq. (A12) for $\psi = \psi_r$. We found

$$2\theta_m = 4K_s\sqrt{\cos\psi_r + (\psi_r - \pi/2)\sin\psi_r}, \tag{A13}$$

so that for $\psi_r = 0$ we recover Eq. (A5) and for $\psi_r = \pi/2$ the trap vanishes ($\theta_m = 0$). The width of the trap is $\psi_2 - \psi_1$.

For other energy conservation constant values $C(\theta(0), \psi(0))$, one gets open trajectories if $C > C^n_{\rm sep}$ and closed trajectories if $C < C^n_{\rm sep}$; see Fig. 30. The open and closed

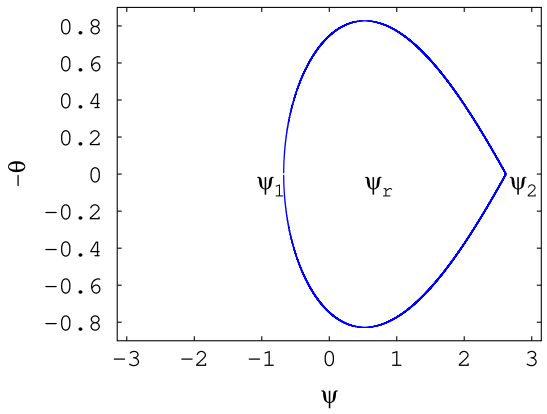

FIG. 31. The separatrix for the $n = 0$ trap in a tapered wiggler for $K_s = 1/\sqrt{2}$ and $\psi_r = \pi/6$. The trap ranges in the region $\psi_1 \leq \psi \leq \psi_2$, where $\psi_2 = \pi - \psi_r$ and ψ_1 has to be calculated numerically and is in this case −0.6752. The height of the trap is 1.6551, according to Eq. (A13).

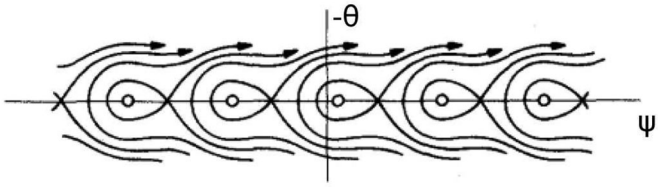

FIG. 32. Separatrix trajectories for trap $n = m$ are unbound around traps $n > m$ and are not allowed near traps $n < m$.

trajectories in phase space $(\psi, -\theta)$ are shown in Fig. 32 (Kroll, Morton, and Rosenbluth, 1981) for the multiple traps.

APPENDIX B: ELECTRON BEAM BUNCHING

While the thrust of this review is the coherent superradiant emission processes, we cannot ignore the processes of prebunching the electron beam.

There is a variety of processes for attaining tight bunches of electron beams. At long wavelength (THz range) single bunch electron beam and periodic bunching can be achieved by direct photoemission from femtosecond laser-illuminated cathodes. This can also be a train of such femtosecond laser beams that are replicated by various optical splitting and delay schemes. In all these schemes, the Gaussian distribution model for the electron bunch [Eq. (27)] is usually a good approximation:

$$f(t) = \frac{1}{\sqrt{2\pi}\sigma_t} e^{-t^2/(2\sigma_{tb}^2)}. \tag{B1}$$

Thus the bunching coefficients of the single electron bunch and periodic Gaussian bunch train, respectively, are Eqs. (28) and (57),

$$M_b(\omega) = e^{-\omega^2\sigma_{tb}^2/2}, \tag{B2}$$

$$b_n = e^{-\omega_n^2\sigma_{tb}^2/2}, \tag{B3}$$

where $\omega_n = n\omega_b$.

At short wavelengths, a most useful scheme of bunching a continuous or long pulse electron beam is to modulate its energy with a high intensity laser beam in a wiggler (or any other interaction scheme), and then turn its energy modulation into density modulation by passing it through a DS, such as a "chicane." This scheme of bunching is useful for a variety of short wavelength radiation emission schemes, including HGHG (Yu, 1991; L. Yu *et al.*, 2000), EEHG (Stupakov, 2009), PEHG (Feng *et al.*, 2014), TESSA (Sudar *et al.*, 2016), and eSASE (Zholents, 2005).

In the laser bunching scheme, the bunch distribution deviates from a single Gaussian shape (B3). Because of the importance of this bunching technique we review here briefly the derivation of the bunching distribution and the bunching coefficient of this case following the parametric notations of Hemsing *et al.* (2014).

The beam is assumed to be initially uniform but has initial energy spread. Its initial normalized energy distribution is

$$f(p) = \frac{1}{\sqrt{2\pi}} e^{-p^2/2}, \tag{B4}$$

where $p = (\gamma - \gamma_0)/\sigma_{\gamma 0}$.

After energy modulation $\gamma = \gamma_0 + \Delta\gamma_{\mathrm{mod}} \sin(\omega_b t)$, the energy distribution is periodically dependent on time t (or z) dependent:

$$f(p) = \frac{1}{\sqrt{2\pi}} e^{-[p - A\sin(\omega_b t)]^2/2}, \tag{B5}$$

where $A = \Delta\gamma_{\mathrm{mod}}/\sigma_{\gamma 0}$.

In a dispersive section of dispersive strength R_{56} the electron time and longitudinal coordinates pass a compression transformation $z' = ct' = z + R_{56}(\gamma - \gamma_0)/\gamma_0 = z + R_{56}p(\sigma_{\gamma 0}/\gamma_0)$, so after the DS

$$f_0(p,t) = \frac{1}{\sqrt{2\pi}} e^{-[p - A\sin(\omega_b t - Bp)]^2/2}. \tag{B6}$$

This current distribution, periodic in time with period $T_b = 2\pi/\omega_b$, depends on the modulation parameter A and the compression parameter B:

$$B = \omega_b\sigma_t = \omega_b(R_{56}/c)(\sigma_{\gamma 0}/\gamma_0). \tag{B7}$$

Figure 33 displays this distribution in $p = (\gamma - \gamma_0)/\sigma_{\gamma 0}$ and t/T_b over one bunching period at A, B parameters choice of maximum bunching.

Integrating over energy and using Eq. (B6), we find the bunching amplitude of harmonic n:

$$\begin{aligned} b_n &= \int_{-T_b/2}^{T_b/2} dt \int_{-\infty}^{\infty} dp e^{-in\omega_b t} f_0(t,p) \\ &= J_n(nAB)e^{-n^2B^2/2} \\ &= J_n(nAB)e^{-\omega_n^2\sigma_t^2/2}. \end{aligned} \tag{B8}$$

For harmonics $n > 4$ the maximum of the Bessel function in Eq. (B8) is about $0.67/n^{1/3}$ and is achieved when the argument is $n + 0.8n^{1/3}$. Thus the optimal strength of the DS for maximal bunching is

$$B = (n + 0.8n^{1/3})/nA \simeq 1/A. \tag{B9}$$

The approximate expression for the bunching parameter is

$$b_n = J_n(n)e^{-n^2B^2/2} \simeq \frac{0.67}{n^{1/3}} e^{\omega_n^2\sigma_t^2/2}, \tag{B10}$$

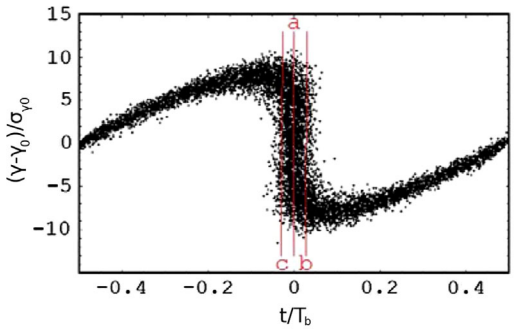

FIG. 33. Longitudinal phase space after the chicane showing microbunching of electrons and an enhanced electron density. From Zholents, 2005.

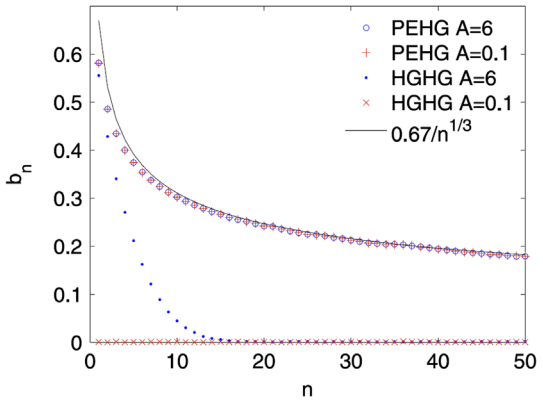

FIG. 34. Comparison of the bunching factor of PEHG and standard HGHG with different energy modulation amplitudes. The black line is the theoretical prediction of the maximal bunching factor of PEHG. From Feng *et al.*, 2014.

where $\sigma_t = B/\omega_b$ is the approximate width of the bunch distribution. The Bessel function factor in Eq. (B10) reduces somewhat the bunching coefficient relative to the Gaussian distribution (B3). Note that the width parameter σ_t is controllable in this case, and the Gaussian factor in Eq. (B8) that is limited by the initial energy spread $\sigma_{\gamma 0}/\gamma_0$ can be enhanced by decreasing B and increasing correspondingly $A \simeq 1/B$. Furthermore, it has been proposed that in a scheme of a transverse gradient wiggler the effect of the energy spread and the Gaussian factor may be nearly eliminated and the bunching factor gets close to (Feng *et al.*, 2014)

$$b_n = \frac{0.67}{n^{1/3}} \tag{B11}$$

as shown in Fig. 34.

Besides the derivation of the bunching coefficient for a laser modulated beam, the formulation here is also useful for calculating the trapping fraction $f_t(\psi_r, A)$ of a laser-prebunched electron beam in the traps of a tapered wiggler FEL characterized by a separatrix

$$\delta\gamma^{\text{sep}} = \delta\gamma^{\text{sep}}(K_s, \psi_n). \tag{B12}$$

The trapping efficiency of harmonic n can then be calculated numerically using the distribution (B6):

$$f_{tn} = \int_{\psi_{n1}}^{\psi_{n2}} d\psi_n \int_{-\delta\gamma^{\text{sep}}/\sigma_{\gamma 0}}^{\delta\gamma^{\text{sep}}/\sigma_{\gamma 0}} dp f_0(p, \psi_n). \tag{B13}$$

This procedure was used to calculate the trapping efficiency in Sec. VII.

APPENDIX C: CONSERVATION OF ENERGY AND THE HARMONIC RADIATION EXCITATION EQUATION IN A WIGGLER

For a single electron

$$\mathbf{J}(t) = -e\mathbf{v}\delta(\mathbf{r}_\perp)\delta[z - z_e(t)] \tag{C1}$$

with the transformation $t_e(z) = \int^z dz'/v_z$

$$\mathbf{J}(z) = -e\frac{\mathbf{v}}{v_z} f(\mathbf{r}_\perp)\delta[t - t_e(z)], \tag{C2}$$

where we replaced $\delta(\mathbf{r}_\perp) \to f(\mathbf{r}_\perp)$ in order to represent a bunch of finite transverse distribution. For a train of electrons

$$\mathbf{J}(z,t) = -e\frac{\mathbf{v}}{v_z} f(\mathbf{r}_\perp) \sum_{n=-\infty}^{\infty} \delta[t - t_e(z) - nT_b], \tag{C3}$$

which may be expressed as a Fourier series

$$\mathbf{J}(z,t) = \sum_{n=-\infty}^{\infty} \tilde{\mathbf{J}}_n e^{-in\omega_b t}, \tag{C4}$$

where the Fourier components are

$$\tilde{\mathbf{J}}_n = \frac{-e\mathbf{v}}{T_b v_z} f(\mathbf{r}_\perp) e^{in\omega_b t_e(z)}, \tag{C5}$$

so that

$$\begin{aligned}\mathbf{J}(z,t) &= \mathbf{J}_0 + \sum_{n=1}^{\infty} [\tilde{\mathbf{J}}_n e^{-in\omega_b t} + \tilde{\mathbf{J}}_n^* e^{in\omega_b t}] \\ &= \mathbf{J}_0 + \sum_{n=1}^{\infty} 2\text{Re}[\tilde{\mathbf{J}}_n e^{-in\omega_b t}].\end{aligned} \tag{C6}$$

For each harmonic n of the current we have

$$\mathbf{J}_n(z,t) = \text{Re}[2\tilde{\mathbf{J}}_n e^{-in\omega_b t}]. \tag{C7}$$

In order to match this formulation to the phasor formulation of Sec. III, we equate Eq. (C7) to the single frequency phasor presentation for ω_0:

$$\mathbf{J}(z,t) = \text{Re}[\tilde{\mathbf{J}} e^{-i\omega_0 t}]. \tag{C8}$$

Therefore, for interaction with a single harmonic $\omega_0 = n\omega_b$

$$\tilde{\mathbf{J}}(\omega_0, z) = 2\tilde{\mathbf{J}}_n = \frac{-e\omega_b \mathbf{v}}{\pi v_z} f(\mathbf{r}_\perp) e^{in\omega_b t_e(z)}. \tag{C9}$$

Substitute this current into the excitation equation (6)

$$\frac{d\tilde{C}_q}{dz} = \frac{-1}{4\mathcal{P}_q} \int \tilde{\mathbf{J}} \cdot \tilde{\boldsymbol{\mathcal{E}}}_q^* d^2\mathbf{r}_\perp, \tag{C10}$$

it can be employed for any harmonic frequency $\omega_0 = n\omega_b$ (in synchronous interaction schemes, such as undulator radiation, only one harmonic is interacting efficiently),

$$\frac{d\tilde{C}_q}{dz} = \frac{1}{4\mathcal{P}_q} \frac{e\omega_b \boldsymbol{\beta}}{\pi\beta_z} e^{i\omega_0 t_e(z)} \cdot \tilde{\boldsymbol{\mathcal{E}}}_q^*. \tag{C11}$$

We will show that the conservation of energy is kept separately for each harmonic. The radiation power is

$$\frac{dP}{dz} = \sum_q \mathcal{P}_q \frac{d}{dz}|C_q(z)|^2 = \sum_q \mathcal{P}_q \left[C_q^* \frac{dC_q}{dz} + C_q \frac{dC_q^*}{dz} \right] = \sum_q \mathcal{P}_q \left[C_q^* \frac{dC_q}{dz} + \text{c.c.} \right]. \tag{C12}$$

Using Eq. (C11) this results in

$$\frac{dP}{dz} = \frac{1}{4}\frac{e\omega_b \boldsymbol{\beta}}{\pi\beta_z} \cdot \sum_q [C_q^* \tilde{\boldsymbol{\mathcal{E}}}_q^* e^{i\omega_0 t_e(z)} + \text{c.c.}] = \frac{1}{4}\frac{e\omega_b \boldsymbol{\beta}}{\pi\beta_z} \cdot 2\mathbf{E}(r, t_e(z)). \tag{C13}$$

On the other hand, the energy equation for each electron interacting with the radiation field $\mathbf{E}(r,t)$ is

$$mc^2 \frac{d\gamma}{dt} = -e\mathbf{v} \cdot \mathbf{E}(\mathbf{r}, t), \tag{C14}$$

so that

$$mc^2 \frac{d\gamma}{dz} = -\frac{e}{\beta_z} \boldsymbol{\beta} \cdot \mathbf{E}(\mathbf{r}, t_e(z)). \tag{C15}$$

The power in the beam at any plane z is $P_e = mc^2(\gamma - 1)/T_b$, and its derivative $dP_e/dz = mc^2(d\gamma/dz)\omega_b/(2\pi)$ satisfies [see Eq. (C13)]

$$\frac{dP}{dz} = -\frac{dP_e}{dz}. \tag{C16}$$

This result of conservation of energy in the interaction between a periodically bunched e beam and a coherent radiation mode is very general. It applies to any kind of interaction scheme including the nonlinear regime. We now specify our formulation to the scheme of radiative interaction in a wiggler structure in order to derive the radiation excitation equation for this case.

To apply the excitation equation (C10) to the case of a wiggler we need to calculate the transverse current component of harmonic n [Eq. (C9)] for this case. For the tight bunching model, replacing e by $N_b e$ in Eq. (C3) we can write for the periodic beam density

$$n(\mathbf{r}, t) = N_b f(\mathbf{r}_\perp) \sum_j \delta\left[z - \int_{t_{oj}}^{t} v_z(t')dt' \right], \tag{C17}$$

where

$$t_{0j} = jT_b + t_0. \tag{C18}$$

Here t_{0j} is the entrance time of bunch j into the wiggler at $z = 0$.

The function $n(\mathbf{r}, t)$ is periodic in time, with a period of $T_b = 2\pi/\omega_b$, so it may be represented by the Fourier series

$$n(\mathbf{r}, t) = \sum_{n=-\infty}^{\infty} \tilde{n}_n(\mathbf{r}) e^{-in\omega_b t}, \tag{C19}$$

where the n harmonic coefficient of the density $\tilde{n}_n(\mathbf{r})$ is given by

$$\tilde{n}_n(\mathbf{r}) = \frac{1}{T_b} \int_{-T_b/2}^{T_b/2} n(\mathbf{r}, t) e^{in\omega_b t} dt. \tag{C20}$$

Setting Eq. (C17) in Eq. (C20) results in

$$\tilde{n}_n(\mathbf{r}) = \frac{N_b \omega_b}{2\pi v_z} f(\mathbf{r}_\perp) e^{in\omega_b [\int_0^z dz'/v_z(z') + t_0]}. \tag{C21}$$

For use in the force equations all bunches are assumed identical, namely, $I(z=0,t) = -eN_b \sum_{j=-\infty}^{\infty} \delta(t - jT_b - t_0)$ (this corresponds to $|\tilde{M}_b| = 1$ in the phasor formulation of Sec. III [Eq. (61)]). This current contains an infinite number of harmonics, but we assume here that only one harmonic at $\omega_0 = n\omega_b$ is interacting synchronously with the wave, so that we need to keep in Eq. (C19) only $\tilde{n}_n(\mathbf{r})$ and $\tilde{n}_{-n}(\mathbf{r}) = \tilde{n}_n^*(\mathbf{r})$. Equating (C9) to the phasor representation (52):

$$n(\mathbf{r}, t) \equiv \text{Re}\{\tilde{n}(\mathbf{r}) e^{-i\omega_0 t}\} = \tfrac{1}{2}\tilde{n}(\mathbf{r}) + \text{c.c.} \tag{C22}$$

we set

$$\tilde{n}(\mathbf{r}) = 2\tilde{n}_n(\mathbf{r}). \tag{C23}$$

Formulating the analysis so that it can be applied to a general wiggler, uniform or tapered, planar or helical, we write the perpendicular velocity of the wiggler as

$$\mathbf{v}_\perp = \text{Re}\{\tilde{\mathbf{v}}_w(z) e^{i\int_0^z k_w(z')dz'}\} = \frac{1}{2}\tilde{\mathbf{v}}_w(z) e^{i\int_0^z k_w(z')dz'} + \text{c.c.}, \tag{C24}$$

and define the perpendicular current density as

$$\mathbf{J}_\perp = -en\mathbf{v}_\perp = \text{Re}\{\tilde{\mathbf{J}}_\perp e^{-i\omega_0 t}\}. \tag{C25}$$

From Eqs. (C23)–(C25) we obtain

$$\tilde{\mathbf{J}}_\perp = -e\frac{1}{2}\tilde{n}(\mathbf{r})\tilde{\mathbf{v}}_w^*(z) e^{-i\int_0^z k_w(z')dz'}, \tag{C26}$$

and using Eq. (C21) in Eq. (C26), and allowing v_z (and in the tapered case also k_w) to change with z, results in

$$\tilde{\mathbf{J}}_\perp = \frac{Q_b \omega_0 \tilde{\boldsymbol{\beta}}_w^*}{2\pi\beta_{zr}} f(\mathbf{r}_\perp) e^{i\int_0^z (\omega_0/v_z(z') - k_w(z'))dz' + i\varphi_{b0}}, \tag{C27}$$

where $\varphi_{b0} = \omega_0 t_0$ is the entrance phase of the bunched beam, and operating near resonance we used $\beta_z \simeq \beta_{zr}$.

By comparing Eq. (60) with (C27), we find that for the model of tightly bunched beam (C3) the wiggling excitation current is

$$\tilde{I}_{m\perp} = \frac{Q_b \omega_0 |\tilde{\boldsymbol{\beta}}_w(z)| e^{i\varphi_{b0}}}{\pi \beta_{zr}}. \tag{C28}$$

Defining

$$\varphi_b(z) = \int_0^z \left(\frac{\omega_0}{v_z} - k_w - k_{zq}\right) dz' + \varphi_{b0}, \tag{C29}$$

and using the excitation equation (C10) one obtains

$$\frac{d\tilde{C}_q(z)}{dz} = -\frac{F Q_b \omega_0 \tilde{\boldsymbol{\beta}}_w(z) \cdot \tilde{\boldsymbol{\mathcal{E}}}_q^*(0)}{8\pi \mathcal{P}_q \beta_{zr}} e^{i\varphi_b(z)}, \tag{C30}$$

where the transverse filling factor F is defined in Eq. (65).

APPENDIX D: PARAMETERS CHOICE AND NORMALIZATION

We normalize the general dynamic equations of a prebunched beam in a tapered wiggler with varying parameters by substituting in Eqs. (105)–(107) or (113)–(115):

$$u = z/L_w, \tag{D1}$$

$$\bar{\theta} = \theta L_w, \tag{D2}$$

$$\bar{E}(z) = \frac{|\tilde{E}(z)|}{b(0) L_w}, \tag{D3}$$

where $b(0)$ is the value of b in Eq. (96) at $z = 0$ (or $u = 0$). This results in

$$\frac{d\bar{E}}{du} = f_B(u) \sin\psi, \tag{D4}$$

$$\frac{d\bar{\theta}}{du} = f_K(u) K_{s0}^2 \bar{E}(u) [\sin\psi - \sin\psi_r(u)], \tag{D5}$$

$$\frac{d\psi}{du} = -\bar{\theta} + \frac{1}{f_B(u)\bar{E}(u)} \cos\psi, \tag{D6}$$

where

$$K_{s0}^2 = \frac{I_0 Z_q k_0 \eta_p^2 \bar{a}_w^2(0) e L_w^3}{4mc^2 \beta_{zr}^5(0) \gamma_{zr}^2(0) \gamma_r^3(0) A_{em\,q}}, \tag{D7}$$

$$f_B(u) = \frac{b(u)}{b(0)} = \frac{\bar{a}_w(u) \beta_{zr}(0) \gamma_r(0)}{\bar{a}_w(0) \beta_{zr}(u) \gamma_r(u)}, \tag{D8}$$

$$f_K(u) = \frac{\beta_{zr}^3(0) \gamma_{zr}^2(0) \gamma_r(0)}{\beta_{zr}^3(u) \gamma_{zr}^2(u) \gamma_r(u)}. \tag{D9}$$

The beam trajectories in the dynamic range $0 < u < 1$ are best displayed in phase space $[\gamma(u) - \gamma_r(0), \psi]$, where

$$\gamma(u) - \gamma_r(0) = \gamma_r(u) - \gamma_r(0) + \delta\gamma(u), \tag{D10}$$

and where for the ultrarelativistic beam case [see Eq. (79)]

$$\delta\gamma(u) = -\frac{\gamma_r(u)\bar{\theta}(u)}{4\pi N_w}. \tag{D11}$$

The consequent radiation mode and beam energy powers are given by

$$P_{em} = \bar{E}^2(u) P_{\mathrm{REF}}, \tag{D12}$$

where

$$P_{\mathrm{REF}} = \frac{\mathcal{P}_q b^2(0) L_w^2}{|\tilde{\boldsymbol{\mathcal{E}}}_q(0)|^2} = \frac{1}{16\pi^2} \frac{\eta_p^2 \bar{a}_w^2(0)}{\beta_{zr}^2(0) \gamma_r^2(0)} \frac{Q_b^2 \omega_0^2 L_w^2 Z_q}{A_{em\,q}}, \tag{D13}$$

and the incremental electron beam power, relative to P_{REF}, is obtained from Eq. (116)

$$\begin{aligned}\Delta P_{\mathrm{el}} &= [\gamma(u) - \gamma(0)] \frac{N_b mc^2}{T_b} \\ &= [\gamma_r(u) - \gamma_r(0) + \delta\gamma(u) - \delta\gamma(0)] \frac{N_b mc^2}{T_b} = \\ &\quad -2P_{\mathrm{REF}} \left[\int_0^u \bar{E}(u') \sin\psi_r(u') du' + [\bar{\theta}(u) - \bar{\theta}(0)]/K_{s0}^2\right].\end{aligned} \tag{D14}$$

Note that $f_B(u)$, $f_K(u)$, and $\sin\psi_r(u)$ depend in general on the tapering scheme. If the tapering is moderate and linear, we may set $f_B(u) \approx 1$, $f_K(u) \approx 1$, and $\sin\psi_r(u) = \text{const}$. In this case Eqs. (D4)–(D6) simplify to

$$\frac{d\bar{E}}{du} = \sin\psi, \tag{D15}$$

$$\frac{d\bar{\theta}}{du} = K_{s0}^2 \bar{E} [\sin\psi - \sin\psi_r], \tag{D16}$$

$$\frac{d\psi}{du} = -\bar{\theta} + \frac{1}{\bar{E}} \cos\psi. \tag{D17}$$

In the numerical computations and the video displays we used the parameters from the Nocibur (Sudar *et al.*, 2016) experiment, from which we calculated $\gamma_r(0) = 127.2$, $P_{\mathrm{REF}} = 37.4$ MW, and $K_{s0}^2 = 1.59$.

For reference, note that when $\bar{E} \approx \text{const}$ (saturation conditions) the first equation is irrelevant and the other two represent a tilted pendulum equation oscillating within the trap at normalized frequency $K_{s0}\sqrt{\bar{E}}$ and in real space at the synchrotron wave number $K_{s0}\sqrt{\bar{E}}/L_w$.

REFERENCES

Abo-Bakr, M., J. Feikes, K. Holldack, G. Wustefeld, and H.-W. Hübers, 2002, Phys. Rev. Lett. **88**, 254801.
Adams, B. W., 2004, Rev. Sci. Instrum. **75**, 1982.

Akre, R., *et al.*, 2008, Phys. Rev. ST Accel. Beams **11**, 030703.

Alexeev, V., E. Alieva, K. Belovintsev, E. Bessonov, A. Serov, and P. Cherenkov, 1989, Nucl. Instrum. Methods Phys. Res., Sect. A **282**, 436.

Allaria, E., *et al.*, 2012, Nat. Photonics **6**, 699.

Andersson, A., M. S. Johnson, and B. Nelander, 2000, Opt. Eng. **39**, 3099.

Arbel, M., A. Abramovich, A. L. Eichnebaum, A. Gover, H. Kleinman, Y. Pinhasi, and I. M. Yakover, 2001, Phys. Rev. Lett. **86**, 2561.

Arbel, M., A. L. Eichenbaum, Y. Pinhasi, Y. Lurie, M. Tecimer, A. Abramovich, H. Kleinman, I. M. Yakover, and A. Gover, 2000, Nucl. Instrum. Methods Phys. Res., Sect. A **445**, 247.

Arbel, M., A. Gover, A. Eichenbaum, and H. Kleinman, 2014, Phys. Rev. ST Accel. Beams **17**, 020705.

Arp, U., *et al.*, 2001, Phys. Rev. ST Accel. Beams **4**, 054401.

Asakawa, M., *et al.*, 1994, Nucl. Instrum. Methods Phys. Res., Sect. A **341**, 72.

Asgekar, V., G. Geloni, V. Kocharyan, N. Stojanovic, P. Michel, and M. Gensch, 2014, Infrared Phys. Technol. **64**, 26.

Balal, N., I. Bandurkin, V. Bratman, E. Magory, and A. Savilov, 2015, Appl. Phys. Lett. **107**, 163505.

Ben-Zvi, I., K. Yang, and L. Yu, 1992, Nucl. Instrum. Methods Phys. Res., Sect. A **318**, 726.

Berryman, K. W., E. R. Crosson, K. N. Ricci, and T. I. Smith, 1996, Nucl. Instrum. Methods Phys. Res., Sect. A **375**, 526.

Bielawski, S., *et al.*, 2008, Nat. Phys. **4**, 390.

Billinghurst, B., J. Bergstrom, L. Dallin, M. de Jong, T. May, J. Vogt, and W. Wurtz, 2013, Phys. Rev. ST Accel. Beams **16**, 060702.

Bluem, H. P., R. H. Jackson, J. D. Jarvis, A. M. Todd, J. Gardelle, P. Modin, and J. T. Donohue, 2015, IEEE Trans. Plasma Sci. **43**, 3176.

Bonifacio, R., L. De Salvo, P. Pierini, N. Piovella, and C. Pellegrini, 1994, Phys. Rev. Lett. **73**, 70.

Bonifacio, R., C. Pellegrini, and L. Narducci, 1984a, AIP Conf. Proc. **118**, 236.

Bonifacio, R., C. Pellegrini, and L. Narducci, 1984b, Opt. Commun. **50**, 373.

Bonifacio, R., N. Piovella, and B. W. McNeil, 1991, Phys. Rev. A **44**, R3441.

Bonifacio, R., L. D. S. Souza, P. Pierini, and N. Piovella, 1990, Nucl. Instrum. Methods Phys. Res., Sect. A **296**, 358.

Boonpornprasert, P., M. Khojoyan, M. Krasilnikov, F. Stephan, B. Marchetti, E. Schneidmiller, M. Yurkov, and S. Rimjaem, 2014, in *Proc. FEL* (Jacow, Geneva), pp. 153–158.

Bostedt, C., *et al.*, 2016, Rev. Mod. Phys. **88**, 015007.

Bratman, V. L., and Yu Lurie, 2018, Phys. Rev. Accel. Beams **21**, 100701.

Brau, C. A., and R. K. Cooper, 1980, in *Free-Electron Generators of Coherent Radiation* (Springer, Berlin/Heidelberg), pp. 647–664.

Brooke, P. G., 2008, J. Mod. Opt. **55**, 2359.

Brownell, J. H., J. Walsh, and G. Ducas, 1998, Phys. Rev. E **57**, 1075.

Byrd, J., W. Leemans, A. Loftsdottir, B. Marcelis, M. C. Martin, W. McKinney, F. Sannibale, T. Scarvie, and C. Steier, 2002, Phys. Rev. Lett. **89**, 224801.

Byrd, J., *et al.*, 2004, Infrared Phys. Technol. **45**, 325.

Carr, G., S. Kramer, J. Murphy, R. Lobo, and D. Tanner, 2001, Nucl. Instrum. Methods Phys. Res., Sect. A **463**, 387.

Carr, G. L., M. C. Martin, W. R. McKinney, K. Jordan, G. R. Neil, and G. P. Williams, 2002, Nature (London) **420**, 153.

Chen, S., K. Fang, X. Huang, C. Pellegrini, J. Wu, C. Emma, C. Hwang, and S. Serkez, 2014, *Proceedings of FEL2014* (Jacow, Geneva).

Cherenkov, P. A., 1934, Doklady Akademii Nauk SSSR **2**, 451.

Ciocci, F., R. Bartolini, A. Doria, G. P. Gallerano, M. F. Kimmitt, G. Messina, and A. Renieri, 1993, Phys. Rev. Lett. **70**, 928.

Cohen, M., A. L. Eichenbaum, M. Arbel, D. Ben-Haim, H. Kleinman, M. Draznin, A. Kugel, I. M. Yakover, and A. Gover, 1995, Phys. Rev. Lett. **74**, 3812.

Collin, R. E., 2007, *Foundations for microwave engineering* (Wiley, New York).

Colson, W., 1977, Phys. Lett. A **64**, 190.

Courant, E., C. Pellegrini, and W. Zakowicz, 1985, AIP Conf. Proc. **127**, 849.

Dattoli, G., L. Giannessi, P. L. Ottaviani, and A. Segreto, 1997, Nucl. Instrum. Methods Phys. Res., Sect. A **393**, 339.

Dattoli, G., S. Pagnutti, P. Ottaviani, and V. Asgekar, 2012, Phys. Rev. ST Accel. Beams **15**, 030708.

Dicke, R. H., 1954, Phys. Rev. **93**, 99.

Dirac, P. A., 1938, Proc. R. Soc. A **167**, 148.

Doria, A., R. Bartolini, J. Feinstein, G. P. Gallerano, and R. H. Pantell, 1993, IEEE J. Quantum Electron. **29**, 1428.

Duris, J., A. Murokh, and P. Musumeci, 2015, New J. Phys. **17**, 063036.

Duris, J., P. Musumeci, N. Sudar, A. Murokh, and A. Gover, 2018, Phys. Rev. Accel. Beams **21**, 080705.

Duris, J., *et al.*, 2014, Nat. Commun. **5**, 4928.

Emma, C., J. Wu, K. Fang, S. Chen, S. Serkez, and C. Pellegrini, 2014, Phys. Rev. ST Accel. Beams **17**, 110701.

Emma, C., K. Fang, J. Wu, and C. Pellegrini, 2016, Phys. Rev. Accel. Beams **19**, 020705.

Emma, C., Y. Feng, D. Nguyen, A. Ratti, and C. Pellegrini, 2017, Phys. Rev. Accel. Beams **20**, 030701.

Emma, C., A. Lutman, M. Guetg, J. Krzywinski, A. Marinelli, J. Wu, and C. Pellegrini, 2017, Appl. Phys. Lett. **110**, 154101.

Emma, C., and C. Pellegrini, 2014, *Proceedings of FEL2014* (Jacow, Geneva).

Emma, C., N. Sudar, P. Musumeci, A. Urbanowicz, and C. Pellegrini, 2017, Phys. Rev. Accel. Beams **20**, 110701.

Faatz, B., A. A. Fateev, J. Feldhaus, J. Krzywinski, J. Pflueger, J. Rossbach, E. L. Saldin, E. A. Schneidmiller, and M. V. Yurkov, 2001, Nucl. Instrum. Methods Phys. Res., Sect. A **475**, 363.

Fawley, W. M., 1995, Center for Beam Physics, Accelerator and Fusion Research Division, Lawrence Berkeley Laboratory, Berkeley, CA.

Fawley, W. M., 1996, Nucl. Instrum. Methods Phys. Res., Sect. A **375**, 550.

Fawley, W. M., Z. Huang, K. J. Kim, and N. A. Vinokurov, 2002, Nucl. Instrum. Methods Phys. Res., Sect. A **483**, 537.

Feist, A., K. E. Echternkamp, J. Schauss, S. V. Yalunin, S. Schafer, and C. Ropers, 2015, Nature (London) **521**, 200.

Feng, C., and H. Deng, 2018, Nucl. Sci. Tech. **29**, 160.

Feng, C., H. Deng, D. Wang, and Z. Zhao, 2014, New J. Phys. **16**, 043021.

Freund, P., D. C. Nguyen, and B. Carlsten, 2012, Phys. Rev. ST Accel. Beams **15**, 030704.

Friedman, A., N. Balal, E. Dyunin, Y. Lurie, E. Magori, V. Bratman, J. Rosenzweig, H. L. To, and A. Gover, 2014, in *Proceedings of the 36th International Conference on Free Electron Lasers* (Jacow, Geneva), p. TUP081.

Friedman, A., A. Gover, G. Kurizki, S. Ruschin, and A. Yariv, 1988, Rev. Mod. Phys. **60**, 471.

Gabriel, F., *et al.*, 2000a, ru.nl/felix.

Gabriel, F., *et al.*, 2000b, Nucl. Instrum. Methods Phys. Res., Sect. B, **161–163**, 1143.

Gallerano, G. P., A. Doria, E. Giovenale, and A. Renieri, 1999, Infrared Phys. Technol., **40**, 161.

Geloni, G., V. Kocharyan, E. Saldin, E. Schneidmiller, and M. Yurkov, 2009, Nucl. Instrum. Methods Phys. Res., Sect. A **605**, 409.

Geloni, G., E. Saldin, E. Schneidmiller, and M. Yurkov, 2003, arXiv: physics/0303113.

Gensch, M., *et al.*, 2008, Infrared Phys. Technol. **51**, 423.

Gensch, M., *et al.*, 2013, *Proceedings of FEL13* (Jacow, Geneva).

Giannessi, L., *et al.*, 2013, Phys. Rev. Lett. **110**, 044801.

Ginzburg, N., I. Zheleznov, A. Malkin, A. Sergeev, I. Zotova, and M. Yalandin, 2015, in *40th International Conference on Infrared, Millimeter, and Terahertz waves (IRMMW-THz)* (IEEE, New York), pp. 1–1.

Ginzburg, N. S., A. M. Malkin, A. S. Sergeev, I. V. Zotova, V. Zaslavsky, and I. V. Zheleznov, 2013, Phys. Rev. Lett. **110**, 184801.

Giovenale, E., A. Doria, G. Gallerano, S. Letardi, G. Messina, C. Ronsivalle, and A. Vignati, 1999, Nucl. Instrum. Methods Phys. Res., Sect. A **437**, 128.

Girard, B., Y. Lapierre, J. M. Ortega, C. Bazin, M. Billardon, P. Elleaume, M. Bergher, M. Velghe, and Y. Petroff, 1984, Phys. Rev. Lett. **53**, 2405.

Gover, A., 2005a, "Lasers: Free Electron Lasers," in *Encyclopedia of Modern Optics*, edited by R. D. Guenther, D. G. Steel, and L. Bayvel (Elsevier, Oxford).

Gover, A., 2005b, Phys. Rev. ST Accel. Beams **8**, 030701.

Gover, A., E. Dyunin, Y. Lurie, Y. Pinhasi, and M. V. Krongauz, 2005, Phys. Rev. ST Accel. Beams **8**, 030702.

Gover, A., A. Friedman, and A. Luccio, 1987, Nucl. Instrum. Methods Phys. Res., Sect. A **259**, 163.

Gover, A., F. V. Hartemann, G. P. Lesage, N. C. Luhmann, R. S. Zhang, and C. Pellegrini, 1994, Phys. Rev. Lett. **72**, 1192.

Gover, A., A. Nause, E. Dyunin, and M. Fedurin, 2012, Nat. Phys. **8**, 877.

Gover, A., and P. Sprangle, 1981, IEEE J. Quantum Electron. **17**, 1196.

Graves, W., *et al.*, 2013, in *Proceedings of the 2013 FEL Conference* (Jacow, Geneva).

Green, B., *et al.*, 2016, Sci. Rep. **6**, 22256.

Green, G. K., 1976, Brookhaven National Lab Report **50522**.

Gross, M., and S. Haroche, 1982, Phys. Rep. **93**, 301.

Gupta, A., and T. Padmanabhan, 1998, Phys. Rev. D **57**, 7241.

Hafizi, B., A. Ting, P. Sprangle, and C. Tang, 1989, in *Proceedings of the Eleventh International Free Electron Laser Conference* (IEEE, New York), pp. 442–447.

Hama, H., M. Yasuda, M. Kawai, F. Hinode, K. Nanbu, and F. Miyahara, 2011, Nucl. Instrum. Methods Phys. Res., Sect. A **637**, S57.

Happek, U., E. B. Blum, and A. J. Sievers, 1991, Phys. Rev. Lett. **67**, 2962.

Hemsing, E., G. Stupakov, D. Xiang, and A. Zholents, 2014, Rev. Mod. Phys. **86**, 897.

Hilbert, S. A., C. Uiterwaal, B. Barwick, H. Batelaan, and A. H. Zewail, 2009, Proc. Natl. Acad. Sci. U.S.A. **106**, 10558.

Hirschmugl, C. J., M. Sagurton, and G. Williams, 1991, Phys. Rev. A **44**, 1316.

Hoffmann, M. C., S. Schulz, S. Wesch, S. Wunderlich, A. Cavalleri, and B. Schmidt, 2011, Opt. Lett. **36**, 4473.

Hoffrogge, J., J. P. Stein, M. Kruger, M. Forster, J. Hammer, D. Ehberger, P. Baum, and P. Hommelhoff, 2014, J. Appl. Phys. **115**, 094506.

Hommelhoff, P., Y. Sortais, A. Aghajani-Talesh, and M. Kasevich, 2006, Phys. Rev. Lett. **96**, 077401.

Huang, Y. C., 2007, Int. J. Mod. Phys. B **21**, 287.

Huang, Y. C., 2010, Appl. Phys. Lett. **96**, 231503.

Huang, Y. C., C. H. Chen, Z. Zhang, and J. Wu, 2014, *Proceedings of FEL2014, Basel, Switzerland* (Jacow, Geneva).

Huang, Y. C., Z. Zhang, C. H. Chen, and M. H. Wu, 2015, Phys. Rev. ST Accel. Beams **18**, 080701.

Ianconescu, R., E. Hemsing, A. Marinelli, A. Nause, and A. Gover, 2015, *FEL 2015 Conference*, MOP078 (Jacow, Geneva).

Ianconescu, R., and L. P. Horwitz, 1992, Phys. Rev. A **45**, 4346.

Ianconescu, R., and L. P. Horwitz, 2002, Found. Phys. Lett. **15**, 551.

Ianconescu, R., and L. P. Horwitz, 2003, Found. Phys. Lett. **16**, 225.

Isermann, S., and R. Graham, 1992, Phys. Rev. A **45**, 4050.

Ismailov, R. A., and A. Y. Kazakov, 1999, J. Exp. Theor. Phys. **89**, 454.

Jaroszynsky, D. A., R. J. Bakker, C. A. J. van der Geer, D. Oepts, and P. W. van Amersfoort, 1993, Phys. Rev. Lett. **71**, 3798.

Jeong, Y. U., Y. Kawamura, K. Toyoda, C. H. Nam, and S. S. Lee, 1992, Phys. Rev. Lett. **68**, 1140.

Jia, Q., 2008, Appl. Phys. Lett. **93**, 141102.

Jiao, Y., J. Wu, Y. Cai, A. Chao, W. Fawley, J. Frisch, Z. Huang, H.-D. Nuhn, C. Pellegrini, and S. Reiche, 2012, Phys. Rev. ST Accel. Beams **15**, 050704.

Kimura, W., *et al.*, 2001, Phys. Rev. Lett. **86**, 4041.

Korbly, S. E., A. S. Kesar, J. R. Sirigiri, and R. J. Temkin, 2005, Phys. Rev. Lett. **94**, 054803.

Kozák, M., N. Schönenberger, and P. Hommelhoff, 2018, Phys. Rev. Lett. **120**, 103203.

Krinsky, S., 1983, IEEE Trans. Nucl. Sci. **30**, 3078.

Krinsky, S., 1999, Phys. Rev. E **59**, 1171.

Kroll, N. M., P. Morton, and M. Rosenbluth, 1981, IEEE J. Quantum Electron. **17**, 1436.

Kroll, N. M., and M. N. Rosenbluth, 1980, in *Free-Electron Generators of Coherent Radiation* (Addison-Wesley, Boston), pp. 147–174.

Krongauz, M., Y. Pinhasi, M. Tecimer, and A. Gover, 2000, Nucl. Instrum. Methods Phys. Res., Sect. A **445**, 28.

Kulipanov, G. N., *et al.*, 2015, IEEE Trans. Terahertz Sci. Technol. **5**, 798.

Kuroda, R., M. Yasumoto, H. Toyokawa, N. Sei, M. Koike, and K. Yamada, 2011, Nucl. Instrum. Methods Phys. Res., Sect. A **637**, S30.

Leemans, W., *et al.*, 2003, Phys. Rev. Lett. **91**, 074802.

Li, W., J. H. Chen, Z. H. Chen, H. X. Deng, J. G. Ding, Y. Fan, G. P. Fang, C. F. L. Feng, and Q. Gu, 2013, Phys. Rev. ST Accel. Beams **16**, 020704.

Lihn, H. C., P. Kung, C. Settakorn, and H. Wiedemann, 1996, Phys. Rev. Lett. **76**, 4163.

Lurie, Y., V. Bratman, and A. Savilov, 2016, Phys. Rev. Accel. Beams **19**, 050704.

Lurie, Y., A. Friedman, and Y. Pinhasi, 2015, Phys. Rev. ST Accel. Beams **18**, 070701.

Lurie, Y., and Y. Pinhasi, 2007, Phys. Rev. ST Accel. Beams **10**, 080703.

Lutman, A. A., *et al.*, 2016, Nat. Photonics **10**, 745.

Madey, J., 1979, Il Nuovo Cimento B **50**, 64.

Mak, A., F. Curbis, and S. Werin, 2017, Phys. Rev. Accel. Beams **20**, 060703.

Marceau, V., P. Hogan-Lamarre, T. Brabec, M. Piche, and C. Varin, 2015, J. Phys. B **48**, 045601.

Marceau, V., C. Varin, T. Brabec, and M. Piche, 2013, Phys. Rev. Lett. **111**, 224801.

Marshall, T., A. Bhattacharjee, S. Cai, Y. Chou, and I. Wernick, 1991, Nucl. Instrum. Methods Phys. Res., Sect. A **304**, 683.

Mayhew, S., A. I. Al-Shamma'a, R. A. Stuart, A. Shaw, C. Balfour, and J. Lucas, 1997, Nucl. Instrum. Methods Phys. Res., Sect. A **393**, 356.

McNeil, B. W. J., G. R. M. Robb, and D. A. Jaroszynski, 1999, Opt. Commun. **165**, 65.

Michel, F. C., 1982, Phys. Rev. Lett. **48**, 580.

Moody, J., S. Anderson, G. Anderson, S. Betts, S. Fisher, A. Tremaine, and P. Musumeci, 2016, Phys. Rev. Accel. Beams **19**, 021305.

Murokh, A., P. Musumeci, S. Nagaitsev, S. Webb, and A. Zholents, 2017, in *Proceedings of International Free Electron Laser Conference (FEL'17)* (Jacow, Geneva).

Musumeci, P., 2005, Phys. Rev. Lett. **94**, 154801.

Musumeci, P., R. Li, K. Roberts, and E. Chiadroni, 2013, Phys. Rev. ST Accel. Beams **16**, 100701.

Musumeci, P., C. Pellegrini, and J. Rosenzweig, 2005, Phys. Rev. E **72**, 016501.

Nasse, M., *et al.*, 2013, Rev. Sci. Instrum. **84**, 022705.

Nause, A., E. Dyunin, and A. Gover, 2014, Phys. Plasmas **21**, 083114.

Neighbors, J. R., F. R. Buskirk, and A. Saglan, 1984, Phys. Rev. A **29**, 3246.

Neuman, C. P., W. S. Graves, and P. G. O'Shea, 2000, Phys. Rev. ST Accel. Beams **3**, 030701.

Neumann, J. G., P. G. O'Shea, D. Demske, W. S. Graves, B. Sheehy, H. Loos, and G. L. Carr, 2003, Nucl. Instrum. Methods Phys. Res., Sect. A **507**, 498.

Nodvick, J. S., and D. S. Saxon, 1954, Phys. Rev. **96**, 180.

Orlandi, G. L., 2002, Opt. Commun. **211**, 109.

Ortega, J., 1996, Synchrotron Radiat. News **9**, 20.

Palmer, R. B., 1972, J. Appl. Phys. **43**, 3014.

Pan, Y., and A. Gover, 2018, J. Phys. Commun. **2**, 115026.

Pellegrini, C., A. Marinelli, and S. Reiche, 2016, Rev. Mod. Phys. **88**, 015006.

Penn, G., M. Reinsch, and J. S. Wurtele, 2006, Phys. Rev. ST Accel. Beams **9**, 060702.

Peralta, E., *et al.*, 2013, Nature (London) **503**, 91.

Piestrup, M. A., and P. F. Finman, 1983, IEEE J. Quantum Electron. **19**, 357.

Pinhasi, Y., and Y. Lurie, 2002, Phys. Rev. E **65**, 026501.

Priebe, K. E., C. Rathje, S. V. Yalunin, T. Hohage, A. Feist, S. SchÃ¤fer, and C. Ropers, 2017, Nat. Photonics **11**, 793.

Prosnitz, D., A. Szoke, and V. Neil, 1981, Phys. Rev. A **24**, 1436.

Qika, J., 2017, Phys. Rev. Accel. Beams **20**, 070702.

Quimby, D., J. Slater, and J. Wilcoxon, 1985, IEEE J. Quantum Electron. **21**, 979.

Ratner, D., E. Hemsing, A. Gover, A. Marinelli, and A. Nause, 2015, Phys. Rev. ST Accel. Beams **18**, 050703.

Ratner, D., and G. Stupakov, 2012, Phys. Rev. Lett. **109**, 034801.

Ratner, D., *et al.*, 2010, Enhancing FEL power with phase shifters, Technical Report (SLAC National Accelerator Laboratory, Menlo Park, CA).

Reiche, S., 1999, Nucl. Instrum. Methods Phys. Res., Sect. A **429**, 243.

Reiche, S., P. Musumeci, C. Pellegrini, and J. B. Rosenzweig, 2008, Nucl. Instrum. Methods Phys. Res., Sect. A **593**, 45.

Saldin, E., E. Schneidmiller, and M. Yurkov, 1993, Opt. Commun. **103**, 297.

Saldin, E. L., E. A. Schneidmiller, and M. V. Yurkov, 2005, Nucl. Instrum. Methods Phys. Res., Sect. A **539**, 499.

Sannibale, F., J. M. Byrd, A. Loftsdottir, and M. Venturini, 2004, Phys. Rev. Lett. **93**, 094801.

Scharlemann, E., A. M. Sessler, and J. Wurtele, 1985, Nucl. Instrum. Methods Phys. Res., Sect. A **239**, 29.

Schneidmiller, E. A., and M. V. Yurkov, 2015, Phys. Rev. ST Accel. Beams **18**, 030705.

Schnitzer, I., and A. Gover, 1985, Nucl. Instrum. Methods Phys. Res., Sect. A **237**, 124.

Schwinger, J., 1949, Phys. Rev. **75**, 1912.

Seo, Y. H., 2013, Phys. Plasmas **20**, 014502.

Shibata, Y., S. Sasaki, and K. Ishi, 2002, Nucl. Instrum. Methods Phys. Res., Sect. A **483**, 440.

Shibata, Y., T. Takahashi, T. Kanai, K. Ishi, M. Ikezawa, J. Ohkuma, S. Okuda, and T. Okada, 1994, Phys. Rev. E **50**, 1479.

Shin, Y. M., J. K. So, K. H. Jang, J. H. Won, A. Srivastava, and G. S. Park, 2007, Appl. Phys. Lett. **90**, 031502.

Smith, S. J., and E. M. Purcell, 1953, Phys. Rev. **92**, 1069.

Snively, E. C., J. Xiong, P. Musumeci, and A. Gover, 2019, Optica Express (to be published).

Stupakov, G., 2009, Phys. Rev. Lett. **102**, 074801.

Su, X., D. Wang, Q. Tian, Y. Liang, L. Niu, L. Yan, Y. Du, W. Huang, and C. Tang, 2018, J. Instrum. **13**, C01020.

Sudar, N., P. Musumeci, and J. Duris, 2017, Nucl. Instrum. Methods Phys. Res., Sect. A **865**, 39.

Sudar, N., *et al.*, 2016, Phys. Rev. Lett. **117**, 174801.

Sudar, N., *et al.*, 2018, Phys. Rev. Lett. **120**, 114802.

Svetina, C., N. Mahne, L. Raimondi, A. Perucchi, P. Di Pietro, S. Lupi, B. Schmidt, and M. Zangrando, 2016, J. Synchrotron Radiat. **23**, 106.

Svidzinsky, A. A., L. Yuan, and M. O. Scully, 2013, Phys. Rev. X **3**, 041001.

Tamada, H., H. Tsutsui, K. Shimoda, and K. Mima, 1993, Nucl. Instrum. Methods Phys. Res., Sect. A **331**, 566.

Tremaine, A., *et al.*, 2011, *Proceedings of the 2011 Particle Accelerator Conference* (Jacow, Geneva).

Tsai, C. Y., J. Wu, C. Yang, M. Yoon, and G. Zhou, 2018, Phys. Rev. Accel. Beams **21**, 060702.

Tsai, C.-Y., C. Emma, J. Wu, M. Yoon, X. Wang, C. Yang, and G. Zhou, 2019, Nucl. Instrum. Methods Phys. Res., Sect. A **913**, 107.

Vanacore, G., *et al.*, 2018, Nat. Commun. **9**, 2694.

Wang, D. X., G. A. Krafft, and C. K. Sinclair, 1998, Phys. Rev. E **57**, 2283.

Wang, F., *et al.*, 2006, Phys. Rev. Lett. **96**, 064801.

Watanabe, T., X. J. Wang, J. B. Murphy, J. Rose, Y. Shen, T. Tsang, L. Giannessi, P. Musumeci, and S. Reiche, 2007, Phys. Rev. Lett. **98**, 034802.

Wheeler, J. A., and R. P. Feynman, 1945, Rev. Mod. Phys. **17**, 157.

Wiggins, M., *et al.*, 2000, Phys. Rev. Lett. **84**, 2393.

Wong, L. J., B. Freelon, T. Rohwer, N. Gedik, and S. G. Johnson, 2015, New J. Phys. **17**, 013051.

Wu, J., X. Huang, T. Raubenheimer, and A. Scheinker, 2018, in *38th International Free Electron Laser Conference (FEL'17), Santa Fe, NM* (Jacow, Geneva), pp. 229–234.

Xiang, D., and G. Stupakov, 2009, Phys. Rev. ST Accel. Beams **12**, 030702.

Yasuda, M., H. Hama, F. Hinode, K. Kasamsook, M. Kawai, A. Kurihara, K. Nanbu, Y. Shibasaki, and S. Takahashi, 2008, in *Proceedings of the FEL Conference FEL2008* (Jacow, Geneva), pp. 71–74.

Yu, L., *et al.*, 2000, Nucl. Instrum. Methods Phys. Res., Sect. A **445**, 301.

Yu, L. H., 1991, Phys. Rev. A **44**, 5178.

Yu, L.-H., *et al.*, 2000, Science **289**, 932.

Zhao, Z. T., and D. Wang, 2016, IEEE Trans. Nucl. Sci. **63**, 930.
Zhaunerchyk, V., R. T. Jongma, Y. Lurie, Y. Pinhasi, and W. J. van der Zande, 2010, Appl. Phys. Lett. **97**, 231109.
Zholents, A. A., 2005, Phys. Rev. ST Accel. Beams **8**, 040701.
Zholents, A. A., and M. S. Zolotorev, 2008, New J. Phys. **10**, 025005.

See the Supplemental Material at http://link.aps.org/supplemental/10.1103/RevModPhys.91.035003. The Supplemental Material consists of six videos from which one can better examine and understand Figs. 9–14.